# Atmospheric dispersion of chemical, biological, and radiological hazardous pollutants: Informing risk assessment for public safety

**Journal Article**

**Author(s):**
Zhang, Xiaole; Wang, Jing

**Publication date:**
2022-12

**Permanent link:**
https://doi.org/https://doi.org/10.3929/ethz-b-000576032



**Originally published in:**
Journal of Safety Science and Resilience 3(4), https://doi.org/10.1016/j.jnlssr.2022.09.001

Journal of Safety Science and Resilience 3 (2022) 372–397

Contents lists available at ScienceDirect

Journal of Safety Science and Resilience

journal homepage: http://www.keaipublishing.com/en/journals/journal-of-safety-science-and-resilience/

# Atmospheric dispersion of chemical, biological, and radiological hazardous pollutants: Informing risk assessment for public safety

Xiaole Zhang[a,b], Jing Wang[a,b,*]

[a] Institute of Environmental Engineering (IfU), ETH Zürich, Zürich, CH 8093, Switzerland
[b] Laboratory for Advanced Analytical Technologies, Empa, Dübendorf, CH 8600, Switzerland

ARTICLE INFO

*Keywords:*
Atmospheric dispersion
Bioaerosols
Toxic and flammable chemicals
Radiation
Nuclear accident
Industrial accident
Data assimilation
Dose-response relations
Exposure
Quantitative risk assessment
Probabilistic risk assessment

ABSTRACT

Modern society is confronted with emerging threats from chemical, biological, and radiological (CBR) hazardous substances, which are intensively utilized in the chemical, medical, and energy industries. The atmospheric dispersion of released CBR hazardous pollutants can influence a large percentage of the population owing to their rapid process with extensive spatial coverage. It is important to comprehensively understand the behaviors of the released CBR pollutants in the atmosphere to fully evaluate the risks and protect public safety. In this study, we reviewed the advancements in the atmospheric transport of CBR pollutants, including the urban atmospheric boundary layer, unique concepts, and models for CBR pollutants. We underlined the development of innovative methodologies (e.g., inverse estimation and data assimilation methods) for the atmospheric transport of accidentally released CBR pollutants to reduce uncertainties in emissions and accumulated errors during dispersion by combining numerical models with monitoring data. Finally, we introduced progress in quantitative risk assessment, including exposure assessment and dose-response relationships for CBR hazardous pollutants. A framework, source, assimilation, fundamentals, exposure, and risk (SAFER), has been proposed to integrate the key components in the risk assessment of airborne CBR hazardous pollutants. These methods and models can contribute to effective risk preparedness, prevention, evidence-based policymaking, and emergency response to airborne CBR pollutants.

## 1. Introduction

With the constant development of economics and technology, people face emerging threats from chemical, biological, and radiological (CBR) hazardous pollutants. The atmospheric dispersion of released CBR hazardous pollutants is a rapid process with extensive spatial coverage, which can influence a large percentage of the population, thereby being an important pathway for human exposure as well as having adverse health and environmental effects.

The spilled hydrogen sulfide from a drilling well in Chongqing, China killed more than 200 people and poisoned more than 9000 people in December 2003 [1]. The methyl isocyanate released from a pesticide plant caused more than 2000 deaths and the exposure of over 500,000 people in the Bhopal disaster, India, in December 1984 [2]. The 1976 dioxin accident in Seveso, Italy prompted the European Union to enact the Seveso Directive in 1982 to prevent and control similar accidents involving hazardous chemicals [3].

Airborne biological particles, namely bioaerosols, have caused significant threats to human society during the past decades, including the severe acute respiratory syndrome coronavirus (SARS-CoV) [4], the Middle Eastern respiratory syndrome coronavirus (MERS-CoV)[5], the swine-origin influenza A (H1N1) virus [6], the severe *Brucella* infection accident in Lanzhou [7], and the recent severe acute respiratory syndrome coronavirus 2 (SARS-CoV-2) [8].

The Chernobyl disaster in 1986 and the Fukushima Daiichi nuclear disaster in 2011 accidentally released a large amount of radioactive pollution, which rapidly dispersed in the atmosphere [9]. The cloud and ground deposition of radionuclides causes external gamma radiation, thereby significantly contributing to radiation exposure, which is indispensable information for risk assessment and effective emergency management, including sheltering, evacuation, and iodine prophylaxis [10,11].

Existing review studies have mainly focused on atmospheric dispersion models as tools for emergency responses [12] and their applications in the modeling of chemicals [13], bioaerosols [14], and radionuclides [15]. Comprehensive reviews of the technical evolution of atmospheric dispersion models for airborne CBR substances between the Chernobyl (1986) and Fukushima (2011) accidents indicated that atmospheric dispersion modeling plays an increasing role in emergency planning and

* Corresponding author.
*E-mail address:* jing.wang@ifu.baug.ethz.ch (J. Wang).

https://doi.org/10.1016/j.jnlssr.2022.09.001
Received 14 August 2022; Received in revised form 4 September 2022; Accepted 4 September 2022

response to CBR accidents, but there are still issues on how to effectively use the model results to support decision making [15]. A recent review of numerical models for the atmospheric transport of radionuclides has suggested that the unknown accidental release rate is the largest uncertain factor, underlining the importance of inverse modeling and data assimilation [16]. Studies on multi-sensing paradigms for detecting and measuring released hazardous gas in urban areas have been reviewed, and a conceptual framework using wireless sensor networks and mobile crowdsensing has been proposed to locate the source of hazardous gasses [17].

The combination of models and observations, for example, data assimilation and inverse modeling, can significantly reduce the uncertainties in emissions and meteorological data in emergency situations [18–21]. For the effective communication of information on atmospheric transport results, quantitative risk assessment can be utilized as an interface between atmospheric transport results and decision-making during an emergency situation [22]. However, there is a lack of comprehensive reviews on model-observation combinations or quantitative risk assessments for the accidental release of CBR hazardous pollutants.

The release of hazardous CBR substances significantly threatens public safety. It is important to comprehensively understand the behaviors of released hazardous pollutants in the ambient atmosphere to evaluate and manage risks and protect public safety. Professor Weicheng Fan, the pioneer of public safety research in China, first proposed comprehensive and integrated risk assessment methods for public safety [23]. Specifically, he developed innovative methodologies to investigate the atmospheric transport of hazardous materials by integrating observations with numerical models to identify sources and reconstruct emissions [24]. The author (X. Zhang) was inspired by these studies as a doctoral student at the Institute of Public Safety Research led by Professor Fan at Tsinghua and has been researching related fields for approximately 10 years.

In this study, we reviewed the progress in the atmospheric transport of CBR pollutants, including the urban atmospheric boundary layer and unique concepts and models for modeling CBR pollutants. We underlined the development of innovative methodologies, such as the development of data assimilation methods for the atmospheric transport of accidentally released CBR pollutants to reduce uncertainties in emissions and dispersion by combining numerical models with monitoring data. Finally, we introduced progress in quantitative risk assessment, including exposure assessment and dose-response relationships for CBR hazardous pollutants. A framework, source, assimilation, fundamentals, exposure, and risk (SAFER), has been proposed to integrate the key components in the risk assessment of airborne CBR hazardous pollutants. This review also contributes to Professor Fan's pioneering work on public safety.

The structure of the review is organized as follows: in Sections 2 and 3, we introduced the common general fundamentals for the atmospheric transport shared by the CBR pollutants, i.e., the structure of the atmospheric boundary layer, turbulent fluxes, relevant horizontal scales, meteorological data, and the various types of models for atmospheric transport. In Sections 4–6, we respectively introduced the unique properties of the airborne toxic and flammable chemicals, bioaerosols, and airborne radionuclides, which will significantly influence their atmospheric transport and associated risks, e.g., density, particle size distribution, and radiation. In Section 7, the development of innovative methodologies, which combine the models and observations, e.g., inverse modeling and data assimilation, were introduced; these methodologies can be used for the atmospheric transport of different CBR pollutants. In Section 8, the quantitative risk assessment methodologies for CBR pollutants were reviewed. In Section 9, we summarized the study and proposed the SAFER integrated framework for the risk assessment of airborne CBR hazardous pollutants.

## 2. Atmospheric boundary layer and relevant scales

Nearly all hazardous materials are released within the atmospheric boundary (ABL), especially the urban boundary layers, where most of the population lives. Consequently, the structure and characteristics of the boundary layer are closely related to the transport of hazardous substances. The atmospheric boundary layer with a thickness of approximately 1–2 km is the lowest part of the troposphere (from the ground to approximately 11 km), and is directly influenced by the planetary surface [25]. The ABL responds rapidly to surface forcing with a timescale of approximately 1 h, and there are significant turbulence and diurnal variations in the ABL. The horizontal transport of pollutants, heat, and momentum in the ABL is dominated by the mean wind, namely advection, whereas vertical transport is dominated by turbulence. The free atmosphere above the ABL lacks turbulence, leading to limited vertical transport of physical quantities. Therefore, the free atmosphere is usually not influenced by surface changes. The urban and rural boundary layers are atmospheric boundary layers in urban and rural areas, respectively. Owing to the enhanced production of turbulence caused by surfacing heating and buildings, urban boundary layers are usually deeper than their rural counterparts [26].

### 2.1. Structure of the atmospheric boundary layer

As shown in Fig. 1(a), the lowest bottom layer in the urban boundary layer is called the urban canopy layer, which is between the ground surface and the average height of the roughness elements or the average building height $H_C$. Above the urban canopy layer is the roughness sublayer, the boundary of which is usually considered to be between 2 $H_C$ and 5 $H_C$ [27]; however, it should be noted that the estimates were mainly based on studies of vegetated surfaces, mostly from wind tunnel experiments. Systematic estimates for urban surfaces are still lacking [28]. The flow and turbulence in the roughness sublayer are directly influenced by individual roughness elements; therefore, the roughness sublayer has a fully three-dimensional structure [28,29]. Within the roughness sublayer, the turbulence fluxes of pollutants, momentum, and energy are significantly dependent on height [30], as indicated by Fig. 1(b) and (c). The influences of individual roughness elements are blended and become spatially homogeneous by turbulence in the upper part of the surface layer, that is, above the roughness sublayer, which is called the inertial sublayer. The turbulence fluxes vary slightly with height in the inertial sublayer [31], as shown in Fig. 1(c).

### 2.2. Parameterizations of turbulent fluxes

In the ABL, the vertical transport is dominated by turbulence. The turbulent fluxes were estimated by the turbulent transport coefficients, namely eddy diffusivity [32]. Most atmospheric models for weather and air quality simulations are based on the Reynolds-averaged Navier-Stokes equations (RANS) and employ first-order turbulence closures [33], which are called gradient transport theory or K-theory. According to K-theory, the vertical turbulent flux ($\overline{w'c'}$) is estimated as

$$\overline{w'c'} = -K_z \frac{\partial \bar{c}}{\partial z} \tag{1}$$

where $w'$and $c'$are, respectively, the fluctuations of the vertical wind speed and concentration of pollutants, $\bar{c}$is the mean concentration, and$K_z$is the eddy diffusivity in units of $m^2s^{-1}$. The turbulent fluxes in the $x$- and $y$-directions can be estimated in a similar manner. The eddy diffusivity$K_z$is approximated as [32]:

$$K_z = u_* \cdot \Phi_s(z) \cdot l \tag{2}$$

where $\Phi_s(z)$is the dimensionless stability function [34] for scalar gradients developed based on field observations, which is referred to as the Monin-Obukhov similarity theory [35], and embodies the influences of

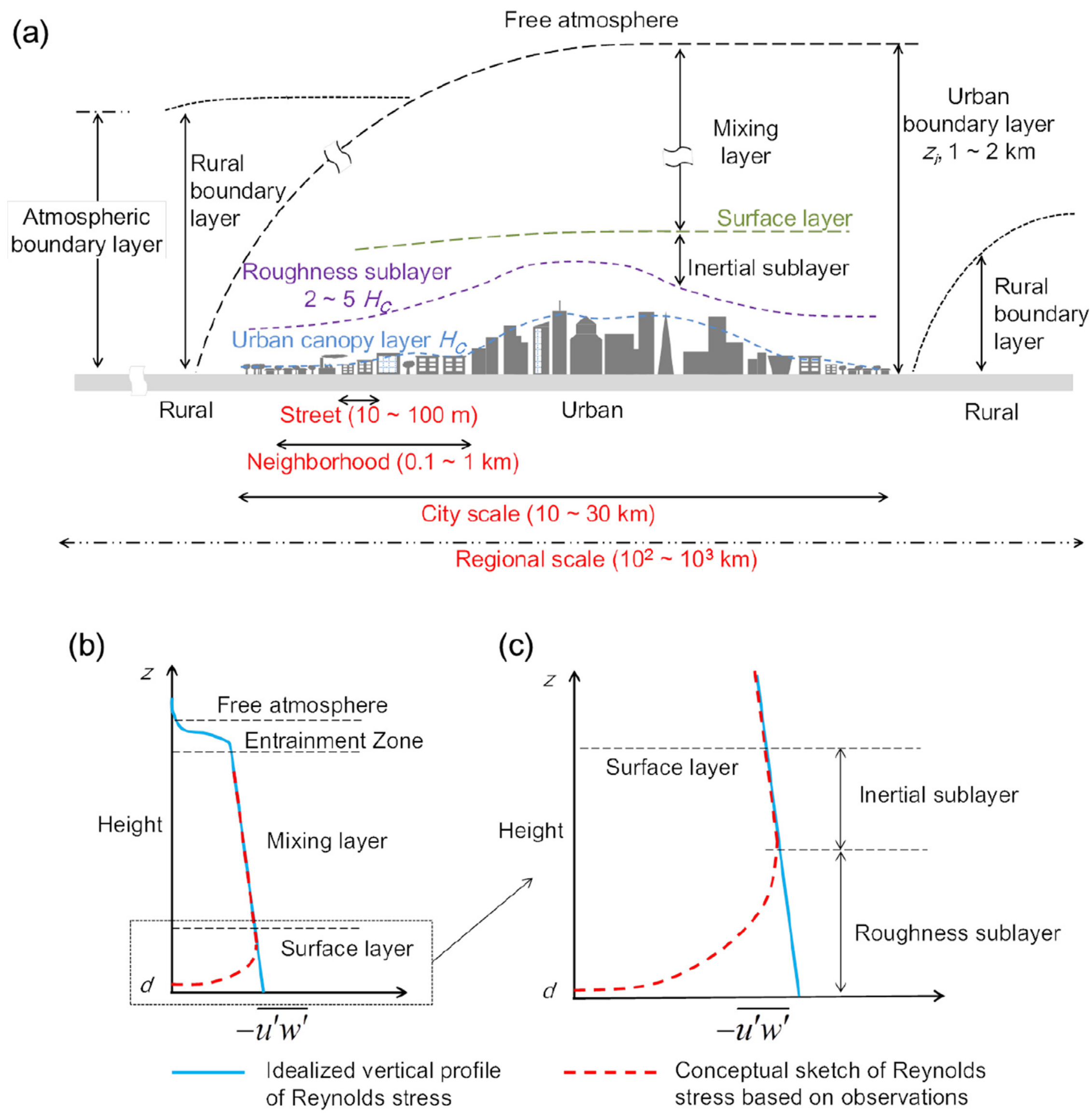


**Fig. 1.** Structure of boundary layer. (a) Structures of urban and rural boundary layers and the relevant horizontal scales for the atmospheric dispersion of hazardous pollutants. (b) Idealized vertical profile of the Reynolds stress [25] and the conceptual sketch of the Reynolds stress based on observations [28] in the atmospheric boundary layer. (c) Enlarged profile of the Reynolds stress in the surface layer.

non-neutral diabatic atmospheric conditions (non-zero gradients of potential temperature), that is, stable and unstable conditions. $l$ is the mixing length (size of the turbulent eddies), and $u_*$ is the friction velocity, which is related to the Reynolds stress and is defined as

$$u_*^2 = -\overline{u'w'} \tag{3}$$

where $u'$is the fluctuation of the horizontal velocity.

It should be noted that the Monin-Obukhov similarity theory is not valid for the roughness sublayer [30], where the turbulence is a fully three-dimensional structure and the turbulence fluxes are height-dependent [28]. Field studies showed that, in contrast to the idealized vertical profile for smooth surfaces, the norm of Reynolds stress appeared to increase with height in the roughness sublayer of the urban boundary layer from a plane displacement height $d$ close to zero before reaching an approximately constant value in the inertial sublayer [28]. As a result, the existing parameterization models for eddy diffusivity based on the Monin-Obukhov similarity theory tend to overestimate the Reynolds stress and eddy diffusivity in the roughness sublayer, leading to a potential underestimation of the concentration near the ground. It is important to consider the turbulent structure in the roughness sublayer for the dispersion of pollutants [28]. However, current studies on the dispersion in the roughness sublayer are still limited.

The thermal stratification of the ABL can significantly influence the atmospheric transport of pollutants. A thermally stratified wind tunnel was built to investigate the effects of atmospheric stability, that is neutral, stable, and unstable conditions, on the dispersion of pollutants over mountainous areas [36–38]. The bulk Richardson number ($Ri_b$) was utilized to satisfy the similarity rule for different atmospheric stabilities, because it is easier to achieve the similarity based on the bulk Richardson number than the others, for example, the gradient Richardson number or the Monin-Obukhov length. The bulk Richardson number is

$$Ri_b = \frac{gL\Delta T}{TU^2} \tag{4}$$

where$\Delta T$is the difference in potential temperature between the source height and ground, and $U$ and $T$ are the potential temperature and velocity at the source height ($L$), respectively. Recent studies using wind tunnel experiments [39] and computational fluid dynamics methods [40–43] have indicated that thermal stratification can significantly influence the transport of pollutants in the roughness sublayer. However, studies on the effects of thermal stratification are still in their infancy.

### 2.3. Relevant horizontal scales for airborne hazards

The atmospheric transport of hazardous substances is related to different horizontal scales. The street scale (10–100 m) and the neighborhood scale (0.1–1 km) are important for all types of hazards to depict the atmospheric transport near the release sources because the concentrations or risks are normally high close to the sources. At these scales, the size of the plume is normally comparable to the depth of the roughness sublayer; therefore, detailed and sophisticated characterizations of the turbulence structure are required for an appropriate assessment of the transport.

Despite the high dilution, the city scale (10–30 km) is still of high importance for bioaerosols and radiological substances because bioaerosols can proliferate and the total amount of radiological substances could be high. Owing to significant public concern, the atmospheric transport of radiological substances at regional ($10^2$–$10^3$ km), continental, and global scales could still be important, for example, atmospheric transport during the Fukushima accident. The transport of substances in large areas (e.g., city or regional scales) is mainly in the inertial sublayer and the mixing layer, so turbulence parameterization models based on the Monin-Obukhov similarity theory can be applied for a reasonable assessment.

### 2.4. Meteorological models and data

Meteorological observations from a monitoring site can be utilized for the estimation of atmospheric dispersion within relatively small horizontal scales, for example, street to city scales, because meteorological conditions are relatively homogeneous within the scale [16]. Downscale modeling is usually required to consider the effects of the terrain and buildings. The GRAMM-GRAL model [44,45], Quick Urban & Industrial Complex (QUIC) Dispersion Modeling System [46–48], and Simulator fOr Wind Farm Applications (SOWFA) [49,50] can take meteorological measurements from a single site as the input and calculate the meteorological field to provide detailed information.

The spatial representativeness of the measurements from a single site becomes limited for dispersion processes at large scales and is circumstantial. As a result, meteorological data from numerical weather prediction (NWP) models are typically adopted. Retrospective studies are usually conducted to investigate the atmospheric dispersion of hazardous pollutants during severe accidents, such as the Chernobyl and Fukushima Daiichi nuclear disasters. Meteorological reanalysis data products can be used in retrospective studies. The reanalysis meteorological data products combine the NWP results with historical observations, so they are generally more accurate than raw NWP data. The current key reanalysis meteorological data products include the fifth generation reanalysis product (ERA5) of the European Center for Medium-Range Weather Forecasts (ECMWF) [51], National Centers for Environmental Prediction/National Center for Atmospheric Research reanalysis [52], Japanese 55-year atmospheric reanalysis [53], and 40-year global reanalysis (CRA-40) dataset from the National Meteorological Information Center (NMIC) of the China Meteorological Administration (CMA) [54]. The resolution of the reanalysis data products is usually tens of kilometers. For local dispersion processes, the aforementioned models can be utilized to dynamically downscale the data into finer resolutions. For regional transport, mesoscale meteorological models, such as the Weather Research and Forecasting model (WRF) [55], can be used to calculate meteorological data at finer resolutions (e.g., several kilometers).

The coupling between meteorological models and atmospheric transport models can be classified into two categories: offline and online [16]. In offline coupling methods, the atmospheric dispersion model directly utilizes the output of NWPs; therefore, there is no feedback from atmospheric dispersion models to the NWPs. Most current dispersion models adopt an offline coupling method owing to its simplicity and relatively low computational cost. However, pollutants might also influence meteorological conditions by acting as cloud condensation nuclei (CCN) or by affecting the radiation budget. Consequently, online coupling methods have been proposed to consider the two-way interactions between meteorological models and atmospheric transport models, for example, WRF-Chem [56]. In accidental releases of hazardous pollutants, it is reasonable to utilize offline coupling methods if the released amount is low and the disturbance on the meteorological conditions is limited. However, when a large amount of pollutants is released, it might significantly alter the meteorological conditions, such as wind and turbulence; therefore, online coupling methods should be adopted.

## 3. Atmospheric transport modeling

The atmospheric transport of hazardous pollutants consists primarily of advection and diffusion, which are driven by meteorological conditions, including the wind field, atmospheric stability, atmospheric boundary layer height, and precipitation. Various methods have been developed to simulate the atmospheric dispersion of hazardous pollutants, including computational fluid dynamics (CFD), Gaussian plume, Lagrangian puff and particle, and chemical transport models. Illustrations of the results from different types of models are shown in Fig. 2, and the representative models or codes for different types of models are summarized in Table 1.

### 3.1. Computational fluid dynamics

CFD methods calculate the transport of pollutants based on the velocity field obtained by solving the Navier-Stokes equations [79,80]. In a comprehensive review of CFD studies on the near-field dispersion of pollutants in the roughness sublayer of an urban environment, the studies were categorized into four typical cases [81]: an isolated building, a single street canyon, building arrays, and building complexes. The complex interaction between the atmospheric flow and buildings makes the flow structure around buildings highly three-dimensional in the near-field dispersion, for example, the street and neighborhood scales. Various factors influence the dispersion process, including horseshoe vortices, vertical diffusion, building wakes, and flow along the street valley.

When a large amount of hazardous pollution is released into the atmosphere, the different physical properties (e.g., temperature and density) between the released pollutants and the ambient atmosphere will alter the flow, which requires an online coupling calculation to take into account the interactions. As a result, CFD models are normally adopted to capture the structures of three-dimensional flow in the near-field dispersion, to achieve online coupling between the ambient flow and the dispersion of pollutants, and to appropriately simulate the physical processes at the street and neighborhood scales [81].

CFD models that solve the RANS equations in conjunction with a turbulence closure model are widely used [82]. The turbulence closure models include the standard $k$–$\varepsilon$ model [83], renormalization group (RNG) $k$–$\varepsilon$ model [84], and Reynolds stress model (RSM) [85]. The $k$–$\varepsilon$ model and its variations usually have better performance than the RSM model [86,87], which might be caused by uncertainties in the parameters of the high number of differential equations involved in the RSM model [81]. Turbulence models derived from the $k$-$\varepsilon$ models are widely adopted in the simulation of accidental releases of hazardous materials [57,88]. In various types of $k$–$\varepsilon$ models, the turbulence flux of pollutants is estimated based on the gradient transport hypothesis with eddy diffusivity, similar to the K-theory adopted in weather prediction and air quality models introduced in the previous section.

In $k$-$\varepsilon$ models, the turbulent Schmidt number ($Sc_t$) is usually adopted to link the eddy diffusivity to the eddy viscosity, which can be calculated from the turbulent kinetic energy ($k$) and turbulent dissipation rate ($\varepsilon$)

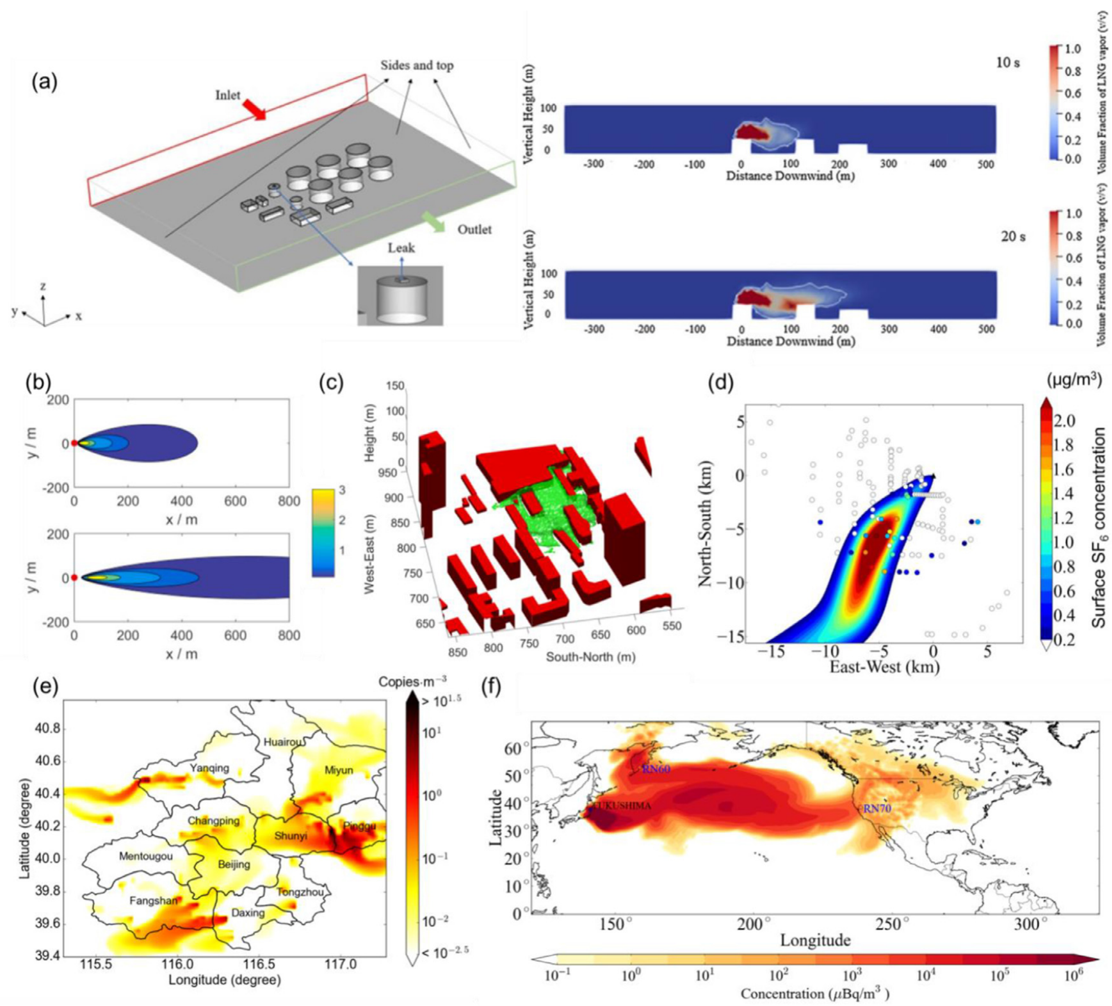


**Fig. 2.** Atmospheric dispersion of chemical, biological, and radiological pollutants calculated by different models. (a) Simulation of atmospheric dispersion of liquefied natural gas leaked from the top of the storage tank using the computational fluid dynamics rhoReactingBuoyantFoam solver in OpenFOAM. Reprinted with permission from ref. [57]. Copyright (2021) Elsevier B.V. (b) Concentration distribution of $SO_2$ predicted by the Gaussian plume model for one case of the Prairie Grass field experiment (mg $m^{-3}$). Reprinted with permission from ref. [58]. Copyright (2018) Elsevier B.V. (c) The plume of virus-laden bioaerosols released from the Wuhan seafood market calculated by the Lagrangian particle model [22], visualized with the urban dispersion visualizer https://github.com/zxiaole/urbanDispersionVisualization. (d) The dispersion of $SF_6$ released in the Kincaid tracer experiment using the Lagrangian puff model. Reprinted with permission from ref. [19]. Copyright (2015) Elsevier B.V. (e) The atmospheric dispersion of bioaerosols containing antimicrobial resistance-related genes from the layer farms in Beijing using the chemistry-transport model [59]. (f) The atmospheric transport of radioactive $^{131}I$ particles released during the Fukushima accident using the chemistry-transport model Polair3D [20].

[89]. It is often assumed that the turbulent Schmidt number is identical to the turbulent Prandtl number in atmospheric models [33]. A Schmidt number of 0.7 to 0.9 is commonly used, but the optimum values in different studies are widely spread from 0.2 to 1.3, depending on the flow properties and geometries [90]. It should be noted that the gradient transport hypothesis cannot depict the anisotropy of turbulent scalar flux, which is common in near-field dispersion. To partially compensate for this inherent limitation, two values of $Sc_t$ can be used to estimate lateral and vertical eddy diffusivities [91].

Large-eddy simulations (LES) are another type of widely utilized turbulence model. Unlike RANS, LES can resolve large-scale eddies, and only the sub-grid scale processes need to be modeled [92]. As a result, the influence of the uncertainties in the turbulent Schmidt number at the sub-grid scale becomes less significant because large-scale fluxes are explicitly resolved in the LES. The performance of LES in estimating the concentration distribution is usually better than that of RANS, even with the simple sub-grid scale model in LES [93], which is mainly attributed to the successful reproduction of the horizontal and vertical diffusions as well as the unsteady fluctuations of concentrations in LES simulations [81]. However, LES simulations are more computationally demanding than RANS ones.

As introduced above, CFD models can capture the fully three-dimensional flow and turbulence structure in the roughness sublayer [28,29]. However, it is difficult and expensive to consider various influencing factors in CFD models, such as atmospheric thermal stratification and buoyancy. The mean inflow and turbulent properties have a strong influence on the flow structure in the roughness sublayer. The inflow properties corresponding to the actual weather conditions should be given [94]. It is more challenging to consider the atmospheric thermal stratification in CFD models. Recent experimental studies [39,95] in wind tunnels and numerical studies [40–42,96] have shown that thermal stratification significantly affects the spread of pollutants and ground-level concentrations.

Model validation is an essential part of the CFD model development. The European COST Action 732 proposed a new protocol for the evaluation and quality assurance of urban meteorology at the microscale

**Table 1**
Representative atmospheric dispersion models of different model types.

| Model type | Model name | Purpose | Developers | Scale | Refs. |
|---|---|---|---|---|---|
| CFD models | OpenFOAM | General purpose | The OpenFOAM Foundation/ ESI Group | Street to neighborhood | [60] |
| | FLACS | Flammable and toxic gas dispersion | GexCon, Norway | Street to neighborhood | [61] |
| | FLUENT | General purpose | Ansys, Inc. | Street to neighborhood | [62] |
| | PALM | General purpose | Leibniz Universität Hannover, Germany | Street to neighborhood | [63] |
| Gaussian plume | HotSpot | Radioactive materials | Lawrence Livermore National Laboratory, U.S. | Neighborhood | [64] |
| | AERMOD | General purpose | U.S. EPA | Neighborhood | [65,66] |
| | Plume model in Polyphemus | general purpose | center d'enseignement et de recherche en environnement atmosphérique, france | Neighborhood | [67] |
| | ALOHA | Chemical emergencies | U.S. EPA | Neighborhood | [68] |
| Lagrangian particle models | FLEXPART | General purpose | University of Vienna, Austria | City, regional, continental, and global scales | [69] |
| | HYSPLIT | General purpose | U.S. National Oceanic and Atmospheric Administration (NOAA) | City, regional, continental, and global scales | [70] |
| | GRAL | General purpose | Air Quality Control, Government of Styria, Graz, Styria, Austria | Street to city | [71] |
| | QUIC | Chemical, biological, and radiological (CBR) agent | University of Utah and Los Alamos National Laboratory | Street to city | [48] |
| Lagrangian puff models | CALPUFF | General purpose | TRC Environmental Corporation | City, regional scale | [72] |
| | RIMPUFF | Chemical, biological, and radiological (CBR) agent | Risø DTU National Laboratory for Sustainable Energy, Denmark | City, regional scale | [73] |
| | ATSTEP | Radioactive materials | Karlsruhe Institute of Technology, Germany | City scale | [74] |
| | Puff model in Polyphemus | general purpose | center d'enseignement et de recherche en environnement atmosphérique, france | Neighborhood | [67] |
| Chemistry transport models | CMAQ | Air quality | U.S. EPA | City, regional, and continental scales | [75] |
| | WRF-Chem | Air quality | U.S. NOAA Earth System Research Laboratories (ESRL) | City, regional, and continental scales | [56] |
| | POLAIR 3D in Polyphemus | general-purpose | center d'enseignement et de recherche en environnement atmosphérique, france | City, regional, and continental scales | [76] |
| | CAMx | Air quality | Ramboll Group | City, regional, and continental scales | [77] |
| | GEOS-Chem | Air quality | Harvard University and Washington University | Global scale | [78] |

[97]. The temporal average of pollution concentrations estimated by the models can be compared with experimental or field measurements because the averages are relatively easy to obtain during measurements. The percentile exceedances of the models should also be evaluated [81].

### 3.2. Gaussian plume model

The Gaussian plume model is a simple approach to calculate the atmospheric transport of pollutants [58]. A number of simplifying assumptions have been made for the original three-dimensional advection-diffusion equation to obtain an approximate analytical solution [98]. It is assumed that (1) the release rate of pollutants is constant from a single point source at $(0, y_0, h_e)$, (2) the wind velocity is constant along the $x$-axis, (3) the dispersion is in a steady state independent of time, (4) the eddy diffusivities are only dependent on the downwind distance, (5) the topography is flat, and (6) the transport in the $x$-direction is dominated by advection, and diffusion is negligible in this direction. The analytical solution to the simplified equation for the average concentration $\bar{c}$ is as follows:

$$\begin{aligned}\bar{c}(x,y,z) = \frac{Q}{\bar{u}}\frac{1}{2\pi\sigma_y\sigma_z}\exp\left(-\frac{(y-y_0)^2}{2\sigma_y^2}\right)\\ \times\left(\exp\left(-\frac{(z-h_e)^2}{2\sigma_z^2}\right)+a\exp\left(-\frac{(z-(-h_e))^2}{2\sigma_z^2}\right)+\exp\left(-\frac{(z-(2h_m-h_e))^2}{2\sigma_z^2}\right)\right)\end{aligned} \tag{5}$$

where $(x, y, z)$ is the position of the target point, $\bar{u}$ is the average wind velocity, $Q$ is the emission rate, $h_e$ is the effective height of the source including the physical height and the plume rise, $h_m$ is the height of the atmospheric boundary layer, $\sigma_y$ and $\sigma_z$ are, respectively, the horizontal and vertical standard deviations, which depict the crosswind diffusion, and $a$ is the reflection coefficient of the ground, which is 1 for complete reflection from the ground and 0 for complete absorption by the ground. The reflections of pollutants at the ground surface and top of the boundary layer are considered in the model.

Different parameterization models have been proposed to estimate the standard deviations in the Gaussian plume model. These models are based on atmospheric stabilities, which are usually categorized as unstable, neutral, and stable boundary layers. Several different subcategories might also be adopted, for example, slightly stable and extremely stable boundary layers. Detailed information about atmospheric stabilities and parameterization models was introduced in the overall reviews [12,99]. The computational cost of the Gaussian plume model is negligible because of its simple form; therefore, it has been widely adopted for operational regulations and emergency responses. It should be noted that because of the assumptions required to obtain the Gaussian plume model, it can only be applied to situations with nearly constant meteorological conditions, simple topography, and constant emission.

### 3.3. Lagrangian puff/particle models

Lagrangian models calculate the transport of pollutants by utilizing a series of released puffs or particles, which carry a certain amount of released pollution and are transported downwind. The key difference between the Lagrangian puff and particle models is the method used to consider the stochastic effects of turbulence. In the Lagrangian puff model, the positions of puffs are deterministically updated based on the mean wind field, the effects of turbulence are considered by assuming a Gaussian distribution of the pollutants within the puffs, and the standard deviations of the puffs increase owing to turbulence [18,58,100–102]. The concentrations at a certain point are calculated as the contributions from all the released puffs. The parameterization models for the standard deviations in the Gaussian plume model are normally applied to Lagrangian puff models.

In Lagrangian particle models, the positions of the released particles are updated both deterministically by the mean wind field and stochastically by a random perturbation owing to turbulent fluctuation, which is a random walk approach described by the Langevin equation [28]. In contrast to the puff models, the particle sizes are assumed to be fixed in the particle models. The concentrations are calculated using the total amount of pollution carried by all particles within a certain volume.

Lagrangian models are much more flexible and powerful than the Gaussian plume model. Discrete puffs and particles can follow complex wind fields, which enables Lagrangian models to simulate the transport of pollutants over different types of topographies. They can also be applied to unsteady situations with changing emissions, as well as to temporal and spatial variations in meteorological conditions.

Owing to their relatively low computational cost, Lagrangian models are widely used, for example, the FLEXPART [69], GRAMM-GRAL [44,45], and RIMPUFF models [103–105]. The RIMPUFF model and other Lagrangian models have been integrated into the Real-time On-line DecisiOn Support (RODOS) system [106–109]. It should be noted that the computational cost increases with an increase in the number of puffs or particles released into the computational domain. If the distances between neighboring puffs or particles become too large, the estimated concentration field will become unrealistically discontinuous. Consequently, problems may arise when applying Lagrangian models to large-scale studies.

### *3.4. Chemistry-transport models*

Global or regional chemistry-transport models (CTM), such as GEOS-Chem [78], Polair3D [20,110], CMAQ [75], and WRF-Chem [111], are widely utilized to investigate and regulate air pollution. The chemistry-transport model calculates the spatial and temporal evolution of the atmospheric concentrations of pollutants [112], which is governed by the advection-diffusion-reaction partial differential equation.

The key physical and chemical processes are modeled by chemistry-transport models, including advection owing to wind transport, diffusion owing to turbulent mixing, and reactions owing to physical (e.g., nucleation and coagulation of particles) and chemical (e.g., photochemistry) processes. These models can also be applied during emergency responses to the accidental release of hazardous materials. The CMAQ [113] and WRF-Chem models [114,115] were used to reconstruct the atmospheric transport and deposition of radionuclides released during the Fukushima nuclear accident.

In addition to the advection-diffusion module, the chemistry-transport models also contain modules for multiphase chemistry and aerosol microphysics, which consume most of the computational time of the chemistry-transport models owing to complicated chemical and physical mechanisms. Chemical mechanism models, for example, the widely adopted carbon bond mechanism [116], are mainly developed for regular pollutants in the atmosphere, for example, $NO_2$, $O_3$, and volatile organic compounds (VOC). However, chemical, biological, and radiological hazardous pollutants are not included in the chemical mechanism models, and it is challenging to investigate the chemical mechanisms of these pollutants because of extremely limited observations. Several attempts have been made to introduce an atmospheric iodine gas-phase mechanism for accidental release from nuclear accidents [117,118]. Most of the time, the changes in these hazardous pollutants are simply described by a model of decay or inactivation instead of the complicated chemical mechanisms in chemistry-transport models. Chemistry-transport models usually include aerosol dynamic modules, which can be utilized to depict the detailed behaviors of hazardous particles.

The spatial resolutions of chemistry-transport models are relatively low (typically several kilometers), which is insufficient for assessments in the vicinity of release sources. Some plume-in-grid approaches [119] exist for the sub-grid calculation, but they are unable to satisfactorily model sub-grid meteorological conditions or simulate fully three-dimensional flow structures in the roughness sublayer. As a result, chemistry-transport models are mainly applicable for regional and continental/global transport, for example, studies related to the Fukushima accident [113].

## 4. Airborne toxic and flammable chemicals

The key atmospheric issues arising from the accidental release of chemicals are introduced in this section, including the source terms, special physical properties of the dispersion of the typical toxic and flammable chemicals, numerical models, and field and laboratory experiments.

### *4.1. Source term*

The source term describes the type, amount, and physical parameters of the released hazardous substance involved in the release (e.g., temperature, pressure, release time, and state of the substance) [120]. The source term is closely related to the status and properties of the released material (e.g., compressed gas, liquefied-pressurized gas, and non-boiling liquid) and the damage mechanisms (e.g., failure of vessel holes and rupture of a vessel) [120]. The release of compressed vapor is usually in the gas phase; however, the release of pressurized liquid is complex with a two-phase flow [121].

The statistics of the hazardous substances involved in the accidents recorded in the major accident reporting system [122] are shown in Fig. 3(a). The results indicate that toxic substances frequently involved in accidents include chlorine, ammonia, hydrogen chloride, hydrogen fluoride, and hydrogen sulfide. Flammable substances with high unintended release frequencies include ethylene, natural gas, hydrogen, butane, and propane. These major substances accounted for approximately 50% of accidents in the database. This agrees with the risk ranking of toxic industrial chemicals developed by the U.S. Department of Homeland Security/Chemical Security Analysis Center and the U.S. Defense Threat Reduction Agency, which indicated that chlorine, anhydrous ammonia, and sulfur dioxide are usually at the top of the ranks, and they are normally stored and transported as liquefied gasses [123].

The release plume could be classified into different zones, as shown in Fig. 3(b). The release flow is usually choked owing to the high pressure in the vessel. The release flow is under-expanded in the first zone, and a corresponding model should be developed to depict the expansion of the flow based on the properties of the released substance. There will be flashing of the pressurized liquid, for example, liquefied natural gas (LNG). The pressure of the flow decreases to the ambient level at the end of this zone [124]. In the jet flow zone, droplets can be formed, and the sizes of the droplets must be estimated, which is important for assessing the rainout of the droplets. Source term models should be developed for zones of under-expansion and jet flow.

The zone of jet flow is the buoyant and neutrally buoyant flow (with sufficient dilution), which can be evaluated using atmospheric dispersion models, for example, CFD and Lagrangian models. For buoyant flow, online coupling between the plume and the ambient environment is required; therefore, CFD methods are more suitable for this phase. After sufficient dilution, the density of the released plume approaches the ambient condition, leading to negligible buoyancy; thus, offline methods, for example, Lagrangian particle models, can be utilized. Models have been developed to estimate the source term of the unintended release of liquid hydrogen, accounting for the transitions between the stagnant location in the tank and the location where the concentration drops to 4% by volume [124]. Toxic and harmful pollutants can also be generated by some special sources with a significant release of heat, for example, volcanic eruptions [125,126] and fire accidents [127–129]. In such cases, plume rise schemes [67] should be included to estimate the source term of the emissions by considering the temperature, initial velocity, and area of the sources. More details regarding the source term models can be found in the Accident Damage Analysis Module (ADAM) – Technical Guidance [121].

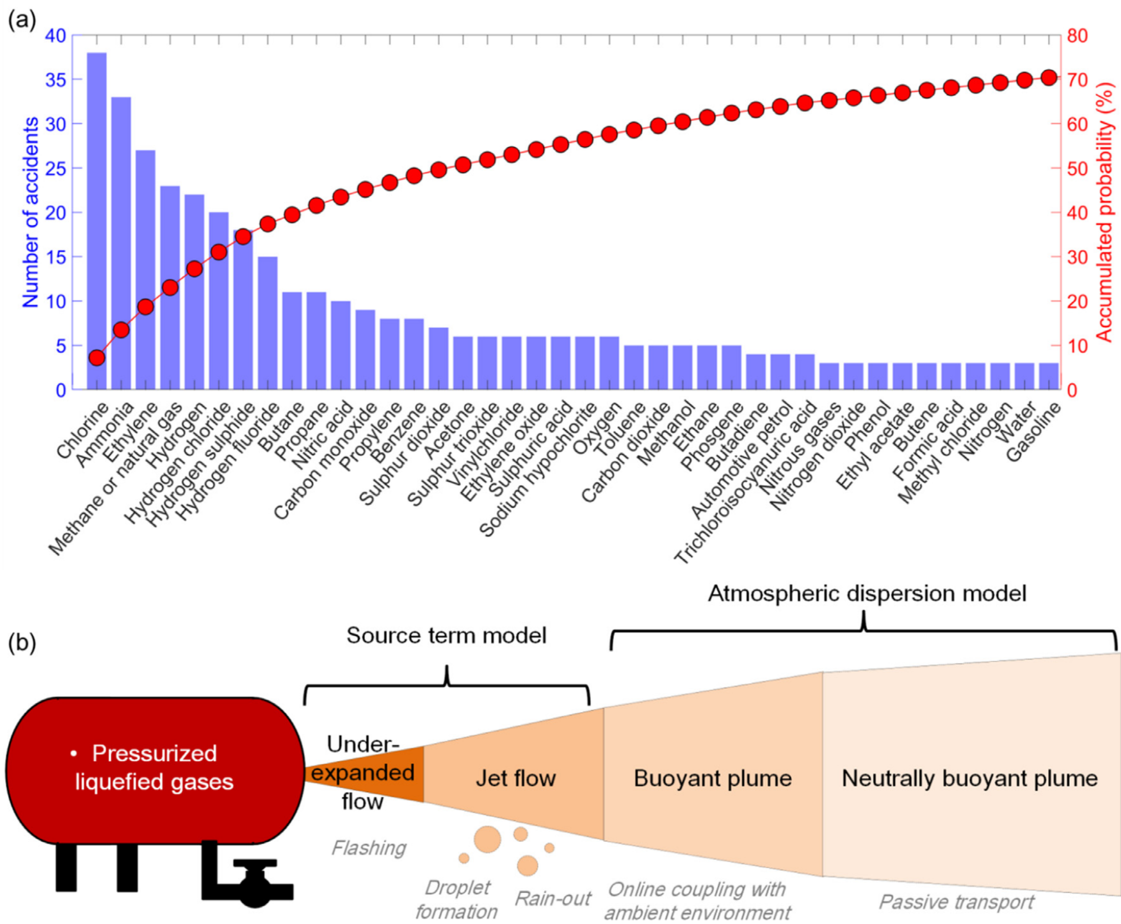


**Fig. 3.** Typical unintended releases of hazardous chemicals: (a) the statistics of the typical toxic and flammable chemicals involved in the release accidents recorded in the database of the European Major Accident Reporting System (eMARS); (b) schematic graph of the key phases of the plume of released pressurized liquefied gasses.

### *4.2. Denser- and lighter-than-air substances*

The atmospheric dispersion of released hazardous substances is highly dependent on the density. In this study, we focused on denser and lighter-than-air substances. Denser-than-air gasses (e.g., chlorine) have higher molecular weights than the ambient air or are released at a sufficiently lower temperature than the ambient conditions (e.g., liquefied natural gas and liquid hydrogen) [130–132]. Two main unique effects were observed from the field experiments of denser-than-air substances, for example, LNG releases: first, the stable stratification owing to the density could suppress the vertical turbulence mixing, and it becomes difficult for the ambient turbulence to penetrate into the cloud of the dense gas, which hinders the dissipation of the cloud; the other unique effect is the gravity-driven flow, tending to follow the topography instead of the ambient wind. These effects lead to a wider and lower cloud near the ground than neutrally buoyant gas [130]. As a result, denser gas stays near the ground and increases the risk [133–135].

Temperature is a critical parameter in the model for the release of dense pressurized liquefied gasses such as LNG. The heat flux from surfaces (e.g., the ground, building walls, and the water surface) to the cold dense substance plays an important role in the mitigation of releases, because the flux can increase the temperature and decrease the density of the cloud, which can also potentially induce turbulence and increase the mixing of the cloud with ambient air [130]. A recent study suggested that the released liquid hydrogen (LH2) initially behaves as a dense gas in the ambient environment, different from the compressed hydrogen gas that will rise and rapidly become diluted, and the lower flammable limit (LFL) distances for LH2 can be significantly larger than that for LNG releases [136]. It was shown that LH2 had dense gas behavior close to the source and became significantly buoyant in the far range after being heated by the ground and buildings [137].

Owing to the increasing demand for green energy, natural gas and hydrogen are gaining popularity, as they are lighter-than-air gasses. The dispersion of these gaseous substances is completely different from that in their liquefied states. Owing to the buoyancy-driven flow, the released plume is vertically lifted and rapidly diluted. It is suggested that the risk of lighter-than-air gasses is much lower than that of dense gasses; therefore, studies on light gasses are scarce. However, it is important to fully understand the transport behavior of light gasses, for example, hydrogen, considering their increasing usage [138]. The release of light gas can cause classical Rayleigh Taylor (R-T) instability [139], which is induced by placing a heavy fluid over a light fluid in a gravitational field [138], and the buoyancy drives the mixing between the light gas and the ambient air. If there was an ignition source, the mixed flammable gas with air would impose a significant risk [140,141]. It is also important to investigate the effects of the relative directions of the jet flow and ambient wind [142] and the thermal stratification of the atmosphere [96,143,144].

### *4.3. Simulations of the atmospheric dispersion of hazardous chemicals*

The released denser- and lighter-than-air substances can influence the ambient flow, so CFD methods with online coupling between the releases and the ambient air provide the most complete description of the physical processes (e.g., mass, momentum, and energy conservation) and become the most suitable tools to calculate the atmospheric dispersion of dense or light substances [130]. The FLACS CFD models have been adopted to simulate the atmospheric dispersion of LNG [61] and LH2 [145], and have shown that similar qualitative trends with field experiments can be produced, but there are still significant quantitative differences. The rhoReactingBuoyantFoam solver of OpenFOAM has been utilized to investigate the leakage and dispersion of LNG [57] and natural gas [88]. ANSYS Fluent has been used to simulate the atmospheric dispersion of ammonia [146,147].

CFD methods are typically computationally expensive; therefore, parameterized Lagrangian models are more suitable for emergency response applications [130]. The parameterization model of buoyancy-driven dynamics was implemented in a Lagrangian puff model to simulate the rise of the buoyant plume and dispersion of dense gas [148]. Various types of simplified models have been developed, such as parameterized plume models, shallow layer models, one-dimensional integral models, and parameterized Lagrangian models. More details about these models can be found in a comprehensive review [149].

### *4.4. Field and laboratory experiments*

Field measurements are indispensable for developing and evaluating atmospheric transport models. Many experiments have been conducted and efforts have been made to archive datasets [150]. Representative experiments under typical conditions, such as urban environment dispersion, large-scale transport, and release of dense gasses, are briefly summarized in Table 2. A more complete introduction to the experiments can be found in the Modelers' Data Archive [13,150].

## 5. Bioaerosols

Bioaerosols are particles that are partially or completely formed by living organisms, such as bacteria, viruses, fungi, or pollen. Bioaerosols can be pathogenic or infectious and can potentially cause diseases, such as SARS-CoV-2, if inhaled by humans or animals.

### *5.1. Size distributions of bioaerosols*

The size of bioaerosols significantly influences their atmospheric transport properties, for example, deposition and the distribution of deposition in different parts of the human respiratory tract; therefore, the size distribution of bioaerosols is an important parameter for the evaluation of their atmospheric transport [14,59]. Viruses are usually in breath aerosols formed by the rupture of fluid film in the lungs during inhalation owing to the expansion of the bronchiole [165]; therefore, viral shedding is usually assumed to be proportional to the volume of the exhaled particles [22]. As shown in Fig. 4, the emission of bioaerosols and their size distribution should first be evaluated.

Measurements have shown that the aerodynamic diameters of the breath droplet nuclei are mainly below 5 $\mu$m at the equilibrium state after evaporation with a concentration of approximately 0.098 particles cm$^{-3}$ for mouth breathing [166]. The respiratory shedding of coronavirus (NL63, OC43, HKU1, and 229E) is approximately $10^2$ to $10^5$ virus copies in particles below 5 $\mu$m with 30 min sampling and without wearing masks [167]. The geometric mean concentrations of the influenza A virus (IAV), porcine reproductive and respiratory syndrome virus (PRRSV), and porcine epidemic diarrhea virus (PEDV) generated by acutely infected pigs were respectively approximately $9.1 \times 10^4$, $5 \times 10^3$, and $9.1 \times 10^7$ copies m$^{-3}$ for particles below 10 $\mu$m sampled with the cyclonic air collector; the measurements also indicated a higher viral load in larger particles [168]. The viable IAV and PRRSV viruses could be isolated in cell cultures only from particles larger than 2.1 $\mu$m [168]. Bioaerosols are also generated during the aeration process at wastewater treatment plants [169]. Existing studies suggest that airborne viruses can be found in a wide range of respiratory

**Table 2**
Representative experiments in typical conditions, including urban environment dispersion, large-scale transport, and releases of dense gasses.

| Experiment name | Year | Tracers | Atmospheric stability | Terrain | Scale | Source geometry | Release duration | Ref. |
|---|---|---|---|---|---|---|---|---|
| JR II (Jack Rabbit II) | 2015–2016 | Dense (liquefied chlorine) | Stable, neutral, and unstable | Mock urban | Neighborhood | Point | Instantaneous | [151] |
| MID05 (Midtown 2005) | 2005 | Neutral (perfluorocarbon and $SF_6$ tracers) | Neutral to unstable | Urban (midtown Manhattan) | Neighborhood | Point | Short time | [152] |
| MSG05 (Madison Square Garden 2005) | 2005 | Neutral (perfluorocarbon tracer) | Slightly unstable to slightly stable | Urban (Madison Square Garden) | Neighborhood | Point | Short time | [153] |
| Joint Urban 2003 (JU2003) | 2003 | Neutral ($SF_6$ as tracer) | Stable, neutral, and unstable | Urban (Oklahoma City) | Neighborhood | Point | Instantaneous and short time | [154] |
| URBAN 2000 Multi-scale Tracer Experiment | 2000 | Neutral ($SF_6$ as tracer) | Neutral to stable | Urban (Salt Lake City) | Neighborhood | Point and line | Short time | [155] |
| MUST (Mock Urban Setting Test) | 2001 | Neutral (Propylene as tracer) | Stable, neutral, and unstable | Mock urban | Neighborhood | Point | Instantaneous and short time | [156] |
| PSB1 (Project Sagebrush Phase 1) | 2013 | Neutral ($SF_6$ as tracer) | Neutral and unstable | Rural | Neighborhood | Point | Short time | [157] |
| METREX (Metropolitan Tracer Experiment) | 1984 | Neutral (perfluorocarbon tracer) | Stable, neutral, and unstable | Urban (Washington, DC metropolitan area) | City scale | Point | Short time | [158] |
| ACURATE (Atlantic Coast Unique Regional Atmospheric Tracer Experiment) | 1982–1983 | Neutral (Kr-85) | Complex | Complex | Regional scale | Point | Hours | [159] |
| SRPTEX (Savanah River Plant Tracer EXperiment) | 1975–1977 | Neutral (Kr-85) | Complex | Complex | Regional scale | Point | Hours | [160] |
| OKTEX (OKlahoma Tracer EXperiment) | 1980 | Neutral (perfluorocarbon tracer) | Complex | Complex | Regional scale | Point | Hours | [161] |
| ETEX (European Tracer EXperiment) | 1994 | Neutral (perfluorocarbon tracer) | Complex | Complex | Continental | Point | Hours | [162] |
| ANATEX (Across North America tracer experiment) | 1987 | Neutral (perfluorocarbon tracer) | Complex | Complex | Continental | Point | Hours | [163] |
| CAPTEX (Cross APpalachian Tracer EXperiment) | 1983 | Neutral (perfluorocarbon tracer) | Complex | Complex | Continental | Point | Hours | [164] |

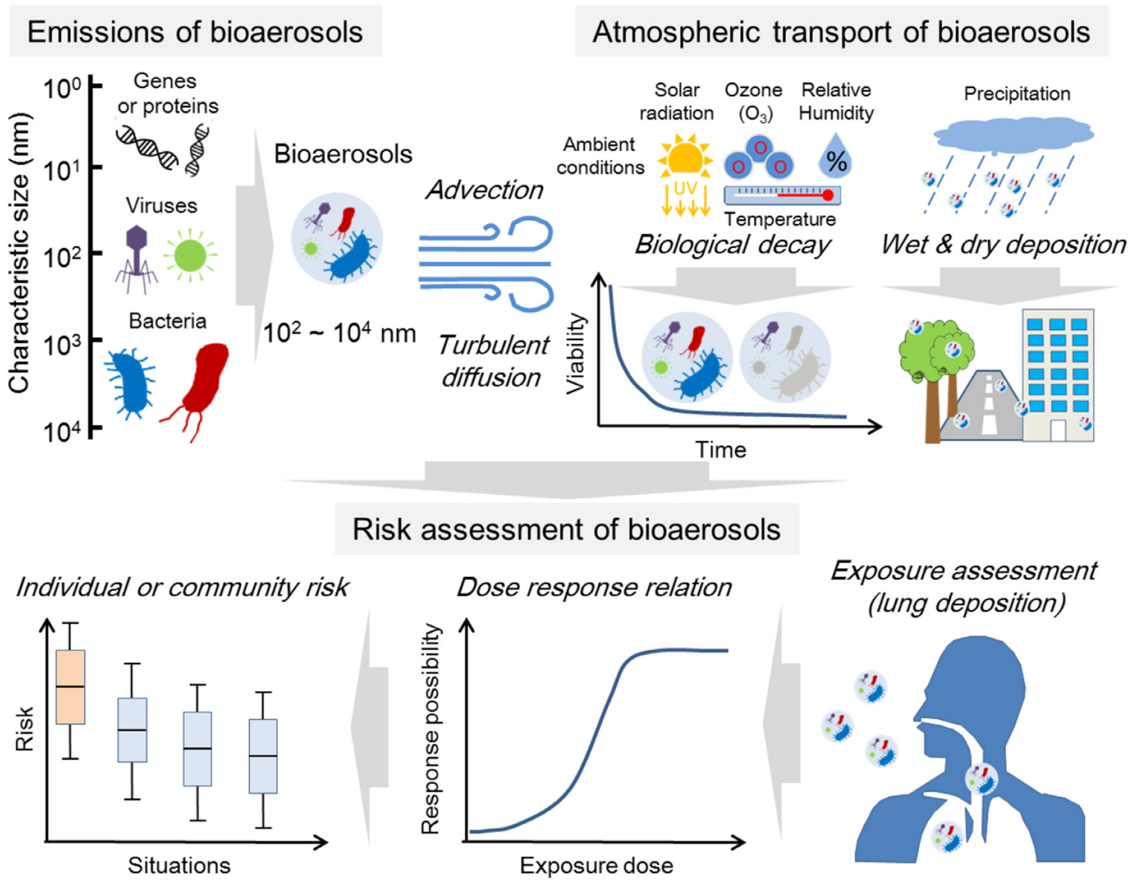


**Fig. 4.** Risk assessment of bioaerosols, including estimation of bioaerosol emission, atmospheric transport, exposure assessment, and risk assessment using dose-response relations.

particles, and virus viability might be dependent on the size of the particles.

The size distributions of bioaerosols containing bacteria, fungi, and actinomycetes have been investigated in a full-scale composting facility in Korea [170]. A six-stage impactor was utilized to sample the bioaerosols onto the agar plates, which were incubated after sampling, and the number of colonies was counted to represent the concentrations of bioaerosols in terms of colony-forming units (CFU) per unit volume of air [170]. The bioaerosol concentrations were nearly constant over the range of measured sizes between 0.65 and 7 $\mu$m at a magnitude of $10^3$ CFU $m^{-3}$, although the particle number concentrations significantly decreased with the size of the particles. The percentages of bacteria, fungi, and actinomycetes were 85.1%, 0.3%, and 14.6%, respectively [170].

## 5.2. Biological decay

The biological decay of bioaerosols is of great importance for understanding their behavior in the environment and for risk assessment. Biological decay affects the viability of airborne organisms. A recent study systematically reviewed the decay characteristics of aerosolized viruses [171]. It was assumed that the viruses followed an exponential decay function; however, an initial decay constant and a secondary decay constant were estimated for the first 5–30 min and after 30 min, respectively. The half-life periods during the initial stage were between $10^{-2}$ and 10 h, and the decay became slower during the second stage, with half-life periods between $10^{-1}$ and $10^2$ h. The data also indicate that the decay became faster with increasing temperature and was fast when the humidity was approximately 50%. More details can be found in [171] and the references therein.

The stability of SARS-CoV-2 has been investigated by considering the influence of sunlight and relative humidity [172]. The results indicated that the decay rates of the viruses in simulated saliva were dependent on the simulated sunlight intensity, with a half-life of approximately 86 min without sunlight, approximately 6 min in sunlight of medium intensity (0.94 W $m^{-2}$ UVB, the solar radiation in March and October), and approximately 2 min in sunlight of high intensity (1.91 W $m^{-2}$ UVB, the solar radiation in June), but they were independent of the relative humidity. The biological decay of coronaviruses, including common human coronavirus (HCoV), MERS-CoV, SARS-CoV, transmissible gastroenteritis virus (TGEV), and mouse hepatitis virus (MHV), reported in the literature was summarized to determine the reasonable parameters for the infection risk assessment of aerosol transmission [22]. The half-life was between 0.5 and $10^2$ h. A recent study found that the viability of both bacteria and viruses decreased with decreasing relative humidity (RH) at intermediate and high RH [173]. Divergences occurred at low RH, where the viability of bacteria continued to decrease with decreasing RH, but the viability of viruses increased with decreasing RH. However, the mechanisms underlying the inactivation of bacteria and viruses remain unclear.

*Bacillus anthracis* is a spore-forming bacterium that causes anthrax infection. The spores are very resistant to extreme physical conditions, and can survive for up to 200 years [174], which is very different from bacteria and viruses. As a result, spore-forming pathogenic microorganisms can be very harmful, and special attention should be paid to them.

It has been shown that various atmospheric conditions will influence the survival of bioaerosols [59,175,176], including solar radiation (ultraviolet radiation), the ozone, relative humidity, and temperature. However, current studies on biological decay are still limited and inconsistent, which might be due to various experimental protocols. Innovative experimental systems [175,177] should be developed to simulate the conditions that bioaerosols will experience in the natural environment, which will enable the robust investigation of the survival of bioaerosols as a function of ambient conditions.

### 5.3. Atmospheric transport model for bioaerosols

Atmospheric dispersion models have been adopted to assess the impact of bioaerosols, including viruses, spores, bacteria, and pollen, with high spatial and temporal resolutions [14], which are difficult to achieve by field sampling and measurements. In addition, the models can also provide forecasts, which are important for effective emergency response during the accidental release of hazardous bioaerosols.

The transport of the foot-and-mouth disease virus (FMDV) has been widely investigated based on atmospheric transport models, especially Lagrangian models, including the Lagrangian puff CALPUFF [178,179], RIMPUFF [180–182], and Lagrangian particle HYSPLIT models [183]. In these studies, the size of FMDV-related bioaerosols was assumed to be approximately 10 $\mu$m [178,179]. The emissions of FMDV were estimated as $10^{4.3}$ to $10^{6.1}$ $TCID_{50}$ (the median tissue culture infective dose) [14] per cattle per day. The biological decay of FMDV was usually included in the studies and it was assumed that it was dependent on ambient parameters, including relative humidity and temperature. The survival rates of FMDV were assumed to be low, with relative humidity lower than 60% and temperature higher than 27 °C [178,179]. As an alternative, an inactivation rate of $3.2 \times 10^{-4}$ $h^{-1}$ [183] was adopted to depict the inactivation process.

Mathematical models were developed to estimate atmospheric transport, evaluate infection risk, and formulate emergency response strategies for airborne anthrax attacks from the spore-forming bacterium *B. anthracis* [184]. The embedded Lagrangian dispersion model in the operational multiscale environment model with grid adaptivity (OMEGA) was used to evaluate the atmospheric dispersion of anthrax spores over an urban region [185]. The influence of the numerical models for biological decay on the assessment of atmospheric transport was investigated using three types of biological decay models: exponential, probability, and catastrophe [186], which were integrated with a simple Gaussian plume model. The study indicated that the models yielded similar results for the first 30 min, but significantly diverged between intermediate and long times. More work should be conducted, including detailed fundamental studies on the responses of microorganisms to environmental stressors, the development of parameterization models for response modeling, and probabilistic assessment considering the uncertainties in the various components of the model.

The Lagrangian particle model GRAL (microphysics Graz Lagrangian Model) and mesoscale numerical weather prediction model GRAMM (Graz Mesoscale Model wind fields) were utilized to evaluate the atmospheric transport of SARS-CoV-2 in the urban area surrounding the Wuhan seafood market [22]. Aerosol dynamics models with detailed microphysics [187–189] can be utilized to improve the model performance for the detailed behavior of bioaerosols in the ambient environment. Computational fluid dynamics (CFD) methods have also been adopted to investigate the transport of some highly pathogenic and lethal viruses, for example SARS [4], but CFD methods are computationally expensive and not suitable for the assessment of large areas.

### 5.4. Bioaerosol measurements

Bioaerosols can be measured using air samples [190,191]. Filter-based sampling methods are typically used to collect ambient particles [192–196]. Portable microsystems for the collection of airborne particles can facilitate the concentration of bioaerosols and enhance the detection performance [197]. Wetted-wall cyclones based on centrifugal impaction are also widely adopted for bioaerosol sampling, as they can protect biological structures and improve the viability of the sampled microorganisms [191]. Other bioaerosol sampling methods include impaction-based samplers, liquid-based samplers, and electrostatic precipitators, which can be referred to in a comprehensive review of bioaerosol sampling [191].

Quantitative polymerase chain reaction (qPCR) analysis or culturing can be subsequently applied to identify the bio-components in the samples, for example, viruses [198,199], bacteria [200,201], and airborne antibiotic resistance genes (ARGs) [202,203]. However, it is difficult for these offline methods to provide real-time information, which may be important to address safety concerns.

The development of real-time detection and measurement methods for bioaerosols is still in its early stages. Laser-induced fluorescence (LIF), which utilizes UV light to excite the biological fluorophores tryptophan and nicotinamide adenine dinucleotide (NADH), is currently a widely adopted and commercialized method for the online detection of bioaerosols [204,205]. A succinimidyl-ester-functionalized plasmonic biosensor was proposed and developed as an alternative technology for measuring total bioaerosols [206]. Colorimetric immunoassay combined with filtration for enrichment [207] and microfluidic analysis [208–211] could be promising low-cost pathways for the detection of pathogenic bioaerosols. However, these methods lack specificity and are unable to distinguish between the types of bioaerosols.

Many innovative bioaerosol detectors with high specificity have emerged since the outbreak of COVID-19. An amplification-free plasmonic biosensor has been fabricated to directly detect the RNA of SARS-CoV-2 with high efficiency and short detection time [212,213]. A low-cost, one-step, sensitive, and accurate multiplex detection electrochemical biochip has recently been developed to detect the spike, nucleocapsid proteins, and IgG antibodies of SARS-CoV-2 [214], which can be easily modified to specifically detect different types of bioaerosols, for example, ARGs [215]. However, there are still many challenges in bioaerosol detection [216].

## 6. Airborne radionuclides

### 6.1. International Nuclear and Radiological Event Scale

A radiological event involves radionuclides that are not induced by nuclear explosions. Radiological events include accidents at nuclear power plants, transportation, and radiological dispersal devices (RDD) [217].

The International Atomic Energy Agency (IAEA) and Organization for Economic Co-operation and Development (OECD) Nuclear Energy Agency (OECD/NEA) developed the International Nuclear and Radiological Event Scale (INES) as an international event rating scale to consistently define the radiation risks of nuclear and radiological events [218]. There are seven levels in the INES, from lowest level 1 (anomaly) to highest level 7 (major accident). The accident level is defined based on the quantity of radioactive substances released and not the dose received.

Radioactive $^{131}I$ was utilized as a reference substance to quantitatively define the INES scales. The released amounts of other radionuclides are converted to the equivalent amount of $^{131}I$ using the defined conversion factors base on the concept of “radiological equivalence,” resulting in the same level of effective dose [218]. There have been two Level 7 accidents: the Chernobyl disaster in 1986 and the Fukushima Daiichi nuclear disaster in 2011 [9].

### 6.2. Source term and particle size distribution

The released radionuclides can be gasses or particles, and they can be in organic or inorganic forms. The forms of the radionuclides, for example, the size distribution of the particles, significantly influence the deposition processes. In nuclear accidents, volatile radionuclides, including noble gasses, iodine, cesium, tellurium, and tritium, can be released into the atmosphere [219,220].

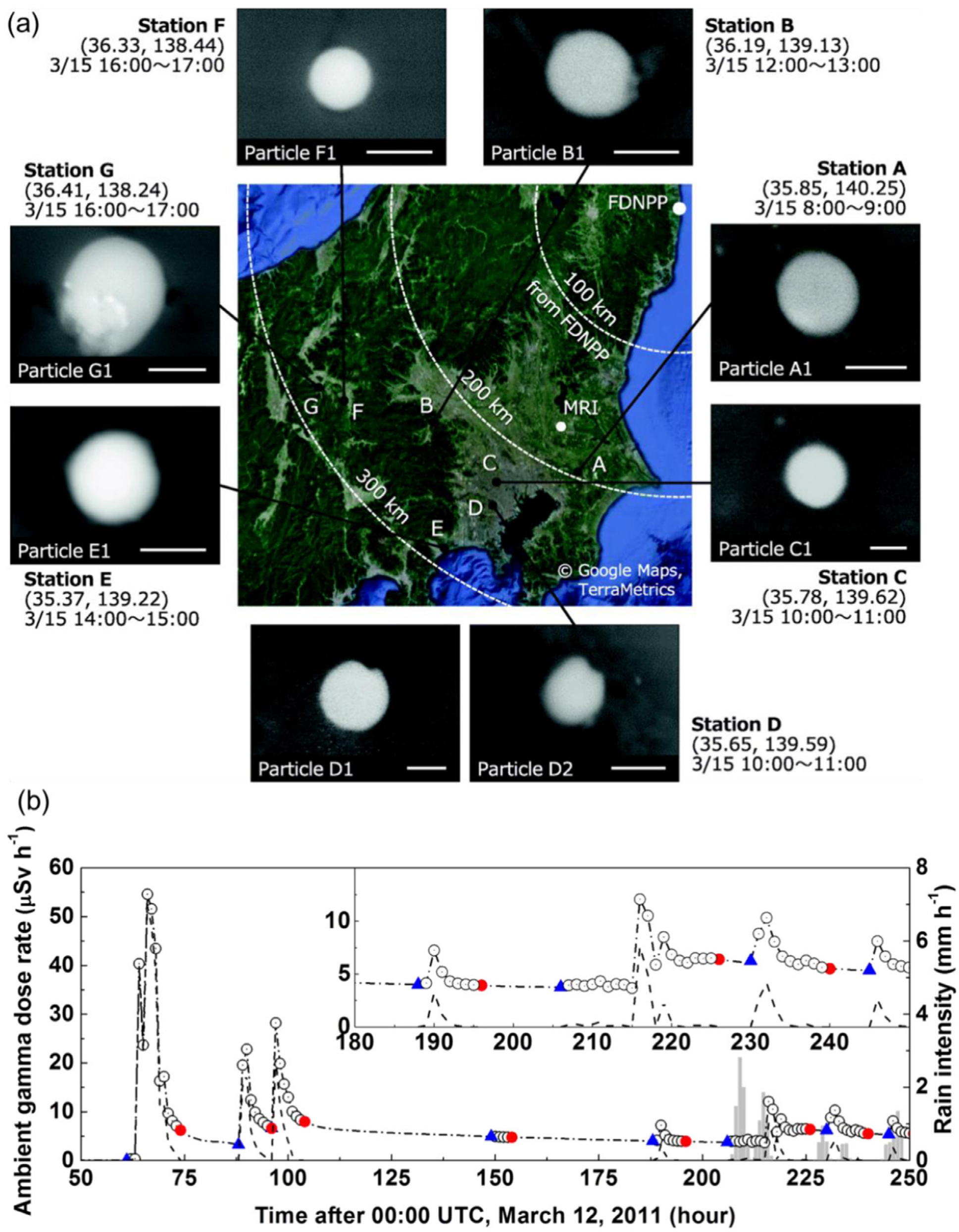


**Fig. 5.** Radioactive particles and ambient gamma dose rate during the Fukushima accident: (a) locations of monitoring stations and the isolated radioactive cesium-bearing microparticles over the greater Kanto Region resulting from the Fukushima nuclear accident; the scale bars indicate a length of 1 $\mu$m. Reprinted with permission from ref. [227] (open access article distributed under the terms of the Creative Commons CC BY license). (b) Identified radioactive plume and reconstructed cloud shine for the in-situ measurements of gamma dose rate obtained at Futatsunuma during the Fukushima accident, between 2:00 UTC, March 14 and 10:00 UTC, March 22, 2011. Reprinted with permission from ref. [228]. Copyright (2017) Elsevier B.V.

Noble gasses, for example, $^{133}$Xe, are first released into the ambient environment if the reactors are damaged. It was estimated that most of the $^{133}$Xe was released over short periods of time by the first venting of the reactors in the Fukushima accident, but other particulate radionuclides, such as $^{137}$Cs, were released over an extended period and only a certain part of the inventory was released [221]. Five representative radionuclides were utilized to approximate the source terms of nuclear accidents, including $^{131}$I, $^{137}$Cs, $^{132}$Te, and $^{140}$La for aerosols and $^{133}$Xe for noble gasses [21]. Iodine can exist in both gaseous and particulate phases, thereby strongly influencing the dry deposition and scavenging of radionuclides [222]. Based on the air samples collected at JAEA-Tokai, it was estimated that approximately 50% of the released $^{131}$I was particulate during the first several days of the release in the Fukushima accident [223]. The ratio of gaseous $CH_3I$ to $I_2$ was assumed to be approximately 0.6 for the accident.

During meltdowns, spherical radioactive cesium-rich microparticles (CsMPs) were released during the Fukushima Daiichi Nuclear Power Plant (FDNPP) accident, as shown in Fig. 5(a). The CsMPs with sizes of 2.0–3.4 $\mu$m were in the soil located approximately 4 km west of the FDNPP [224]. The size of the particles was approximately 2 $\mu$m and these were sampled 50 km from the FDNPP [225]. Radioactive cesium-bearing microparticles were also observed in the greater Kanto Region, more than 250 km from the FDNPP, and the particles were approximately 1.3 $\mu$m (0.9–1.8 $\mu$m) [225]. The median aerodynamic diameters of the $^{131}$I, $^{137}$Cs, and $^{134}$Cs particles ranged from 0.56 to 0.60 $\mu$m; these measurements were based on the particles collected with the Andersen-type classifier combined with a high volume air samplers in Nagano, approximately 300 km away from the nuclear power plant [226].

Airborne particles can be deposited on the ground via wet and dry deposition. Wet deposition is dependent on the wet scavenging rates, which are usually estimated based on the precipitation intensity in the following form [229]:

$$\Lambda^s = A \cdot p^B \tag{6}$$

where $A$ and $B$ are the fitted parameters and $p$ is the precipitation intensity. The dry deposition velocities depend on the particle size, density, atmospheric turbulence, and land-use type [230]. This can be estimated as follows [231]:

$$v^{dep} = \frac{u_{grav}}{1 - e^{(R_a+R_b)u_{grav}}} \quad (7)$$

where $u_{grav}$ is the gravitational settling velocity, $R_a$ is the aerodynamic resistance, and $R_b$ is the quasilaminar layer resistance. There are various types of parameterization models for wet and dry deposition [232], which can be referred to in a comprehensive review of the deposition models of dry deposition and radionuclide scavenging [222].

### 6.3. Radiation from cloud and ground deposition

The atmospheric transport model is usually coupled with a gamma radiation model to evaluate radiation exposure [233–236]. Monte Carlo codes are important tools for simulating interactions between neurons, protons, photons, and electrons with other particles and media. Radiation exposure can be evaluated using Monte Carlo codes, e.g., the Monte Carlo N-Particle Transport Code (MCNP) [237,238], FLUktuierende KAskade (FLUKA) [239], and GEometry and Tracking (GEANT4) [240]. The MCNP code has been utilized with Gaussian plume models to estimate the gamma radiation from the overhead plume [241] and the photon count rate from the plume of $^{41}$Ar emitted from a training reactor [242]. Monte Carlo codes are currently the most sophisticated and reliable method to evaluate the gamma dose, but the method requires detailed information on the properties of the medium and is time-consuming, making it impractical to couple with atmospheric transport models, especially during an emergency. As an alternative, a simplified methodology, for example, the point kernel method, is usually integrated online with atmospheric dispersion models.

In the RODOS system [106,107], a rapid gamma dose assessment model [233] based on the point kernel method was developed to combine with the Lagrangian puff dispersion models in RODOS, including the DIPCOT model [243] and RIMPUFF model [103,104], which has been adopted for off-site emergency management in Europe. In the proposed model [233], the three-dimensional radiation from each puff was analytically integrated, which simplified the problem to a one-dimensional calculation and significantly reduced the computational cost. The point kernel method has also been implemented in the FLEXPART model [244] for gamma dose calculation, and has been applied to the assessment of atmospheric dispersion and radiological impact during the Fukushima accident [245,246]. In the Japanese System for Prediction of Environmental Emergency Dose Information (SPEEDI) [247,248] and the Worldwide Version of SPEEDI [249], integration based on the point kernel method is applied for radioactive plume gamma dose computation. The point kernel method has been combined with the Lagrangian puff model to evaluate the ground radiation due to deposition, and the differences between the proposed method and the traditional "infinite plane" source assumption have been investigated under various meteorological conditions [234]. The Lagrangian CALPUFF model has been utilized to investigate external and internal radiation from hypothesized severe accidents at the Daya Bay Nuclear Power Plant (DBNPP) [250]. The internal radiation from the deposited radionuclides in the lung is also important for the evaluation of health effects; the internal radiation will be discussed in detail in [Section 8.2 (exposure assessment).

The calculation of gamma radiation is still relatively computationally expensive even with the simplified point kernel method because all radioactive pollutants in the computational domain will contribute to the radiation at each location, and spatial three-dimensional integration is required. An accelerated method using the fast Fourier transform has been proposed for the calculation of gamma radiation, and it has been implemented using the Lagrangian puff model RIMPUFF [251,252].

## 7. Combination of models and observations

The results of the models have high temporal and spatial resolutions, but it is difficult to directly utilize the models during an emergency because of the limited available information on the accidental release of hazardous substances. As shown in Fig. 6, models suffer from various types of uncertainties, including uncertainties in the emission and meteorological data. Emission information is an essential component of atmospheric transport models [18,20,253–255], but it is typically unavailable during an emergency, for example, in the Fukushima accident [256], making it the largest single source of uncertainties in the assessment [221,257]. Adding to the myriad challenges are the large uncertainties of meteorological fields, which cause cumulative errors in the model results. Environmental observations are also important for evaluating risk and supporting emergency responses [228]. Unlike these models, environmental observations are considered to be more reliable, but the spatial distributions of observation networks are usually sparse. Without the support of theoretical models, observations alone cannot predict future situations. Models and observations are mutually complementary [258]. By combining models and observations, the emission can be inversely estimated [21], and the uncertainties of the model results can be significantly alleviated [20,259].

### 7.1. Algebraic reverse method

The effective emergency response was significantly hindered by the lack of emission information during the Fukushima nuclear accident. Various methods have been proposed to reconstruct the source term of the Fukushima accident. The measurements of radionuclide concentrations were usually combined with the atmospheric dispersion models to estimate the emission. The United Nations Scientific Committee on the Effects of Atomic Radiation (UNSCEAR) defined two types of estimation methods, reverse modeling and inverse modeling [260], which are referred to as the algebraic reverse method and regularized regression inverse method, respectively, based on the mathematical methods involved.

In the algebraic reverse method, the dilution factor $D_i$ for time period $i$ is first calculated as the ratio between the concentration at a given location by the atmospheric transport model and the corresponding release rate, and a unit release rate is usually assumed [261]. Then, the actual emission rate $Q_i$ is estimated as the ratio between the measurement $M_i$ at the location and the dilution factor, as follows:

$$Q_i = M_i / D_i \quad (8)$$

Measurements at different locations were considered independently and utilized to estimate emissions within different periods. The reverse method was applied to obtain a preliminary estimation of the release of $^{131}$I and $^{137}$Cs into the atmosphere within a short time after the Fukushima accident using Lagrangian particle models and measurements (mainly dust sampling data for the activity concentrations) [261]. Multiple measurements may have been simultaneously available for the same period, and only the maximum value was adopted to avoid errors caused by the data obtained at the edges of the plume [261]. It was also claimed that the ground radiation due to deposition made the background radiation too high to use the gamma radiation measurements for the reverse estimations, which indicated the necessity to distinguish between ground and cloud radiation. Similar methods were used to update the emissions with more available measurements [249,256,262,263].

The algebraic reverse method is simple and easy to apply, which is advantageous for rapid estimations during emergencies. However, the uncertainties in the atmospheric dispersion model and the measurements are not considered in this approach, and the measurements are considered independently, which might compromise the quality of the estimations [260].

### 7.2. Regularized regression inverse method

More sophisticated mathematical methods are involved in the inverse method [260]. The source-receptor sensitivity (SRS) matrix, which relates the changes in emission to the response of measurements, was

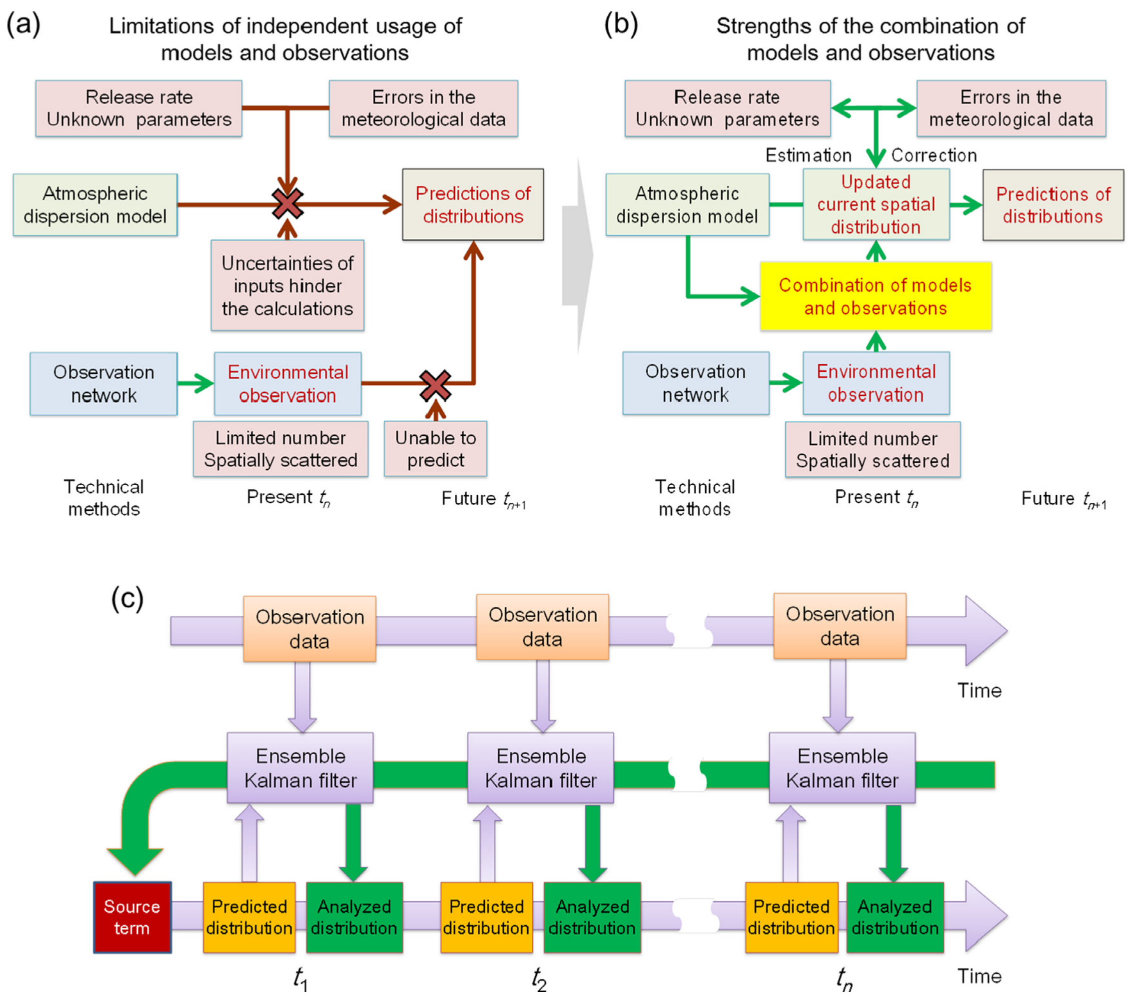


**Fig. 6.** Schematic graph for data assimilation: (a) the limitations of the independent usage of atmospheric transport models and observations in emergency situations; (b) the strengths of the combination of models and observations; (c) the working procedure of the ensemble Kalman filter sequential data assimilation methods.

first constructed using atmospheric dispersion models. The SRS matrix is based on the assumption of linearity. This is a reasonable assumption for chemical, biological, and radiological substances, as most of the substances are dominated by linear removal processes, for example, radioactive or biological decay, and wet and dry depositions, without nonlinear chemical transformations [59,228,264]. Then, the optimal estimation of the emissions is achieved by minimizing a cost function, which includes the differences between the model results and the measurements (likelihood), as well as the deviations from the *a priori* information about the emissions. Inverse problems are normally ill-conditioned, so additional constraints or regularizations are usually required [265]. The uncertainties of the model results, measurements, and *a priori* information are considered in the cost function. The regularized weighted least-squares problem cost function is usually expressed as follows [21]:

$$J\left(\dot{Q}\right) = \left(\boldsymbol{Y} - \boldsymbol{H}\cdot\dot{Q}\right)^{\mathrm{T}} \boldsymbol{R}^{-1}\left(\boldsymbol{Y} - \boldsymbol{H}\cdot\dot{Q}\right) + \left(\dot{Q} - \dot{Q}_0\right)^{\mathrm{T}} \boldsymbol{B}_0^{-1}\left(\dot{Q} - \dot{Q}_0\right) \quad (9)$$

where $\boldsymbol{Y}$ is the vector of the measurements, $\dot{\boldsymbol{Q}}$is the optimal estimation of emissions, $\boldsymbol{H}$ is the SRS matrix, $\dot{\boldsymbol{Q}}_0$is the *a priori* emission rate, $\boldsymbol{R}$is the covariance matrix of the combination of the model and measurement errors, and $\boldsymbol{B}_0$is the covariance matrix of the *a priori* estimation error.

The release of radioactive noble gas $^{133}$Xe and particulate $^{137}$Cs was estimated using the SRS matrix generated by the Lagrangian particle model FLEXPART and the measurements of activity concentrations as well as the deposition of $^{137}$Cs [221] based on the regularized least squares method. The preliminary guess of release rates based on fuel inventories and information about the events in the accident were utilized as *a priori* knowledge in inverse modeling [221]. Similar methods have been utilized to reconstruct source terms using long-range transport models and continental or global monitoring data, but there are great uncertainties in the meteorological data [221,266–270]. A Bayesian approach is often combined with inverse estimation to evaluate the *a posteriori* probability density of estimations [264,271].

For radioactive substances, detectors for gamma dose rates have been widely adopted for radiation monitoring. However, the gamma dose is the integration of the contributions from all radionuclides, so extra constraints must be introduced to reconstruct the releases of different types of radionuclides [228]. Methods were first proposed to estimate the release of a single type of radionuclide using GDR measurements [272–274]. The *a priori* information regarding the ratios of the released radionuclides was applied to regularize the inverse problem and reconstruct the multi-nuclide release for the Fukushima accident based on bulk GDR measurements [275–277]. The Kalman filter sequential multi-nuclide emission reconstruction method has also been proposed based on GDR measurements, which can evaluate the uncertainties in the estimations [21]. The updated Bayesian methodology was developed to determine the source term based on gamma dose rate measurements during an accidental release [278]. Machine learning methods, such as recurrent neural networks [279] and convolutional networks [280], have recently been utilized to estimate multi-nuclide emissions using GDR measurements.

### 7.3. Localization of release sources

In some cases, the location of the release source is also unknown [281–284]. Various source-localization methods have been developed to identify and localize accidental release sources. The Markov Chain Monte Carlo (MCMC) method combined with Bayesian methodology is the most widely used framework for retrieving source parameters [24]. Owing to the large number of potential release locations, the adjoint atmospheric dispersion model is typically utilized to calculate the SRS matrix for the MCMC methodology to reduce the computational cost [285,286]. The MCMC method has been applied to localize the sources of CBR substances in urban environments and has been validated using twin experiments [24], the classic Prairie Grass experiment [287], the Joint Urban 2003 field campaign [288], and 2007 FUSION Field Trial concentration data [289]. The MCMC method has also been applied to identify indoor sources of hazards [290–292] and reconstruct the source of a real accidental radioactive release at the end of May 1998 on a continental scale [293]. Modified methods have been proposed to localize the potential source of $^{131}$I emissions in Europe in the fall of 2011 [264] using the tuning-free method [271].

Heuristic algorithms are another important category of methods that are widely adopted to estimate source parameters, including locations and release rates. By combining field sensor data and atmospheric dispersion models, a mixed integer genetic algorithm (GA) was proposed to optimize the source location and strength of chemical or biological releases, as well as key meteorological parameters such as atmospheric stability, wind speed, and precipitation [294–296]. The influence of cost functions on the performance of GA inverse modeling has been investigated [58]. Bioinspired particle swarm optimization (PSO) was combined with models to localize release sources [297], and the PSO algorithm was directly embedded in unmanned aerial vehicles to search for sources in complex urban environments [298]. The simulated annealing (SA) algorithm was utilized to localize a gas source and estimate its strength [299]. The SA method can prevent convergence to the local minima [300]. Recently, an integrated framework, Multi-Agents for sensing, monitoring, estimating, and determining (MAsmed), has been proposed to monitor and reconstruct source parameters in emergency responses by leveraging multiple sensing methods, including wireless sensor networks (WSNs) and mobile crowdsensing (MCS) [17].

### 7.4. Data assimilation

Data assimilation (DA) is similar to inverse modeling and combines the model and observations. Inverse modeling can be considered as a type of data assimilation. However, in contrast to inverse modeling, DA methods focus on sequentially correcting the biases in the predicted state of the system, for example, the concentration distribution, to avoid the accumulation of errors caused by uncertainties in the model input, including emissions and meteorological data [259]. As a result, the DA normally simultaneously corrects the biases in the atmospheric transport model and reconstructs the emissions [19,20,301].

Variational methods [302–306] and particle filter data assimilation methods [307,308] have been combined with plume or puff models to improve model predictions. The variational methods are similar to the regularized regression inverse method, as shown in Eq. (9); however, the optimized state vector is the concentration of pollutants instead of emissions. The Kalman filter [309] sequential data assimilation method has been used to improve the predictions of the Gaussian plume model under quasi-steady states [310–312].

Release estimation can benefit from the simultaneous correction of transport biases. Sequential methods, such as the Kalman filter method, have been applied to sequentially update the emissions and plume height and to simultaneously correct the biases caused by meteorological data, such as wind speed and wind direction [313,314]. Modified and augmented ensemble Kalman filter (EnKF) methods were proposed to estimate the emissions by simultaneously considering the uncertainties in the emissions and meteorological data [18–20,100], as shown in Fig. 7. Modified EnKF methods have also been applied to reconstruct the concentration field and estimate the release of natural gas in underground tunnels [315,316]. A bilinear inverse model [317] was proposed to estimate the release by simultaneously correcting the bias in the atmospheric transport model, that is, the SRS matrix. An ensemble-based method has been proposed to evaluate the spatial correlation and update the predictions using observations, which improves the reconstruction of the source term estimation [301,318]. Machine learning methods, for example, physics-guided deep learning, have been recently utilized to combine observations and physical models [319].

## 8. Risk assessment

The risk assessments of airborne chemical, biological, and radiological substances have many common features. We introduce frameworks for these hazardous substances, for example, probabilistic or quantitative risk assessment, and the key components in risk assessment, including exposure and dose-response relations.

### 8.1. Probabilistic/quantitative risk assessment

This risk-informed methodology is widely adopted in the nuclear industry and can be dated back to the 1975 Reactor Safety Study (WASH 1400) [320]. The United States Nuclear Regulatory Commission (U.S. NRC) proposes utilizing probabilistic risk assessment (PRA) for risk-informed regulation. As shown in Fig. 8(a), PRA has three levels [321]. The conditional probabilities are determined at each level and adopted as the input for the next level. The final risk is a combination of the consequence and associated probabilities. Levels 1 and 2 are used to analyze the accident progress inside the plant. The atmospheric transport of radionuclides is utilized in Level 3 PRA, which is often called consequence analysis.

A similar framework for risk assessment in the chemical industry is usually called quantitative risk analysis (QRA) [322–325]. Quantitative Microbial Risk Assessment (QMRA) is an effective method for estimating the risk of airborne microorganisms. QMRA has been widely adopted for the risk assessment of bioaerosols originating from wastewater treatment plants [326,327] and waste management facilities [328,329]. The QMRA method has been utilized to evaluate the infection risk of MERS-CoV in hospitals [5] and SARS-CoV-2 in the Wuhan seafood market [22] through aerosol transmission.

As shown in Fig. 4 and atmospheric transport is an important component of the PRA, QRA, and QMRA frameworks. The spatial and temporal distributions of the released hazardous substances should first be evaluated using models or measurements. Comprehensive and sophisticated PRA methods are important for understanding the risks associated with airborne chemical, biological, and radiological hazardous substances, and they are useful tools for risk preparedness, prevention, and evidence-based policymaking during the preparation phase, as shown in Fig. 8(b). Historical databases play a key role in understanding risk during the preparation phase.

Atmospheric transport calculations are mainly used to evaluate $P(E|R)$ in Level 3, as shown in Fig. 8(a), including exposure assessment and dose-response relations, which relate the exposure dose to a certain effect (endpoint). Risk assessment is also important for an effective emergency response and management when accidents occur. $P(E|R)$ is the only relevant factor because $P(R)$ becomes 1. As introduced in Section 7, observations and data assimilation become more critical during an emergency response when the uncertainties in the information of the accident should be minimized.

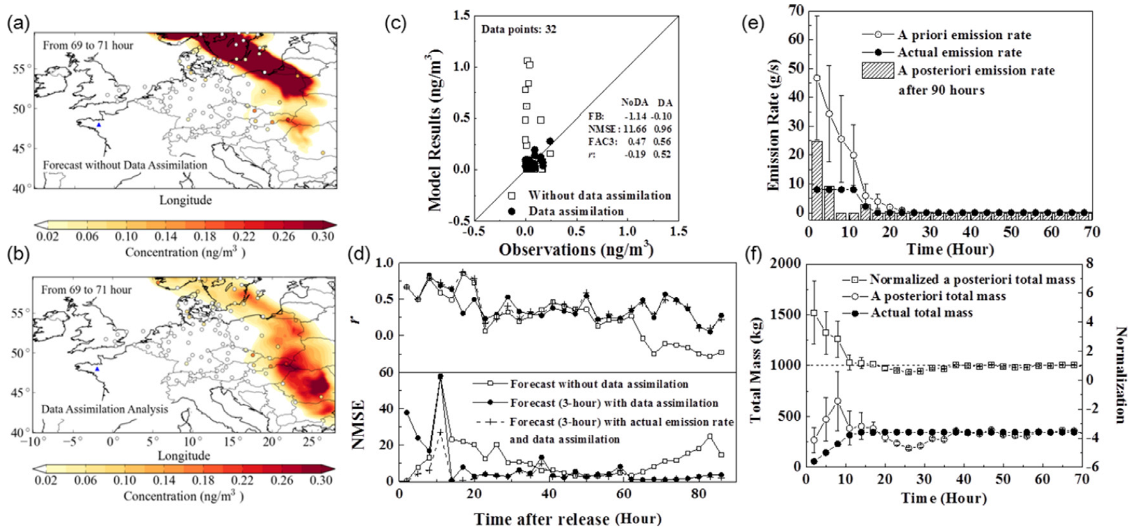


**Fig. 7.** Demonstration and validation of the performance of the ensemble Kalman filter method for the reconstruction of the source term and improvement of model accuracy with the European Tracer EXperiment (ETEX) [20]: (a) forecast with the actual emissions but without assimilation for the spatial distribution of tracers between hours 69 and 71 after release; (b) the same with (a) but with reconstructed releases and data assimilation; (c) scatter plots of model results versus observed surface concentrations of tracers; (d) correlation coefficient (top) and normalized mean square error (bottom) between the measurements and model results for surface concentrations of tracers with and without assimilation; (e) the actual (solid circles), the *a priori* (open circles), and the *a posteriori* (shaded bars) emission rates; (f) the actual total mass of the release tracer, the *a posteriori* reconstructed total mass of tracers. Figures (a) to (f) are reprinted with permission from Ref. [20]. Copyright (2015) Elsevier B.V.

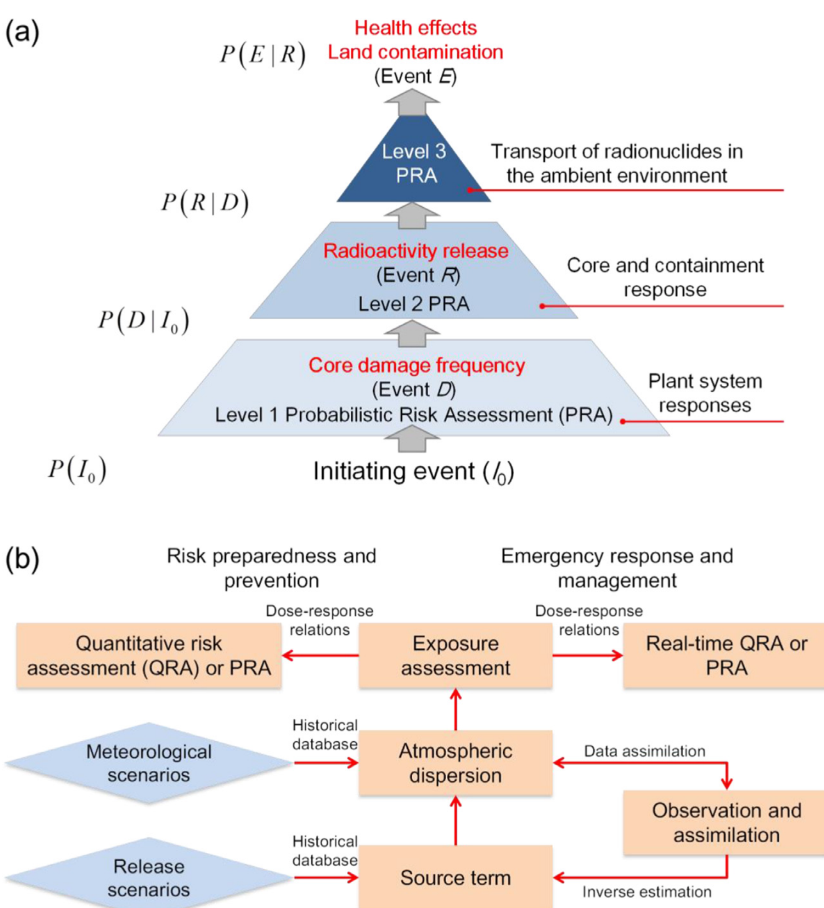


**Fig. 8.** Schematic graph for the risk assessment: (a) three levels of the PRA in the nuclear industry; (b) risk assessment during the preparation phase and the real-time dynamic risk assessment during the emergency situation.

### 8.2. Exposure assessment

Inhalation and lung deposition are important for assessing the exposure to airborne hazardous substances. The tidal volume of respiration is dependent on activities such as resting, light activity, and heavy activity [330], which influence the inhalation of hazardous substances. To accurately evaluate the exposure, lung deposition models are used to estimate the deposition of size-specific particles in various parts of the respiratory tract, including the anterior nasal, naso-oropharynx/larynx, bronchi, bronchioles, and alveolar interstitial [331,332]. Various lung deposition models have been developed, such as the multiple-path particle dosimetry model (MPPD v 3.04) [333] and the model adopted by the International Commission on Radiological Protection (ICRP) [334]. Deposition models have also been extended to pathogenic bioaerosols [335]. These models can be utilized simultaneously to estimate the associated uncertainties.

The effects of personal protective equipment (PPE) and air-cleaning systems, such as masks and electronic air cleaners, should be considered in the assessment [336–341]. Their filtration efficiency should be appropriately evaluated for exposure assessment [342–345]. High-fidelity models should be developed to understand the deposition and filtration of particles considering the physical shape, agglomeration, and aerodynamic properties of airborne particles [346–353]. Filter-based antimicrobial technologies have been developed to inhibit the airborne transport of bioaerosols and related exposure [354,355]. The degradation of the performance of PPE and air-cleaning systems is also an important factor for exposure assessment [356–361].

The system of radiation protection worldwide is based on the ICRP recommendations. The current recommendations are in ICRP Publication 103 (ICRP-103) [362], which was issued in 2007. Three categories of exposure situations were defined in ICRP-103: planned, emergency, and existing exposure situations. The measurements of ambient radiation are the physical quantities, e.g., absorbed dose (the energy deposited in matters by ionizing radiation per unit mass), which have to be converted into “equivalent dose” by taking into account the biological effectiveness of different types of radiation, e.g., gamma rays, beta particles, alpha particles, and neutrons. The “effective dose” for different organs, tissues, and the entire body is further estimated based on the equivalent dose and sensitivity of different body parts to radiation [362]. The effective dose is used for external radiation, and its counterpart committed dose is adopted for internal radiation, for example, the radiation from the deposited radionuclides in the lung, which can last for a certain time period depending on the physical decay of the radionuclides and the biological retention within the body [363]. The effective and committed doses have the same risk-dose relationship.

It should be noted that vulnerabilities to fires and explosions of vapor clouds should also be considered in the risk assessment of unintended releases of hazardous chemicals [121,364,365]. The intensities of combustion and explosion must be evaluated first, which is beyond the scope of this study. More information on exposure to fires and explosions can be found in other reviews [121].

### 8.3. Dose-response relationships

For the quantitative risk analysis of the exposure to toxic chemicals, the relationship between the exposure dose and a certain effect (endpoint) is required, which is referred to as a “probit function” [366]. Such relationships are usually developed based on data from animal experiments. Lethality is chosen as the endpoint for the safety assessment of the implementation of the Seveso III directive in the Netherlands [366].

The dose-response relationships for radiation exposure are largely determined based on the Life Span Study (LSS), a long-term cohort epidemiological study on atomic bomb survivors in Hiroshima and Nagasaki [367–369], which had high doses and high dose rates. ICRP classifies radiation effects into stochastic effects and tissue reactions [362]. The stochastic effects include cancer and heritable effects. The probability of stochastic effects is a function of the effective dose without a threshold. A linear no-threshold relation (LNT model) was adopted by the radiation protection community for the stochastic effects [370]. It should be noted that there might be a “dose-rate” effect, which suggests that chronic exposures with low dose rates will have less of an effect than acute exposures with high dose rates, despite using the same dose [371]. The risk values are usually determined in high exposure situations, which might overestimate the risk for low-dose and low-dose-rate conditions owing to the dose-rate effect. The ICRP adopted a dose and dose-rate effectiveness factor (DDREF) to adjust the risk; however, there are substantial debates on the use of DDREF [371,372]. Tissue reactions are defined as the collective injury of the proportions of cells in affected tissues, such as cataracts and non-malignant skin damage. The induction of tissue reactions is based on a threshold dose because radiation damage to a critical proportion of cells must be sustained before injury can be clinically detected [362]. Above the threshold, the severity of injury increases with the dose. The dose thresholds are defined as the doses resulting in an effect in approximately 1% of exposed individuals [362].

The dose-response relationship is also an important component of QMRA to link the exposure level and infection risk. The dose-response relationship depicts the possibility of infection or other outcomes of disease after exposure to a certain number of pathogens, such as viruses and bacteria. Experimental studies based on animal models (e.g., mice, ferrets, and monkeys) are usually conducted to develop a dose-response relationship because it is normally unethical to challenge human beings with harmful pathogens. Toxicology studies have also been conducted *in vitro* to investigate the toxicity and cellular response to hazardous substances [373–377], and have been widely adopted to evaluate the environmental, health, and safety (EHS) issues of emerging materials [378].

During the COVID-19 pandemic, ferrets and hamsters [379–381] have been used to investigate the dose of SARS-CoV-2 required to induce severe clinical infections. In addition to animal studies, the dose-response relationship in humans can be deduced based on epidemiological investigations, systematic reviews, and meta-analyses. Using the results from the meta-analysis for the transmission risk of SARS-CoV-2 by the WHO COVID-19 Systematic Urgent Review Group Effort (SURGE) [382], a simple framework was developed to integrate the *a priori* dose-response relationship for SARS-CoV based on mouse experiments [383] and the reconstructed exposure dose to estimate the dose-response relationship for humans [384].

### 8.4. Uncertainties of risk assessment

Probabilistic and quantitative risk assessments can be conducted based on the exposure results and dose–response relationships. Monte Carlo simulations can be performed to consider the uncertainties in the risk assessment caused by uncertainties in key components, for example, emissions, atmospheric transport, decay, deposition, and dose-response parameters [22,385]. In QMRA studies, Monte Carlo methods have also been applied to evaluate the infection risks in four different typical scenarios, i.e., hospital rooms, gyms, public indoor environments (e.g., restaurants and banks), and conference rooms or auditoriums [330].

The susceptible exposed infectious removed (SEIR) model has been widely utilized in the assessment of the community risk of aerosols [386]. Special attention should be paid to risk assessment in crowded situations [387–390]. The SEIR models have been adopted to evaluate the effectiveness of different intervention measures [391,392]. The dose-response relations and QMRA methods could be applied to better quantify the infection probability in SEIR and improve its performance for community risk assessment.

It has been suggested that the uncertainties in health effect models are larger than those in atmospheric dispersion models, and they are the dominant factors for the risk assessment of exposure to toxic chemicals [123]. As a result, the current best practices are to evaluate the “enve-

**Table 3**
Important characteristics, issues, and recommended methods for the airborne CBR pollutants.

| | | Chemical hazards | Biological hazards | Radiological hazards |
|---|---|---|---|---|
| Risk assessment | | Lower flammability limit<br>Dose-response relationship | Dose-response relationship | Dose-response relationship |
| Exposure assessment | | Concentration distribution<br>Population distribution | Concentration distribution<br>Lung deposition<br>Population distribution | Concentration distribution<br>Lung deposition<br>Internal and external exposure<br>Population distribution |
| Unique problems | | Buoyancy (density, temperature)<br>Gravity driven flow<br>(Rapid) phase transition | Particle size distribution<br>Biological decay<br>Wet and dry deposition | Particle size distribution<br>Multi-nuclides<br>Gamma radiation<br>Wet and dry deposition |
| Recommended methods | | CFD<br>Lagrangian particle/puff models (emergency use) | Lagrangian particle/puff models | Chemical transport models<br>CFD and Lagrangian particle/puff models (emergency use) for the local scale |
| Importance of online coupling | | High | Low | Medium |
| Importance of relevant scale | Street | High | High | High |
| | Neighborhood | High | High | High |
| | City | Medium | High | High |
| | Regional scale | Low | Medium | High |
| | Continental/global | Low | Low | High |
| Common problems | | Meteorological data, atmospheric boundary layer, turbulent diffusion (atmospheric stability), surface roughness | | |
| Emergency response | | Near real-time quantification of emissions during emergencies | | |

lope" of the plausible concentrations, which could be further utilized to evaluate the magnitude of the potential risk and impact [393].

## 9. Summary and implications

The risk assessment of airborne CBR pollutants is a highly interdisciplinary problem that involves information and knowledge on atmospheric boundary layers, atmospheric transport of pollutants, source terms, physical and chemical properties of hazardous substances, aerosol dynamics, sampling and measurements, numerical simulation, data processing, epidemiology, and toxicology. The atmospheric transport of CBR pollutants is a critical component of risk assessment. In this study, we reviewed the key relevant concepts, methods, and models of the atmospheric transport of CBR pollutants. The important characteristics, issues, and recommended methods for airborne CBR pollutants are summarized in Table 3.

(1) The impacts of released toxic and flammable chemicals are mainly on the street and neighborhood scales. The released denser- and lighter-than-air substances can influence the ambient flow; therefore, CFD methods with online coupling between the releases and ambient air provide the most complete description of the physical processes. The parameterized Lagrangian models can be used for emergency response applications.
(2) Bioaerosols are able to proliferate, so the scale from street to city is of high importance for bioaerosols. The amount of bioaerosols released is typically low. The influence of released bioaerosols on the ambient flow is limited; therefore, it can be treated as a neutrally buoyant flow, and offline coupling methods, for example, Lagrangian particle or puff models, are the most suitable models. Additional models are required for biological decay and wet and dry depositions.
(3) Owing to significant public concern, the atmospheric transport of radiological substances at the regional ($10^2$–$10^3$ km), continental, and global scales could still be important, for example, atmospheric transport during the Fukushima accident. Chemical transport models are suitable and computationally efficient for large-scale dispersion, but CFD methods or Lagrangian particle/puff models may be required for local-scale investigations. Special models are required for radiation calculations and deposition.


**Fig. 9.** Source, Assimilation, Fundamentals, Exposure, and Risk (SAFER), an integrated framework for the risk assessment of airborne chemical, biological, and radiological hazardous pollutants.

In summary, we propose a framework, SAFER, to integrate the key components in the risk assessment of airborne CBR hazardous pollutants, as shown in Fig. 9.

(1) Source (S): The physical and chemical properties of hazardous substances (e.g., density, particle size distribution, and phase) and relevant physical processes (e.g., phase transition, biological decay, and radiation) should be considered in the assessment.
(2) Assimilation (A): In emergency situations, the near real-time quantification of emissions and reduction of the accumulated errors owing to meteorological data are required; therefore, data assimilation and inverse modeling become critical by combining models and observations.
(3) Fundamentals (F): Theoretical models for the atmospheric boundary layer, atmospheric dispersion of different CBR substances, and

submodules for relevant processes should be developed, and experiments should be conducted to evaluate the models.

(4) Exposure (E): Spatial and temporal distributions of CBR hazardous pollutants must be calculated, and lung deposition, including internal/external radiation exposure, should be evaluated and combined with the demographic population for further analysis.

(5) Risk (R): Dose-response relationships are needed to link the exposure and the effects, and lower flammability limits are required for flammable chemicals. There are still significant uncertainties in the dose-response relationships for CBR pollutants. It has been suggested that uncertainties in health effect models are the dominant factors in risk assessment.

## Declaration of Competing Interest

The authors declare that they have no known competing fifinancial interests or personal relationships that could have appeared to inflfluence the work reported in this paper.

## Acknowledgments

This study was partially supported by the Clean Air China Project sponsored by the Swiss Agency for Development and Cooperation.

## Supplementary materials

Supplementary material associated with this article can be found, in the online version, at doi:10.1016/j.jnlssr.2022.09.001.

## References

[1] Q.C. Ma, L.B. Zhang, CFD simulation study on gas dispersion for risk assessment: a case study of sour gas well blowout, Saf. Sci. 49 (2011) 1289–1295.
[2] I. Yet-Pole, S.G. Gu, J.P. Gupta, A preliminary explore to the forced ventilation on the toxic gas release/dispersion and the hazard mitigation within a petrochemical plant, J. Loss Prev. Process Ind. 69 (2021) 1–11.
[3] The European Commission, 2020. Major Accident Hazards: the Seveso Directive –Technological Disaster Risk Reduction. https://ec.europa.eu/environment/seveso/. Accessed 21 September 2022.
[4] I.T.S. Yu, Y. Li, T.W. Wong, W. Tam, A.T. Chan, J.H.W. Lee, D.Y.C. Leung, T. Ho, Evidence of airborne transmission of the severe acute respiratory syndrome virus, N. Engl. J. Med. 350 (2004) 1731–1739.
[5] U. Adhikari, A. Chabrelie, M. Weir, K. Boehnke, E. McKenzie, L. Ikner, M. Wang, Q. Wang, K. Young, C.N. Haas, J. Rose, J. Mitchell, A case study evaluating the risk of infection from middle eastern respiratory syndrome coronavirus (MERS-CoV) in a hospital setting through bioaerosols, Risk Anal. 39 (2019) 2608–2624.
[6] N. Naffakh, S. van der Werf, April 2009: an outbreak of swine-origin influenza A(H1N1) virus with evidence for human-to-human transmission, Microbes Infect. 11 (2009) 725–728.
[7] Z. Liu, M. Wang, Y. Tian, Z. Li, L. Gao, Z. Li, A systematic analysis of and recommendations for public health events involving brucellosis from 2006 to 2019 in China, Ann. Med. 54 (2022) 1859–1866.
[8] C.C. Wang, K.A. Prather, J. Sznitman, J.L. Jimenez, S.S. Lakdawala, Z. Tufekci, L.C. Marr, Airborne transmission of respiratory viruses, Science 373 (2021) 1–12.
[9] P. Burgherr, S. Hirschberg, Comparative risk assessment of severe accidents in the energy sector, Energy Policy 74 (2014) S45–S56.
[10] NEA, in: Chernobyl: Assessment of Radiological and Health Impacts –2002 Update of Chernobyl: Ten Years On in, Nuclear Energy Agency (NEA), Paris, 2002, p. 155.
[11] , The implementation of short-term countermeasures after a nuclear accident (stable iodine, sheltering and evacuation), in: Proceedings of the An NEA Workshop, Stockholm, Sweden, 1994.
[12] Á. Leelőssy, F. Molnár, F. Izsák, Á. Havasi, I. Lagzi, R. Mészáros, Dispersion modeling of air pollutants in the atmosphere: a review, Cent. Eur. J. Geosci. 6 (2014) 257–278.
[13] S. Hanna, J. Chang, Acceptance criteria for urban dispersion model evaluation, Meteorol. Atmos. Phys. 116 (2012) 133–146.
[14] J.P.G. Van Leuken, A.N. Swart, A.H. Havelaar, A. Van Pul, W. Van der Hoek, D. Heederik, Atmospheric dispersion modelling of bioaerosols that are pathogenic to humans and livestock – a review to inform risk assessment studies, Microb. Risk Anal. 1 (2016) 19–39.
[15] Y. Benamrane, J.L. Wybo, P. Armand, Chernobyl and Fukushima nuclear accidents: what has changed in the use of atmospheric dispersion modeling? J. Environ. Radioact. 126 (2013) 239–252.
[16] A. Leelossy, I. Lagzi, A. Kovacs, R. Meszaros, A review of numerical models to predict the atmospheric dispersion of radionuclides, J. Environ. Radioact. 182 (2018) 20–33.
[17] Z. Zhu, B. Chen, Y. Zhao, Y. Ji, Multi-sensing paradigm based urban air quality monitoring and hazardous gas source analyzing: a review, J. Saf. Sci. Resil. 2 (2021) 131–145.
[18] X.L. Zhang, G.F. Su, H.Y. Yuan, J.G. Chen, Q.Y. Huang, Modified ensemble Kalman filter for nuclear accident atmospheric dispersion: prediction improved and source estimated, J. Hazard. Mater. 280 (2014) 143–155.
[19] X.L. Zhang, G.F. Su, J.G. Chen, W. Raskob, H.Y. Yuan, Q.Y. Huang, Iterative ensemble Kalman filter for atmospheric dispersion in nuclear accidents: an application to Kincaid tracer experiment, J. Hazard. Mater. 297 (2015) 329–339.
[20] X.L. Zhang, Q.B. Li, G.F. Su, M.Q. Yuan, Ensemble-based simultaneous emission estimates and improved forecast of radioactive pollution from nuclear power plant accidents: application to ETEX tracer experiment, J. Environ. Radioact. 142 (2015) 78–86.
[21] X. Zhang, W. Raskob, C. Landman, D. Trybushnyi, Y. Li, Sequential multi-nuclide emission rate estimation method based on gamma dose rate measurement for nuclear emergency management, J. Hazard. Mater. 325 (2017) 288–300.
[22] X. Zhang, Z. Ji, Y. Yue, H. Liu, J. Wang, Infection risk assessment of COVID-19 through aerosol transmission: a case study of South China seafood market, Environ. Sci. Technol. 55 (2021) 4123–4133.
[23] X. Ji, W. Weng, X. Shu, S. Shen, W. Fan, Research on the risk analysis of urban accidents, China Saf. Sci. J. 11 (2006) 119–123.
[24] S. Guo, R. Yang, H. Zhang, W. Weng, W. Fan, Source identification for unsteady atmospheric dispersion of hazardous materials using Markov Chain Monte Carlo method, Int. J. Heat Mass Transf. 52 (2009) 3955–3962.
[25] R.B. Stull, An Introduction to Boundary Layer Meteorology, Springer, Netherlands, 1988.
[26] A. Christen, G. Mills, J.A. Voogt, T.R. Oke, Urban heat Island, in: Urban Climates, Cambridge University Press, Cambridge, 2017, pp. 197–237.
[27] M.R. Raupach, R.A. Antonia, S. Rajagopalan, Rough-wall turbulent boundary layers, Appl. Mech. Rev. 44 (1991) 1–25.
[28] M.W. Rotach, Simulation of urban-scale dispersion using a lagrangian stochastic dispersion model, Bound. Layer Meteorol. 99 (2001) 379–410.
[29] M.W. Rotach, On the influence of the urban roughness sublayer on turbulence and dispersion, Atmos. Environ. 33 (1999) 4001–4008.
[30] M. Piringer, C.S.B. Grimmond, S.M. Joffre, P. Mestayer, D.R. Middleton, M.W. Rotach, A. Baklanov, K. De Ridder, J. Ferreira, E. Guilloteau, A. Karppinen, A. Martilli, V. Masson, M. Tombrou, Investigating the surface energy balance in urban areas – recent advances and future needs, water, Air Soil Pollut. Focus 2 (2002) 1–16.
[31] J.F. Barlow, Progress in observing and modelling the urban boundary layer, Urban Clim. 10 (2014) 216–240.
[32] C.B. Senel, O. Temel, S. Porchetta, D. Muñoz-Esparza, J. van Beeck, A new planetary boundary layer scheme based on les: application to the XPIA campaign, J. Adv. Model. Earth Syst. 11 (2019) 2655–2679.
[33] D. Li, Turbulent Prandtl number in the atmospheric boundary layer - where are we now? Atmos. Res. 216 (2019) 86–105.
[34] A.J. Dyer, A review of flux-profile relationships, Bound. Layer Meteorol. 7 (1974) 363–372.
[35] A. Monin, A.M. Obukhov, Basic laws of turbulent mixing in the surface layer of the atmosphere, Contrib. Geophys. Inst. Acad. Sci. USSR 24 (1954) 163–187.
[36] R. Ohba, N. Ukeguchi, S. Kakishima, B. Lamb, Wind tunnel experiment of gas diffusion in stably stratified flow over a complex terrain, Atmos. Environ. Part A Gen. Top. 24 (1990) 1987–2001.
[37] R. Ohba, T. Hara, S. Nakamura, Y. Ohya, T. Uchida, Gas diffusion over an isolated hill under neutral, stable and unstable conditions, Atmos. Environ. 36 (2002) 5697–5707.
[38] R. Ohba, A. Kouchi, T. Hara, V. Vieillard, D. Nedelka, Validation of heavy and light gas dispersion models for the safety analysis of LNG tank, J. Loss Prev. Process Ind. 17 (2004) 325–337.
[39] I. Kanda, Y. Yamao, Passive scalar diffusion in and above urban-like roughness under weakly stable and unstable thermal stratification conditions, J. Wind Eng. Ind. Aerodyn. 148 (2016) 18–33.
[40] J. Cai, J. Chen, H. Cheng, S. Zi, J. Xiao, F. Xia, J. Zhao, The effects of thermal stratification on airborne transport within the urban roughness sublayer, Int. J. Heat Mass Transf. 184 (2022) 122289.
[41] S. Masoumi-Verki, P. Gholamalipour, F. Haghighat, U. Eicker, Embedded LES of thermal stratification effects on the airflow and concentration fields around an isolated high-rise building: spectral and POD analyses, Build. Environ. 206 (2021) 108388.
[42] Z. Shen, G. Cui, Z. Zhang, Turbulent dispersion of pollutants in urban-type canopies under stable stratification conditions, Atmos. Environ. 156 (2017) 1–14.
[43] D. Guo, P. Zhao, R. Wang, R. Yao, J. Hu, Numerical simulation studies of the effect of atmospheric stratification on the dispersion of LNG vapor released from the top of a storage tank, J. Loss Prev. Process Ind. 61 (2019) 275–286.
[44] A. Berchet, K. Zink, C. Muller, D. Oettl, J. Brunner, L. Emmenegger, D. Brunner, A cost-effective method for simulating city-wide air flow and pollutant dispersion at building resolving scale, Atmos. Environ. 158 (2017) 181–196.
[45] A. Berchet, K. Zink, D. Oettl, J. Brunner, L. Emmenegger, D. Brunner, Evaluation of high-resolution GRAMM–GRAL (v15.12/v14.8) NOx simulations over the city of Zürich, Switzerland, Geosci. Model Dev. 10 (2017) 3441–3459.
[46] M.A. Nelson, M.J. Brown, S.A. Halverson, P. Bieringer, A. Annunzio, G. Bieberbach, Assimilation of WRF mesoscale meteorological simulations into the QUIC atmospheric dispersion modeling system: wind fields, turbulence, and contaminant dispersion, Chemical and Biological Warfare Weaponization & Consequence Assessment Modeling Symposium, 2014.

[47] A.A. Gowardhan, E.R. Pardyjak, I. Senocak, M.J. Brown, A CFD-based wind solver for an urban fast response transport and dispersion model, Environ. Fluid Mech. 11 (2011) 439–464.
[48] M. Brown, QUIC: a fast, high-resolution 3D building-aware urban transport and dispersion modeling system, AWMA Environ. Manag. 64 (2014) 28–31.
[49] M.J. Churchfield, S. Lee, P.J. Moriarty, Adding complex terrain and stable atmospheric condition capability to the OpenFOAM-based flow solver of the simulator for on/offshore wind farm applications (SOWFA), in: Proceedings of the 1st Symposium on OpenFOAM in Wind Energy, Oldenburg, Germany, 2013.
[50] P. Fleming, J. Annoni, J.J. Shah, L.P. Wang, S. Ananthan, Z.J. Zhang, K. Hutchings, P. Wang, W.G. Chen, L. Chen, Field test of wake steering at an offshore wind farm, Wind Energy Sci. 2 (2017) 229–239.
[51] H. Hersbach, B. Bell, P. Berrisford, S. Hirahara, A. Horányi, J. Muñoz-Sabater, J. Nicolas, C. Peubey, R. Radu, D. Schepers, The ERA5 global reanalysis, Q. J. R. Meteorolog. Soc. 146 (2020) 1999–2049.
[52] E. Kalnay, M. Kanamitsu, R. Kistler, W. Collins, D. Deaven, L. Gandin, M. Iredell, S. Saha, G. White, J. Woollen, Y. Zhu, A. Leetmaa, R. Reynolds, M. Chelliah, W. Ebisuzaki, W. Higgins, J. Janowiak, K.C. Mo, C. Ropelewski, J. Wang, R. Jenne, D. Joseph, The NCEP/NCAR 40-year reanalysis project, Bull. Am. Meteorol. Soc. 77 (1996) 437–471.
[53] S. Kobayashi, Y. Ota, Y. Harada, A. Ebita, M. Moriya, H. Onoda, K. Onogi, H. Kamahori, C. Kobayashi, H. Endo, K. Miyaoka, K. Takahashi, The JRA-55 reanalysis: general specifications and basic characteristics, J. Meteorol. Soc. Jpn. Ser. 93 (2015) 5–48 II.
[54] X. Liang, L. Jiang, Y. Pan, C. Shi, Z. Liu, Z. Zhou, A 10-yr global land surface reanalysis interim dataset (CRA-Interim/Land): implementation and preliminary evaluation, J. Meteorol. Res. 34 (2020) 101–116.
[55] W.C. Skamarock, J.B. Klemp, J. Dudhia, D.O. Gill, Z. Liu, J. Berner, W. Wang, J.G. Powers, M.G. Duda, D.M. Barker, in: A Description of the Advanced Research WRF Model Version 4, National Center for Atmospheric Research, Boulder, CO, USA, 2019, p. 145. 145.
[56] Peckham, E. Steven, WRF/Chem version 3.3 user's guide, in: NOAA technical memorandum OAR GSD ; 40, Earth System Research Laboratory, Global Systems Division, Boulder, Colorado, USA, 2012. https://repository.library.noaa.gov/view/noaa/11119. Accessed 21 September 2022.
[57] J.S. Wu, J.T. Cai, S.Q. Yuan, X.L. Zhang, G. Reniers, CFD and EnKF coupling estimation of LNG leakage and dispersion, Saf. Sci. 139 (2021) 1–13.
[58] Y. Wang, H. Huang, L. Huang, X. Zhang, Source term estimation of hazardous material releases using hybrid genetic algorithm with composite cost functions, Eng. Appl. Artif. Intell. 75 (2018) 102–113.
[59] M. Gao, X. Zhang, Y. Yue, T. Qiu, J. Wang, X. Wang, Air path of antimicrobial resistance related genes from layer farms: emission inventory, atmospheric transport, and human exposure, J. Hazard. Mater. 430 (2022) 128417.
[60] H. Jasak, A. Jemcov, Z. Tukovic, OpenFOAM: a C++ library for complex physics simulations, in: International Workshop On Coupled Methods in Numerical Dynamics, IUC Dubrovnik Croatia, 2007, pp. 1–20.
[61] O.R. Hansen, F. Gavelli, M. Ichard, S.G. Davis, Validation of FLACS against experimental data sets from the model evaluation database for LNG vapor dispersion, J. Loss Prev. Process Ind. 23 (2010) 857–877.
[62] J.E. Matsson, An Introduction to ANSYS Fluent 2021, SDC Publications, 2021.
[63] B. Maronga, M. Gryschka, R. Heinze, F. Hoffmann, F. Kanani-Sühring, M. Keck, K. Ketelsen, M.O. Letzel, M. Sühring, S. Raasch, The parallelized large-eddy simulation model (PALM) version 4.0 for atmospheric and oceanic flows: model formulation, recent developments, and future perspectives, Geosci. Model Dev. 8 (2015) 2515–2551.
[64] S.G. Homann, F. Aluzzi, HotSpot Health Physics Codes Version 3.0 User's Guide, Lawrence Livermore National Laboratory, CA, USA, 2013.
[65] A.J. Cimorelli, S.G. Perry, A. Venkatram, J.C. Weil, R.J. Paine, R.B. Wilson, R.F. Lee, W.D. Peters, R.W. Brode, AERMOD: a dispersion model for industrial source applications. Part I: general model formulation and boundary layer characterization, J. Appl. Meteorol. 44 (2005) 682–693.
[66] S.G. Perry, A.J. Cimorelli, R.J. Paine, R.W. Brode, J.C. Weil, A. Venkatram, R.B. Wilson, R.F. Lee, W.D. Peters, AERMOD: a dispersion model for industrial source applications. Part II: model performance against 17 field study databases, J. Appl. Meteorol. 44 (2005) 694–708.
[67] I. Korsakissok, V. Mallet, Comparative study of gaussian dispersion formulas within the polyphemus platform: evaluation with prairie grass and Kincaid experiments, J. Appl. Meteorol. Climatol. 48 (2009) 2459–2473.
[68] NOAAALOHA ® (Areal Locations of Hazardous Atmospheres) 5.4.4 in: NOAA Technical Memorandum NOS OR&R 43, National Oceanic and Atmospheric Administration (NOAA), 2013.
[69] A. Stohl, M. Hittenberger, G. Wotawa, Validation of the lagrangian particle dispersion model FLEXPART against large-scale tracer experiment data, Atmos. Environ. 32 (1998) 4245–4264.
[70] R.R. Draxler, G.D. Hess, A.R. Laboratory, E.R. Laboratories, Description of the HYSPLIT-4 Modeling System, National Oceanic and Atmospheric Administration, 1997.
[71] D. Oettl, R.A. Almbauer, P.J. Sturm, A new method to estimate diffusion in stable, low-wind conditions, J. Appl. Meteorol. 40 (2001) 259–268.
[72] J.S. Scire, D.G. Strimaitis, R.J. Yamartino, A user's guide for the CALPUFF dispersion model (Version 5), in: User's Guide, Earth Tech, Inc, Concord, MA 01742, 2000, pp. 1-521. http://www.src.com/calpuff/download/CALPUFF_UsersGuide.pdf. Accessed 21 September 2022.
[73] S. Thykier-Nielsen, S. Deme, T. Mikkelsen, in: Description of the Atmospheric Dispersion Module RIMPUFF, Riso National Laboratory, PO Box, 1999, p. 49.
[74] Päsler-Sauer, J., 2000. Description of the atmospheric dispersion model ATSTEP, RODOS (WG2)-TN (99)-11. Forschungszentrum Karlsruhe, D-76021 Karlsruhe, Germany. https://resy5.iket.kit.edu/RODOS/Documents/Public/CD1/Wg2_CD1_General/WG2_TN99_11.pdf. Accessed 21 September 2022.
[75] D. Byun, K.L. Schere, Review of the governing equations, computational algorithms, and other components of the models-3 community multiscale air quality (CMAQ) modeling system, Appl. Mech. Rev. 59 (2006) 51–77.
[76] V. Mallet, B. Sportisse, 3-D chemistry-transport model Polair: numerical issues, validation and automatic-differentiation strategy, Atmos. Chem. Phys. Discuss. 4 (2004) 1371–1392.
[77] U. Nopmongcol, Z. Liu, T. Stoeckenius, G. Yarwood, Modeling intercontinental transport of ozone in North America with CAMx for the air quality model evaluation international initiative (AQMEII) Phase 3, Atmos. Chem. Phys. 17 (2017) 9931–9943.
[78] I. Bey, D.J. Jacob, R.M. Yantosca, J.A. Logan, B.D. Field, A.M. Fiore, Q.B. Li, H.G.Y. Liu, L.J. Mickley, M.G. Schultz, Global modeling of tropospheric chemistry with assimilated meteorology: model description and evaluation, J. Geophys. Res. Atmos. 106 (2001) 23073–23095.
[79] B. Blocken, T. Stathopoulos, P. Saathoff, X. Wang, Numerical evaluation of pollutant dispersion in the built environment: comparisons between models and experiments, J. Wind Eng. Ind. Aerodyn. 96 (2008) 1817–1831.
[80] G.C. Efthimiou, J.G. Bartzis, Atmospheric dispersion and individual exposure of hazardous materials, J. Hazard. Mater. 188 (2011) 375–383.
[81] Y. Tominaga, T. Stathopoulos, CFD simulation of near-field pollutant dispersion in the urban environment: a review of current modeling techniques, Atmos. Environ. 79 (2013) 716–730.
[82] G.C. Efthimiou, S. Andronopoulos, R. Tavares, J.G. Bartzis, CFD-RANS prediction of the dispersion of a hazardous airborne material released during a real accident in an industrial environment, J. Loss Prev. Process Ind. 46 (2017) 23–36.
[83] B.E. Launder, D.B. Spalding, Lectures in mathematical models of turbulence, Academic Press, London, New York, 1972.
[84] V. Yakhot, S.A. Orszag, S. Thangam, T.B. Gatski, C.G. Speziale, Development of turbulence models for shear flows by a double expansion technique, Phys. Fluids A 4 (1992) 1510–1520.
[85] B.E. Launder, G.J. Reece, W. Rodi, Progress in the development of a reynolds-stress turbulence closure, J. Fluid Mech. 68 (1975) 537–566.
[86] N. Koutsourakis, J.G. Bartzis, N.C. Markatos, Evaluation of Reynolds stress, k-$\varepsilon$ and RNG k-$\varepsilon$ turbulence models in street canyon flows using various experimental datasets, Environ. Fluid Mech. 12 (2012) 379–403.
[87] X. Wang, K.F. McNamara, Evaluation of CFD simulation using RANS turbulence models for building effects on pollutant dispersion, Environ. Fluid Mech. 6 (2006) 181–202.
[88] J.T. Cai, J.S. Wu, S.Q. Yuan, D.S. Kong, X.L. Zhang, Prediction of gas leakage and dispersion in utility tunnels based on CFD-EnKF coupling model: a 3D full-scale application, Sustain. Cities Soc. 80 (2022) 1–13.
[89] P. Gousseau, B. Blocken, T. Stathopoulos, G.J.F. van Heijst, CFD simulation of near-field pollutant dispersion on a high-resolution grid: a case study by LES and RANS for a building group in downtown Montreal, Atmos. Environ. 45 (2011) 428–438.
[90] Y. Tominaga, T. Stathopoulos, Turbulent Schmidt Numbers for CFD analysis with various types of flowfield, Atmos. Environ. 41 (2007) 8091–8099.
[91] F.J.M. Simoes, S.S.Y. Wang, Numerical prediction of three-dimensional mixing in a compound open channel, J. Hydraul. Res. 35 (1997) 619–642.
[92] H. Zhang, Y. Li, J. Xiao, T. Jordan, Detached eddy simulation of hydrogen turbulent dispersion in nuclear containment compartment using GASFLOW-MPI, Int. J. Hydrog. Energy 43 (2018) 13659–13675.
[93] Y. Tominaga, A. Mochida, S. Murakami, S. Sawaki, Comparison of various revised k–$\varepsilon$ models and LES applied to flow around a high-rise building model with 1:1:2 shape placed within the surface boundary layer, J. Wind Eng. Ind. Aerodyn. 96 (2008) 389–411.
[94] A. Mochida, S. Iizuka, Y. Tominaga, I.Y.F. Lun, Up-scaling CWE models to include mesoscale meteorological influences, J. Wind Eng. Ind. Aerodyn. 99 (2011) 187–198.
[95] K. Uehara, S. Murakami, S. Oikawa, S. Wakamatsu, Wind tunnel experiments on how thermal stratification affects flow in and above urban street canyons, Atmos. Environ. 34 (2000) 1553–1562.
[96] T. Jin, Y. Liu, J. Wei, D. Zhang, X. Wang, G. Lei, T. Wang, Y. Lan, H. Chen, Numerical investigation on the dispersion of hydrogen vapor cloud with atmospheric inversion layer, Int. J. Hydrog. Energy 44 (2019) 23513–23521.
[97] R. Britter, M. Schatzmann, Model Evaluation Guidance and Protocol Document, University of Hamburg Hamburg, Germany, 2007.
[98] J.M. Stockie, The mathematics of atmospheric dispersion modeling, SIAM Rev. 53 (2011) 349–372.
[99] A.K. Blackadar, Turbulence and Diffusion in the Atmosphere: Lectures in Environmental Sciences, Springer, Berlin Heidelberg, 1997.
[100] X.L. Zhang, J.G. Chen, G.F. Su, H.Y. Yuan, Study on source inversion technology for nuclear accidents based on Gaussian puff model and EnKF, in: T. Comes, F. Fiedrich, S. Fortier, J. Geldermann, T. Müller (Eds.), 10th International Conference on Information Systems for Crisis Response and Management, Baden-Baden, Germany, 2013, pp. 634–639.
[101] H. Snoun, G. Bellakhal, H. Kanfoudi, X. Zhang, J. Chahed, One-way coupling of WRF with a Gaussian dispersion model: a focused fine-scale air pollution assessment on southern Mediterranean, Environ. Sci. Pollut. Res. 26 (2019) 22892–22906.
[102] Z.H.A.O. Quanlai, S.U. Guofeng, C.H.E.N. Jianguo, Y.U.A.N. Hongyong, Z.H.A.N.G. Xiaole, C.H.E.N. Peng, N. Shunjiang, Development and application of a serious nuclear accident scenario library, J. Tsinghua Univ. (Sci. Technol.) 55 (2015) 808–814.

[103] O. Connan, K. Smith, C. Organo, L. Solier, D. Maro, D. Hébert, Comparison of RIMPUFF, HYSPLIT, ADMS atmospheric dispersion model outputs, using emergency response procedures, with 85Kr measurements made in the vicinity of nuclear reprocessing plant, J. Environ. Radioact. 124 (2013) 266–277.
[104] S. Thykier-Nielsen, S. Deme, T. Mikkelsen, Description of the Atmospheric Dispersion Module RIMPUFF, Forschungszentrum Karlsruhe GMBH, 1999 Technical Report RODOS(WG2)-TN(98)-02.
[105] C. Rojas-Palma, H.K. Aage, P. Astrup, K. Bargholz, M. Drews, H.E. Jørgensen, U. Korsbech, B. Lauritzen, T. Mikkelsen, S. Thykier-Nielsen, R. Van Ammel, Experimental evaluation of gamma fluence-rate predictions from Argon-41 releases to the atmosphere over a nuclear research reactor site, Radiat. Prot. Dosim. 108 (2004) 161–168.
[106] W. Raskob, D. Trybushnyi, I. Ievdin, M. Zheleznyak, JRODOS: platform for improved long term countermeasures modelling and management, Radioprotection 46 (2011) S731–S736.
[107] W. Raskob, J. Ehrhardt, C. Landman, J. PÄSler-Sauer, Status of the Rodos system for off-site emergency management after nuclear and radiological accidents, in: S. Apikyan, D. Diamond (Eds.), Countering Nuclear and Radiological Terrorism, Springer, Netherlands, 2006, pp. 151–166.
[108] W. Raskob, Brief description of the RODOS installation PV5.0, in: Rodos Version 5 handbook, User guide, Forschungszentrum Karlsruhe, Technik und Umwelt, PO Box 3640, D-76021, Karlsruhe, Germany, 2003. https://resy5.iket.kit.edu/RODOS/Documents/Public/HandbookV5/UserGuide/Summary_5.pdf. Accessed 21 September 2022.
[109] W. Raskob, J. Ehrhardt, The RODOS system: decision support for nuclear off-site emergency management in Europe, in: IRPA-10 Proceedings of the 10th International Congress of the International Radiation Protection Association on harmonization of radiation, human life and the ecosystem, Japan, Japan Health Physics Society, 2000, p. 1. v.
[110] V. Mallet, D. Quélo, B. Sportisse, M. Ahmed de Biasi, É. Debry, I. Korsakissok, L. Wu, Y. Roustan, K. Sartelet, M. Tombette, H. Foudhil, Technical Note: the air quality modeling system polyphemus, Atmos. Chem. Phys. 7 (2007) 5479–5487.
[111] G.A. Grell, S.E. Peckham, R. Schmitz, S.A. McKeen, G. Frost, W.C. Skamarock, B. Eder, Fully coupled "online" chemistry within the WRF model, Atmos. Environ. 39 (2005) 6957–6975.
[112] X. Feng, X. Zhang, C. He, J. Wang, Contributions of traffic and industrial emission reductions to the air quality improvement after the lockdown of Wuhan and neighboring cities due to COVID-19, Toxics 9 (2021) 358.
[113] T. Nakajima, S. Misawa, Y. Morino, H. Tsuruta, D. Goto, J. Uchida, T. Takemura, T. Ohara, Y. Oura, M. Ebihara, M. Satoh, Model depiction of the atmospheric flows of radioactive cesium emitted from the Fukushima Daiichi Nuclear Power station accident, Prog. Earth Planet. Sci. 4 (2017) 2.
[114] X. Hu, D. Li, H. Huang, S. Shen, E. Bou-Zeid, Modeling and sensitivity analysis of transport and deposition of radionuclides from the Fukushima Dai-ichi accident, Atmos. Chem. Phys. 14 (2014) 11065–11092.
[115] S. Fang, S. Zhuang, D. Goto, X. Hu, L. Sheng, S. Huang, Coupled modeling of in- and below-cloud wet deposition for atmospheric 137Cs transport following the Fukushima Daiichi accident using WRF-Chem: a self-consistent evaluation of 25 scheme combinations, Environ. Int. 158 (2022) 106882.
[116] G. Sarwar, D. Luecken, G. Yarwood, G.Z. Whitten, W.P.L. Carter, Impact of an updated carbon bond mechanism on predictions from the CMAQ modeling system: preliminary assessment, J. Appl. Meteorol. Climatol. 47 (2008) 3–14.
[117] C. Fortin, V. Fèvre-Nollet, F. Cousin, P. Lebègue, F. Louis, Box modelling of gas-phase atmospheric iodine chemical reactivity in case of a nuclear accident, Atmos. Environ. 214 (2019) 116838.
[118] J. Trincal, L. Cantrel, F. Cousin, V. Fevre-Nollet, P. Lebegue, Impact of atmospheric species reactivity on radioactive gaseous iodine transport in severe accident conditions, in: Proceedings of the 23rd International Conference on Modelling, Monitoring and Management of Air Pollution, Valencia, SPAIN, 2015, pp. 77–86.
[119] J. Rissman, S. Arunachalam, M. Woody, J.J. West, T. BenDor, F.S. Binkowski, A plume-in-grid approach to characterize air quality impacts of aircraft emissions at the Hartsfield–Jackson Atlanta International Airport, Atmos. Chem. Phys. 13 (2013) 9285–9302.
[120] L. Fabbri, M.H. Wood, Accident damage analysis module (ADAM): novel European commission tool for consequence assessment—scientific evaluation of performance, Process Saf. Environ. Prot. 129 (2019) 249–263.
[121] Y. Bruinen de Bruin, M. Binda, L. Fabbri, Accident Damage Analysis Module (ADAM) : Technical Guidance : Software Tool for Consequence Analysis Calculations, European Commission, Joint Research Centre, Publications Office, 2017.
[122] C. Kirchsteiger, Status and functioning of the European Commission's major accident reporting system, J. Hazard. Mater. 65 (1999) 211–231.
[123] S. Hanna, T. Mazzola, J. Chang, T. Spicer, S. Gant, R. Batt, in: Gaps in Toxic Industrial Chemical Model systems: Improvements and Changes Over Past 10 years, 41, Process Safety Progress, 2022, pp. 151–166.
[124] W.G. Houf, W.S. Winters, Simulation of high-pressure liquid hydrogen releases, Int. J. Hydrog. Energy 38 (2013) 8092–8099.
[125] A. Stohl, A.J. Prata, S. Eckhardt, L. Clarisse, A. Durant, S. Henne, N.I. Kristiansen, A. Minikin, U. Schumann, P. Seibert, K. Stebel, H.E. Thomas, T. Thorsteinsson, K. Tørseth, B. Weinzierl, Determination of time- and height-resolved volcanic ash emissions and their use for quantitative ash dispersion modeling: the 2010 Eyjafjallajökull eruption, Atmos. Chem. Phys. 11 (2011) 4333–4351.
[126] R. D'Amours, A. Malo, R. Servranckx, D. Bensimon, S. Trudel, J.-.P. Gauthier–Bilodeau, Application of the atmospheric Lagrangian particle dispersion model MLDP0 to the 2008 eruptions of Okmok and Kasatochi volcanoes, J. Geophys. Rese. Atmos. 115 (2010) D00L11.
[127] D. Yang, R. Huo, X.L. Zhang, X.Y. Zhao, Comparison of the distribution of carbon monoxide concentration and temperature rise in channel fires: reduced-scale experiments, Appl. Therm. Eng. 31 (2011) 528–536.
[128] D. Yang, R. Huo, X.L. Zhang, X.Y. Zhao, On the front velocity of buoyancy-driven transient ceiling jet in a horizontal corridor: comparison of correlations with measurements, Appl. Therm. Eng. 31 (2011) 2992–2999.
[129] D. Yang, R. Huo, X.L. Zhang, S. Zhu, X.Y. Zhao, Comparative study on carbon monoxide stratification and thermal stratification in a horizontal channel fire, Build. Environ. 49 (2012) 1–8.
[130] R.P. Koopman, D.L. Ermak, Lessons learned from LNG safety research, J. Hazard. Mater. 140 (2007) 412–428.
[131] Y. Liu, Z. Liu, J. Wei, Y. Lan, S. Yang, T. Jin, Spread characteristics of hydrogen vapor cloud for liquid hydrogen spill under different source conditions, Int. J. Hydrog. Energy 46 (2021) 4606–4613.
[132] Y. Liu, J. Wei, Z. Liu, G. Lei, T. Jin, Dilution of flammable vapor cloud formed by liquid hydrogen spill, Int. J. Hydrog. Energy 45 (2020) 5067–5072.
[133] J. He, L. Liu, A. Li, Y. Ma, D. Zhou, Q. Zhou, Y. Zhan, A dense gas dispersion model based on revised meteorological parameters and its performance evaluation, Atmos. Environ. 244 (2021) 117953.
[134] C. Rauchegger, S. Bayley, V. Schröder, D. Thévenin, Dispersion of heavy gases – experimental results and numerical simulations, Process Saf. Prog. 34 (2015) 280–285.
[135] Q. Liu, H. Zhang, Y. Liu, H. Huang, X. Zhang, Z. Li, W. Yao, Influencing factors of flammable refrigerants leaking in building air- conditioning system, Procedia Eng. 62 (2013) 648–654.
[136] O.R. Hansen, Liquid hydrogen releases show dense gas behavior, Int. J. Hydrog. Energy 45 (2020) 1343–1358.
[137] J.C. Statharas, A.G. Venetsanos, J.G. Bartzis, J. Würtz, U. Schmidtchen, Analysis of data from spilling experiments performed with liquid hydrogen, J. Hazard. Mater. 77 (2000) 57–75.
[138] A. Banerjee, Buoyancy driven effects in formation of mixing zones, in: Proceedings of the ASME International Mechanical Engineering Congress and Exposition, Boston, MA, 2008, pp. 315–322. Asme.
[139] D.L. Youngs, Numerical simulation of turbulent mixing by Rayleigh-Taylor instability, Phys. D 12 (1984) 32–44.
[140] A.G. Venetsanos, T. Huld, P. Adams, J.G. Bartzis, Source, dispersion and combustion modelling of an accidental release of hydrogen in an urban environment, J. Hazard. Mater. 105 (2003) 1–25.
[141] F. Rigas, S. Sklavounos, Evaluation of hazards associated with hydrogen storage facilities, Int. J. Hydrog. Energy 30 (2005) 1501–1510.
[142] D.P. Hoult, J.C. Weil, Turbulent plume in a laminar cross flow, Atmos. Environ. 6 (1972) 513–531 (1967).
[143] Z. Shu, G. Lei, Z. Liu, W. Liang, X. Zheng, J. Ma, F. Lu, H. Qian, Motion trajectory prediction model of hydrogen leak and diffusion in a stable thermally-stratified environment, Int. J. Hydrog. Energy 47 (2022) 2040–2049.
[144] H.A. Olvera, A.R. Choudhuri, Numerical simulation of hydrogen dispersion in the vicinity of a cubical building in stable stratified atmospheres, Int. J. Hydrogen Energy 31 (2006) 2356–2369.
[145] P.G. Holborn, C.M. Benson, J.M. Ingram, Modelling hazardous distances for large-scale liquid hydrogen pool releases, Int. J. Hydrog. Energy 45 (2020) 23851–23871.
[146] W. Tan, H. Du, L.Y. Liu, T. Su, X.Y. Liu, Experimental and numerical study of ammonia leakage and dispersion in a food factory, J. Loss Prev. Process Ind. 47 (2017) 129–139.
[147] W. Tan, D. Lv, X.Y. Guo, H. Du, L.Y. Liu, Y. Wang, Accident consequence calculation of ammonia dispersion in factory area, J. Loss Prev. Process Ind. 67 (2020) 1–10.
[148] R.I. Sykes, C.P. Cerasoli, D.S. Henn, The representation of dynamic flow effects in a Lagrangian puff dispersion model, J. Hazard. Mater. 64 (1999) 223–247.
[149] M. Markiewicz, A review of mathematical models for the atmospheric dispersion of heavy gases. Part I. A classification of models, Ecol. Chem. Eng. S 19 (2012) 297–314.
[150] J.C. Chang, S.R. Hanna, Modelers' data archive – a collection of atmospheric transport and dispersion data sets, in: Proceedings of the 20th GMU Conference on Atmospheric Transport and Dispersion Modeling, Fairfax, Virginia, 2016.
[151] S. Fox, S. Hanna, T. Mazzola, T. Spicer, J. Chang, S. Gant, Overview of the Jack Rabbit II (JR II) field experiments and summary of the methods used in the dispersion model comparisons, Atmos. Environ. 269 (2022) 118783.
[152] J. Allwine, J. Flaherty, Urban Dispersion Program Overview and MID05 Field Study Summary, Urban Dispersion Program (UDP), Pacific Northwest National Laboratory, 99352, Richland, Washington, 2007.
[153] K.J. Allwine, J.E. Flaherty, Urban Dispersion Program MSG05 Field Study: Summary of Tracer and Meteorological Measurements, United States, 2006.
[154] J. Allwine, J. Flaherty, Joint Urban 2003 (2006).
[155] K.J. Allwine, J.H. Shinn, G.E. Streit, K.L. Clawson, M. Brown, Overview of urban 2000 a multiscale field study of dispersion through an urban environment, Bull. Am. Meteorol. Soc. 83 (2002) 521–536.
[156] S. Warner, N. Platt, J.F. Heagy, J.E. Jordan, G. Bieberbach, Comparisons of transport and dispersion model predictions of the mock urban setting test field experiment, J. Appl. Meteorol. Climatol. 45 (2006) 1414–1428.
[157] D.D. Finn, K.L. Clawson, R.M. Eckman, R.G. Carter, J.D. Rich, T.W. Strong, S.A. Beard, B.R. Reese, D. Davis, H. Liu, E. Russell, Z. Gao, S. Brooks, Project Sage-Brush phase 1, in: L.Air Resources (Ed.), Air Resources Laboratory, 2015, p. 362.
[158] R.R. Draxler, Metropolitan Tracer Experiment (METREX), in: NOAA Technical Memorandum ERL ARL-140, Air Resources Laboratory, Silver Spring, Maryland, 1985.
[159] J.L. Heffter, J.F. Schubert, G.A. Mead, Atlantic Coast Unique Regional Atmospheric Tracer Experiment (ACURATE), in: NOAA Techinical Memoradum, Air Resources

Laboratory, National Oceanic and Atmospheric Administration, Rockville, Maryland, United States, 1984.
[160] K. Telegadas, G. Ferber, R. Draxler, M. Pendergast, A. Boni, J. Hughes, J. Gray, Measured Weekly and Twice-Daily krypton-85 Surface Air Concentrations Within 150Km of the Savannah River Plant (March 1975 Through September 1977), National Oceanic and Atmospheric Administration, Silver Spring, MD, 1980 Final report.
[161] G.J. Ferber, K. Telegadas, J.L. Heffter, C.R. Dickson, R.N. Dietz, P.W. Krey, Demonstration of a long-range atmospheric tracer system using perfluorocarbons, Air Resources Laboratories, Silver Spring, Maryland, 1981.
[162] F. Girardi, G. Graziani, D. Van Velzen, S. Galmarini, S. Mosca, R. Bianconi, R. Bellasio, W. Klug, G. Fraser, ETEX - The European Tracer Experiment, Official publications of the European Communities, Luxembourg, 1998 EUR 18143 EN,.
[163] R.R. Draxler, R. Dietz, R.J. Lagomarsino, G. Start, Across North America tracer experiment (ANATEX): sampling and analysis, Atmos. Environ. Part A Gen. Top. 25 (1991) 2815–2836.
[164] T. Chai, A. Stein, F. Ngan, Weak-constraint inverse modeling using HYSPLIT-4 Lagrangian dispersion model and cross-Appalachian tracer experiment (CAPTEX) observations – effect of including model uncertainties on source term estimation, Geosci. Model Dev. 11 (2018) 5135–5148.
[165] G.R. Johnson, L. Morawska, The mechanism of breath aerosol formation, J. Aerosol. Med. Pulm. Drug Deliv. 22 (2009) 229–237.
[166] L. Morawska, G.R. Johnson, Z.D. Ristovski, M. Hargreaves, K. Mengersen, S. Corbett, C.Y.H. Chao, Y. Li, D. Katoshevski, Size distribution and sites of origin of droplets expelled from the human respiratory tract during expiratory activities, J. Aerosol Sci. 40 (2009) 256–269.
[167] N.H.L. Leung, D.K.W. Chu, E.Y.C. Shiu, K.H. Chan, J.J. McDevitt, B.J.P. Hau, H.L. Yen, Y. Li, D.K.M. Ip, J.S.M. Peiris, W.H. Seto, G.M. Leung, D.K. Milton, B.J. Cowling, Respiratory virus shedding in exhaled breath and efficacy of face masks, Nat. Med. 26 (2020) 676–680.
[168] C. Alonso, P.C. Raynor, P.R. Davies, M. Torremorell, Concentration, size distribution, and infectivity of airborne particles carrying swine viruses, PLoS One 10 (2015) e0135675.
[169] M.A. Sánchez-Monedero, M.I. Aguilar, R. Fenoll, A. Roig, Effect of the aeration system on the levels of airborne microorganisms generated at wastewater treatment plants, Water Res. 42 (2008) 3739–3744.
[170] J.H. Byeon, C.W. Park, K.Y. Yoon, J.H. Park, J. Hwang, Size distributions of total airborne particles and bioaerosols in a municipal composting facility, Bioresour. Technol. 99 (2008) 5150–5154.
[171] Z. Yang, Q. Wang, L. Zhao, E. Long, Decay characteristics of aerosolized viruses in the air and control strategy of thermal and humid environment for epidemic prevention, Indoor Built Environ. 31 (2022) 1287–1305.
[172] M. Schuit, S. Ratnesar-Shumate, J. Yolitz, G. Williams, W. Weaver, B. Green, D. Miller, M. Krause, K. Beck, S. Wood, B. Holland, J. Bohannon, D. Freeburger, I. Hooper, J. Biryukov, L.A. Altamura, V. Wahl, M. Hevey, P. Dabisch, Airborne SARS-CoV-2 Is rapidly inactivated by simulated sunlight, J. Infect. Dis. 222 (2020) 564–571.
[173] K. Lin, L.C. Marr, Humidity-dependent decay of viruses, but not bacteria, in aerosols and droplets follows disinfection kinetics, Environ. Sci. Technol. 54 (2020) 1024–1032.
[174] M. Pohanka, P. Skládal, Bacillus anthracis, Francisella tularensis and Yersinia pestis. The most important bacterial warfare agents — review, Folia Microbiol. (Praha) 54 (2009) 263–272.
[175] A.E. Haddrell, R.J. Thomas, Aerobiology: experimental Considerations, observations, and future tools, Appl. Environ. Microbiol. 83 (2017) e00809–e00817.
[176] W. He, Y. Guo, H. Gao, J. Liu, Y. Yue, J. Wang, Evaluation of regeneration processes for filtering facepiece respirators in terms of the bacteria inactivation efficiency and influences on filtration performance, ACS Nano 14 (2020) 13161–13171.
[177] O. Fernandez Mara, J. Thomas Richard, J. Garton Natalie, A. Hudson, A. Haddrell, P. Reid Jonathan, Assessing the airborne survival of bacteria in populations of aerosol droplets with a novel technology, J. R. Soc. Interface 16 (2019) 20180779.
[178] P. Kritana, K. Taehyeung, K. Hyeontae, K. Ki Youn, S. Wongeun, Atmospheric pathway: a possibility of continuous outbreaks of foot-and-mouth disease in South Korea in 2010–2011, Comput. Electron. Agric. 108 (2014) 95–104.
[179] J. Gloster, H.J. Champion, L.M. Mansley, P. Romero, T. Brough, A. Ramirez, The 2001 epidemic of foot-and-mouth disease in the United Kingdom: epidemiological and meteorological case studies, Vet. Rec. 156 (2005) 793–803.
[180] I. Traulsen, G. Rave, J. Krieter, Sensitivity analysis of a stochastic simulation model for foot and mouth disease, Arch. Anim. Breed. 53 (2010) 529–544.
[181] I. Traulsen, J. Krieter, Assessing airborne transmission of foot and mouth disease using fuzzy logic, Expert Syst. Appl. 39 (2012) 5071–5077.
[182] J.H. Sørensen, C.Ø. Jensen, T. Mikkelsen, D.K.J. Mackay, A.I. Donaldson, Modelling the atmospheric dispersion of foot-and-mouth disease virus for emergency preparedness, Phys. Chem. Earth Part B 26 (2001) 93–97.
[183] M.G. Garner, G.D. Hess, X. Yang, An integrated modelling approach to assess the risk of wind-borne spread of foot-and-mouth disease virus from infected premises, Environ. Model. Assess. 11 (2006) 195–207.
[184] L.M. Wein, D.L. Craft, E.H. Kaplan, Emergency response to an anthrax attack, Proc. Natl. Acad. Sci. 100 (2003) 4346–4351.
[185] A. Nicogossian, L.A. Schintler, Z. Boybeyi, Modeling urban atmospheric anthrax spores dispersion: assessment of health impacts and policy implications, World Med. Health Policy 3 (2011) 1–16.
[186] A.L. Stuart, D.A. Wilkening, Degradation of biological weapons agents in the environment: implications for terrorism response, Environ. Sci. Technol. 39 (2005) 2736–2743.
[187] M. Karl, L. Pirjola, T. Grönholm, M. Kurppa, S. Anand, X. Zhang, A. Held, R. Sander, M. Dal Maso, D. Topping, S. Jiang, L. Kangas, J. Kukkonen, Description and evaluation of the community aerosol dynamics model MAFOR v2.0, Geosci, Model. Dev. 15 (2022) 3969–4026.
[188] X. Zhang, M. Karl, L. Zhang, J. Wang, Influence of aviation emission on the particle number concentration near Zurich airport, Environ. Sci. Technol. 54 (2020) 14161–14171.
[189] X. Zhang, X. Chen, L. Zhang, J. Wang, A number-based inventory of particle emissions by civil aviation and the influences on the particle number concentration near Zurich airport, in: C.P.M. Strohmeier (Ed.), Proceedings of the 7th OpenSky workshop 2019 EPiC series in computing, Zurich, Switzerland, 2019, pp. 109–116. Vol. 67.
[190] E. Mescioglu, A. Paytan, B.W. Mitchell, D.W. Griffin, Efficiency of bioaerosol samplers: a comparison study, Aerobiologia 37 (2021) 447–459 Bologna.
[191] G. Mainelis, Bioaerosol sampling: classical approaches, advances, and perspectives, Aerosol Sci. Technol. 54 (2020) 496–519.
[192] S.C. Chen, J. Wang, H. Fissan, D.Y.H. Pui, Use of nuclepore filters for ambient and workplace nanoparticle exposure assessment—spherical particles, Atmos. Environ. 77 (2013) 385–393.
[193] S.-.C. Chen, J. Wang, H. Fissan, D.Y.H. Pui, Exposure assessment of nanosized engineered agglomerates and aggregates using nuclepore filter, J. Nanopart. Res. 15 (2013) 1955.
[194] S.-.C. Chen, Y. Hu, D.Y.H. Pui, J. Wang, Explicit expressions for the minimum efficiency and most penetrating particle size of nuclepore filters, J. Aerosol Sci. 100 (2016) 108–117.
[195] T.Y. Ling, J. Wang, D.Y.H. Pui, Measurement of filtration efficiency of Nuclepore filters challenged with polystyrene latex nanoparticles: experiments and modeling, J. Nanopart. Res. 13 (2011) 5415.
[196] Y.B. Zhao, T. Cen, J. Tang, W. He, C. Ludwig, S.C. Chen, J. Wang, An elution-based method for estimating efficiencies of aerosol collection devices not affected by their pressure drops, Sep. Purif. Technol. 287 (2022) 120590.
[197] Y.-.B. Zhao, J. Tang, T. Cen, G. Qiu, W. He, F. Jiang, R. Yu, C. Ludwig, J. Wang, Integrated aerodynamic/electrochemical microsystem for collection and detection of nanogram-level airborne bioaccessible metals, Sens. Actuators B 351 (2022) 130903.
[198] Y. Tao, X. Zhang, G. Qiu, M. Spillmann, Z. Ji, J. Wang, SARS-CoV-2 and other airborne respiratory viruses in outdoor aerosols in three Swiss cities before and during the first wave of the COVID-19 pandemic, Environ. Int. 164 (2022) 107266.
[199] Y. Tao, Y. Yue, G. Qiu, Z. Ji, M. Spillman, Z. Gai, Q. Chen, M. Bielecki, M. Huber, A. Trkola, Q. Wang, J. Cao, J. Wang, Comparison of analytical sensitivity and efficiency for SARS-CoV-2 primer sets by TaqMan-based and SYBR Green-based RT-qPCR, Appl. Microbiol. Biotechnol. 106 (2022) 2207–2218.
[200] Y. Yue, H. Chen, A. Setyan, M. Elser, M. Dietrich, J. Li, T. Zhang, X. Zhang, Y. Zheng, J. Wang, M. Yao, Size-resolved endotoxin and oxidative potential of ambient particles in Beijing and Zürich, Environ. Sci. Technol. 52 (2018) 6816–6824.
[201] H. Liu, Z. Hu, M. Zhou, H. Zhang, X. Zhang, Y. Yue, X. Yao, J. Wang, C. Xi, P. Zheng, X. Xu, B. Hu, PM2.5 drives bacterial functions for carbon, nitrogen, and sulfur cycles in the atmosphere, Environ. Pollut. 295 (2022) 118715.
[202] J. Li, J. Cao, Y.G. Zhu, Q.L. Chen, F. Shen, Y. Wu, S. Xu, H. Fan, G. Da, R.J. Huang, J. Wang, A.L. de Jesus, L. Morawska, C.K. Chan, J. Peccia, M. Yao, Global survey of antibiotic resistance genes in air, Environ. Sci. Technol. 52 (2018) 10975–10984.
[203] Y. Tao, Y. Yue, J. Wang, Abundance and diversity of antibiotic resistance genes possibly released to ambient air by experiments in biology laboratories, Sci. Total Environ. 797 (2021) 149147.
[204] J.A. Huffman, A.E. Perring, N.J. Savage, B. Clot, B. Crouzy, F. Tummon, O. Shoshanim, B. Damit, J. Schneider, V. Sivaprakasam, M.A. Zawadowicz, I. Crawford, M. Gallagher, D. Topping, D.C. Doughty, S.C. Hill, Y. Pan, Real-time sensing of bioaerosols: review and current perspectives, Aerosol Sci. Technol. 54 (2020) 465–495.
[205] H.K. Paul, H. Edwin, E.F. Virginia, M.C. James, L.B. Karen, A low-cost multichannel aerosol fluorescence sensor for networked deployment, Proceeding of the SPIE, 2004.
[206] G. Qiu, Y. Yue, J. Tang, Y.-.B. Zhao, J. Wang, Total bioaerosol detection by a succinimidyl-ester-functionalized plasmonic biosensor to reveal different characteristics at three locations in Switzerland, Environ. Sci. Technol. 54 (2020) 1353–1362.
[207] J. Tang, Y. Meng, L. Bezinge, G. Qiu, Y. Yue, X. Zhang, J. Wang, Colorimetric immunodetection of bacteria enriched on membranes within a compact multichannel filtration device, Sens. Actuators B 353 (2022) 131142.
[208] J. Tang, G. Qiu, X. Cao, Y. Yue, X. Zhang, J. Schmitt, J. Wang, Self-aligned 3D microlenses in a chip fabricated with two-photon stereolithography for highly sensitive absorbance measurement, Lab Chip 20 (2020) 2334–2342.
[209] J. Tang, G. Qiu, J. Wang, Recent development of optofluidics for imaging and sensing applications, Chemosensors 10 (2022) 1–20.
[210] J. Tang, X. Cao, G. Qiu, A. deMello, J. Wang, Optical-switch-enabled microfluidics for sensitive multichannel colorimetric analysis, Anal. Chem. 93 (2021) 6784–6791.
[211] J. Tang, G. Qiu, X. Zhang, J. Wang, A 3D-cascade-microlens optofluidic chip for refractometry with adjustable sensitivity, Lab Chip 21 (2021) 3784–3792.
[212] G. Qiu, Z. Gai, Y. Tao, J. Schmitt, G.A. Kullak-Ublick, J. Wang, Dual-functional plasmonic photothermal biosensors for highly accurate severe acute respiratory syndrome coronavirus 2 detection, ACS Nano 14 (2020) 5268–5277.
[213] G. Qiu, Z. Gai, L. Saleh, J. Tang, T. Gui, G.A. Kullak-Ublick, J. Wang, Thermoplasmonic-assisted cyclic cleavage amplification for self-validating plasmonic detection of SARS-CoV-2, ACS Nano 15 (2021) 7536–7546.
[214] F.Z. Jiang, Z. Xiao, T. Wang, J.J. Wang, L.H. Bie, L. Saleh, K. Frey, L.J. Zhang, J. Wang, Rapid and sensitive multiplex detection of COVID-19 antigens and an-

tibody using electrochemical immunosensor-/aptasensor-enabled biochips, Chem. Commun. 58 (2022) 7285–7288.
[215] B. Liu, F. Jiang, Y. Tao, T. Zheng, Y. Yue, V. Tepper, X. Cao, J. Wang, Measuring airborne antibiotic resistance genes in Swiss cities via a DNA-enabled electrochemical chip-based sensor, ACS ES&T Eng. 2 (2022) 1677–1683.
[216] M. Li, L. Wang, W. Qi, Y. Liu, J. Lin, Challenges and Perspectives for Biosensing of Bioaerosol containing pathogenic microorganisms, Micromachines 12 (2021) 1–19 Basel.
[217] B. Bernard, Regulating nuclear safety through safety culture, J. Saf. Sci. Resil. 2 (2021) 172–178.
[218] IAEAINES: The International Nuclear and Radiological Event Scale : User's Manual, International Atomic Energy Agency, VIENNA, 2013.
[219] G. Steinhauser, A. Brandl, T.E. Johnson, Comparison of the Chernobyl and Fukushima nuclear accidents: a review of the environmental impacts, Sci. Total Environ. 470 (2014) 800–817.
[220] D. Chen, B. Nie, D. Bing, D. Yang, S. Wu, J. He, G. Weiguo, D. Wang, Revisiting atmospheric dispersion characteristics of multi-form tritium, SSRN Electron. J. (2022) 1–26, doi:10.2139/ssrn.4139191.
[221] A. Stohl, P. Seibert, G. Wotawa, D. Arnold, J.F. Burkhart, S. Eckhardt, C. Tapia, A. Vargas, T.J. Yasunari, Xenon-133 and caesium-137 releases into the atmosphere from the Fukushima Dai-ichi nuclear power plant: determination of the source term, atmospheric dispersion, and deposition, Atmos. Chem. Phys. 12 (2012) 2313–2343.
[222] B. Sportisse, A review of parameterizations for modelling dry deposition and scavenging of radionuclides, Atmos. Environ. 41 (2007) 2683–2698.
[223] T. Ohkura, T. Oishi, M. Taki, Y. Shibanuma, M. Kikuchi, H. Akino, Y. Kikuta, M. Kawasaki, J. Saegusa, M. Tsutsumi, H. Ogose, S. Tamura, T. Sawahata, Emergency monitoring of environmental radiation and atmospheric radionuclides at nuclear science research institute, jaea following the accident of Fukushima Dai-ichi nuclear power plant, Department of Radiation Protection JAEA-Data/Code 2012-01, Nuclear Science Research Institute, Ibaraki, Japan, 2012 Tokai Research and Development Center, Japan Atomic Energy Agency.
[224] G. Furuki, J. Imoto, A. Ochiai, S. Yamasaki, K. Nanba, T. Ohnuki, B. Grambow, R.C. Ewing, S. Utsunomiya, Caesium-rich micro-particles: a window into the meltdown events at the Fukushima Daiichi nuclear power plant, Sci. Rep. 7 (2017) 42731.
[225] Y. Kurihara, N. Takahata, T.D. Yokoyama, H. Miura, Y. Kon, T. Takagi, S. Higaki, N. Yamaguchi, Y. Sano, Y. Takahashi, Isotopic ratios of uranium and caesium in spherical radioactive caesium-bearing microparticles derived from the Fukushima Dai-ichi nuclear power plant, Sci. Rep. 10 (2020) 3281.
[226] H. Muramatsu, K. Kawasumi, T. Kondo, K. Matsuo, S. Itoh, Size-distribution of airborne radioactive particles from the Fukushima accident, J. Radioanal. Nucl. Chem. 303 (2015) 1459–1463.
[227] Y. Abe, S. Onozaki, I. Nakai, K. Adachi, Y. Igarashi, Y. Oura, M. Ebihara, T. Miyasaka, H. Nakamura, K. Sueki, H. Tsuruta, Y. Moriguchi, Widespread distribution of radiocesium-bearing microparticles over the greater Kanto Region resulting from the Fukushima nuclear accident, Progr. Earth Planet. Sci. 8 (2021) 13.
[228] X. Zhang, W. Raskob, C. Landman, D. Trybushnyi, C. Haller, H. Yuan, Automatic plume episode identification and cloud shine reconstruction method for ambient gamma dose rates during nuclear accidents, J. Environ. Radioact. 178 (2017) 36–47.
[229] C. Andronache, Estimated variability of below-cloud aerosol removal by rainfall for observed aerosol size distributions, Atmos. Chem. Phys. 3 (2003) 131–143.
[230] J.A. Garland, On the size dependence of particle deposition, Water Air Soil Pollut. Focus 1 (2001) 323–332.
[231] A. Venkatram, J. Pleim, The electrical analogy does not apply to modeling dry deposition of particles, Atmos. Environ. 33 (1999) 3075–3076.
[232] A. Baklanov, J.H. Sørensen, Parameterisation of radionuclide deposition in atmospheric long-range transport modelling, Phys. Chem. Earth Part B 26 (2001) 787–799.
[233] S. Andronopoulos, J.G. Bartzis, A gamma radiation dose calculation method for use with Lagrangian puff atmospheric dispersion models used in real-time emergency response systems, J. Radiol. Prot. 30 (2010) 747–759.
[234] X. Zhang, G. Efthimiou, Y. Wang, M. Huang, Comparisons between a new point kernel-based scheme and the infinite plane source assumption method for radiation calculation of deposited airborne radionuclides from nuclear power plants, J. Environ. Radioact. 184-185 (2018) 32–45.
[235] V. Simsek, L. Pozzoli, A. Unal, T. Kindap, M. Karaca, Simulation of 137Cs transport and deposition after the chernobyl nuclear power plant accident and radiological doses over the Anatolian peninsula, Sci. Total Environ. 499 (2014) 74–88.
[236] B. Nie, M. Jiang, M. Ni, F. Li, Preliminary environmental radiation considerations for CFETR, Fusion Eng. Des. 140 (2019) 16–22.
[237] C.J. Werner, MCNP Users Manual-Code Version 6.2, in, Los Alamos National Laboratory, 2017.
[238] D. Sardari, S. Baradaran, Semi-empirical relationship for photon buildup factor in soft tissue and water, Radiat. Prot. Dosim. 142 (2010) 209–212.
[239] G. Battistoni, T. Boehlen, F. Cerutti, P.W. Chin, L.S. Esposito, A. Fassò, A. Ferrari, A. Lechner, A. Empl, A. Mairani, A. Mereghetti, P.G. Ortega, J. Ranft, S. Roesler, P.R. Sala, V. Vlachoudis, G. Smirnov, Overview of the FLUKA code, Ann. Nucl. Energy 82 (2015) 10–18.
[240] S. Agostinelli, J. Allison, K. Amako, J. Apostolakis, H. Araujo, P. Arce, M. Asai, D. Axen, S. Banerjee, G. Barrand, F. Behner, L. Bellagamba, J. Boudreau, L. Broglia, A. Brunengo, H. Burkhardt, S. Chauvie, J. Chuma, R. Chytracek, G. Cooperman, G. Cosmo, P. Degtyarenko, A. Dell'Acqua, G. Depaola, D. Dietrich, R. Enami, A. Feliciello, C. Ferguson, H. Fesefeldt, G. Folger, F. Foppiano, A. Forti, S. Garelli, S. Giani, R. Giannitrapani, D. Gibin, J.J. Gómez Cadenas, I. González, G. Gracia Abril, G. Greeniaus, W. Greiner, V. Grichine, A. Grossheim, S. Guatelli, P. Gumplinger, R. Hamatsu, K. Hashimoto, H. Hasui, A. Heikkinen, A. Howard, V. Ivanchenko, A. Johnson, F.W. Jones, J. Kallenbach, N. Kanaya, M. Kawabata, Y. Kawabata, M. Kawaguti, S. Kelner, P. Kent, A. Kimura, T. Kodama, R. Kokoulin, M. Kossov, H. Kurashige, E. Lamanna, T. Lampén, V. Lara, V. Lefebure, F. Lei, M. Liendl, W. Lockman, F. Longo, S. Magni, M. Maire, E. Medernach, K. Minamimoto, P. Mora de Freitas, Y. Morita, K. Murakami, M. Nagamatu, R. Nartallo, P. Nieminen, T. Nishimura, K. Ohtsubo, M. Okamura, S. O'Neale, Y. Oohata, K. Paech, J. Perl, A. Pfeiffer, M.G. Pia, F. Ranjard, A. Rybin, S. Sadilov, E. Di Salvo, G. Santin, T. Sasaki, N. Savvas, Y. Sawada, S. Scherer, S. Sei, V. Sirotenko, D. Smith, N. Starkov, H. Stoecker, J. Sulkimo, M. Takahata, S. Tanaka, E. Tcherniaev, E. Safai Tehrani, M. Tropeano, P. Truscott, H. Uno, L. Urban, P. Urban, M. Verderi, A. Walkden, W. Wander, H. Weber, J.P. Wellisch, T. Wenaus, D.C. Williams, D. Wright, T. Yamada, H. Yoshida, D. Zschiesche, Geant4—a simulation toolkit, nuclear instruments and methods in physics research section a: accelerators, spectrometers, Detect. Assoc. Equip. 506 (2003) 250–303.
[241] M.W. McNaughton, J.M. Gillis, E. Ruedig, J.J. Whicker, D.P. Fuehne, Gamma-ray dose from an overhead plume, Health Phys. 112 (2017) 445–450.
[242] G.A. Sandler, H. Gardiner, K. Stadnikia, A. Enqvist, J. Baciak, Verification and validation of atmospheric transport models with the UF training reactor, Nucl. Instrum. Methods Phys. Res. A 954 (2020) 161386.
[243] S. Andronopoulos, E. Davakis, J.G. Bartzis, RODOS-DIPCOT model description and evaluation, RODOS(RA2)-TN(09)-01, Environmental Research Laboratory, Institute of Nuclear Technology and Radiation Protection, National Centre for Scientific Research "Demokritos", 15310 Aghia Paraskevi, Greece, 2009.
[244] P.T. Rakesh, R. Venkatesan, T. Hedde, P. Roubin, R. Baskaran, B. Venkatraman, Simulation of radioactive plume gamma dose over a complex terrain using Lagrangian particle dispersion model, J. Environ. Radioact. 145 (2015) 30–39.
[245] C.V. Srinivas, P.T. Rakesh, K.B.R.R. Hari Prasad, R. Venkatesan, R. Baskaran, B. Venkatraman, Assessment of atmospheric dispersion and radiological impact from the Fukushima accident in a 40-km range using a simulation approach, Air Qual. Atmos. Health 7 (2014) 209–227.
[246] C.V. Srinivas, R. Venkatesan, R. Baskaran, V. Rajagopal, B. Venkatraman, Regional scale atmospheric dispersion simulation of accidental releases of radionuclides from Fukushima Dai-ichi reactor, Atmos. Environ. 61 (2012) 66–84.
[247] H. Terada, M. Chino, Improvement of worldwide version of system for prediction of environmental emergency dose information (WSPEEDI), (II), J. Nucl. Sci. Technol. 42 (2005) 651–660.
[248] H. Terada, M. Chino, Development of an atmospheric dispersion model for accidental discharge of radionuclides with the function of simultaneous prediction for multiple domains and its evaluation by application to the Chernobyl nuclear accident, J. Nucl. Sci. Technol. 45 (2008) 920–931.
[249] G. Katata, H. Terada, H. Nagai, M. Chino, Numerical reconstruction of high dose rate zones due to the Fukushima Dai-ichi nuclear power plant accident, J. Environ. Radioact. 111 (2012) 2–12.
[250] J. Cai, K.F. Ip, C. Eze, J. Zhao, J. Cai, H. Zhang, Dispersion of radionuclides released by nuclear accident and dose assessment in the Greater Bay Area of China, Ann. Nucl. Energy 132 (2019) 593–602.
[251] X. Li, W. Xiong, X. Hu, S. Sun, H. Li, X. Yang, Q. Zhang, M. Nibart, A. Albergel, S. Fang, An accurate and ultrafast method for estimating three-dimensional radiological dose rate fields from arbitrary atmospheric radionuclide distributions, Atmos. Environ. 199 (2019) 143–154.
[252] S. Fang, X. Li, N. Wu, J. Li, Y. Liu, N. Xue, H. Li, J. Liu, W. Xiong, Q. Zhang, A. Albergel, Fast evaluation of three-dimensional gamma dose rate fields on non-equispaced grids for complex atmospheric radionuclide distributions, J. Environ. Radioact. 222 (2020) 106355.
[253] X.L. Zhang, X. Chen, J. Wang, A number-based inventory of size-resolved black carbon particle emissions by global civil aviation, Nat. Commun. 10 (2019) 534.
[254] J. Zhang, S. Zhang, X. Zhang, J. Wang, Y. Wu, J. Hao, Developing a high-resolution emission inventory of China's aviation sector using real-world flight trajectory data, Environ. Sci. Technol. 56 (2022) 5743–5752.
[255] C. Zhang, L. Chen, S. Ding, X. Zhou, R. Chen, X. Zhang, Z. Yu, J. Wang, Mitigation effects of alternative aviation fuels on non-volatile particulate matter emissions from aircraft gas turbine engines: a review, Sci. Total Environ. 820 (2022) 153233.
[256] G. Katata, M. Ota, H. Terada, M. Chino, H. Nagai, Atmospheric discharge and dispersion of radionuclides during the Fukushima Dai-ichi nuclear power plant accident. Part I: source term estimation and local-scale atmospheric dispersion in early phase of the accident, J. Environ. Radioact. 109 (2012) 103–113.
[257] T.J. Yasunari, A. Stohl, R.S. Hayano, J.F. Burkhart, S. Eckhardt, T. Yasunari, Cesium-137 deposition and contamination of Japanese soils due to the Fukushima nuclear accident, Proc. Natl. Acad. Sci. 108 (2011) 19530–19534.
[258] X. Zhang, M. Huang, Ensemble-based release estimation for accidental river pollution with known source position, J. Hazard. Mater. 333 (2017) 99–108.
[259] E. Kalnay, Atmospheric modeling, Data Assimilation and Predictability, Cambridge University Press, 2003.
[260] UNSCEAR(United Nations Scientific Committee on the Effects of Atomic Radiation), UNSCEAR 2013 Report: Sources, Effects and Risks of Ionizing Radiation, Vol. I, SCIENTIFIC ANNEX A: Levels and Effects of Radiation Exposure Due to the Nuclear Accident After the 2011 Great East-Japan Earthquake and Tsunami, UNSCEAR, New York, 2014 (Ed.).
[261] M. Chino, H. Nakayama, H. Nagai, H. Terada, G. Katata, H. Yamazawa, Preliminary estimation of release amounts of 131I and 137Cs accidentally discharged from the fukushima daiichi nuclear power plant into the atmosphere, J. Nucl. Sci. Technol. 48 (2011) 1129–1134.

[262] G. Katata, M. Chino, T. Kobayashi, H. Terada, M. Ota, H. Nagai, M. Kajino, R. Draxler, M.C. Hort, A. Malo, T. Torii, Y. Sanada, Detailed source term estimation of the atmospheric release for the Fukushima Daiichi nuclear power station accident by coupling simulations of an atmospheric dispersion model with an improved deposition scheme and oceanic dispersion model, Atmos. Chem. Phys. 15 (2015) 1029–1070.

[263] H. Terada, G. Katata, M. Chino, H. Nagai, Atmospheric discharge and dispersion of radionuclides during the Fukushima Dai-ichi nuclear power plant accident. Part II: verification of the source term and analysis of regional-scale atmospheric dispersion, J. Environ. Radioact. 112 (2012) 141–154.

[264] O. Tichý, V. Šmídl, R. Hofman, K. Šindelářová, M. Hýža, A. Stohl, Bayesian inverse modeling and source location of an unintended 131I release in Europe in the fall of 2011, Atmos. Chem. Phys. 17 (2017) 12677–12696.

[265] I.G. Enting, Inverse Problems in Atmospheric Constituent Transport, Cambridge University Press, Cambridge, 2002.

[266] X. Davoine, M. Bocquet, Inverse modelling-based reconstruction of the Chernobyl source term available for long-range transport, Atmos. Chem. Phys. 7 (2007) 1549–1564.

[267] M. Krysta, M. Bocquet, Source reconstruction of an accidental radionuclide release at European scale, Q. J. R. Meteorol. Soc. 133 (2007) 529–544.

[268] M. Bocquet, Parameter-field estimation for atmospheric dispersion: application to the Chernobyl accident using 4D-Var, Q. J. R. Meteorol. Soc. 138 (2012) 664–681.

[269] V. Winiarek, M. Bocquet, O. Saunier, A. Mathieu, Estimation of errors in the inverse modeling of accidental release of atmospheric pollutant: application to the reconstruction of the cesium-137 and iodine-131 source terms from the Fukushima Daiichi power plant, J. Geophys. Res. Atmos. 117 (2012) 1–16.

[270] L. Robertson, J. Langner, Source function estimate by means of variational data assimilation applied to the ETEX-I tracer experiment, Atmos. Environ. 32 (1998) 4219–4225.

[271] O. Tichý, V. Šmídl, R. Hofman, A. Stohl, LS-APC v1.0: a tuning-free method for the linear inverse problem and its application to source-term determination, Geosci. Model Dev. 9 (2016) 4297–4311.

[272] V. Tsiouri, I. Kovalets, S. Andronopoulos, J.G. Bartzis, Development and first tests of a data assimilation algorithm in a Lagrangian puff atmospheric dispersion model, Int. J. Environ. Pollut. 44 (2011) 147–155.

[273] V. Tsiouri, S. Andronopoulos, I. Kovalets, L.L. Dyer, J.G. Bartzis, Radiation source rate estimation through data assimilation of gamma dose rate measurements for operational nuclear emergency response systems, Int. J. Environ. Pollut. 50 (2012) 386–395.

[274] V. Tsiouri, I. Kovalets, S. Andronopoulos, J.G. Bartzis, Emission rate estimation through data assimilation of gamma dose measurements in a Lagrangian atmospheric dispersion model, Radiat. Prot. Dosim. 148 (2012) 34–44.

[275] O. Saunier, A. Mathieu, D. Didier, M. Tombette, D. Quelo, V. Winiarek, M. Bocquet, An inverse modeling method to assess the source term of the Fukushima nuclear power plant accident using gamma dose rate observations, Atmos. Chem. Phys. 13 (2013) 11403–11421.

[276] R. Hofman, P. Seibert, I. Kovalets, S. Andronopoulos, Analytical source term optimization for radioactive releases with approximate knowledge of nuclide ratios, in: Proceedings of the EGU General Assembly Conference Abstracts, 2015.

[277] X. Li, S. Sun, X. Hu, H. Huang, H. Li, Y. Morino, S. Wang, X. Yang, J. Shi, S. Fang, Source inversion of both long- and short-lived radionuclide releases from the Fukushima Daiichi nuclear accident using on-site gamma dose rates, J. Hazard. Mater. 379 (2019) 120770.

[278] O. Tichý, V. Šmídl, R. Hofman, N. Evangeliou, Source term estimation of multi--specie atmospheric release of radiation from gamma dose rates, Q. J. R. Meteorol. Soc. 144 (2018) 2781–2797.

[279] Y. Ling, Q. Yue, T. Huang, Q. Shan, D. Hei, X. Zhang, W. Jia, Multi-nuclide source term estimation method for severe nuclear accidents from sequential gamma dose rate based on a recurrent neural network, J. Hazard. Mater. 414 (2021) 125546.

[280] Y. Ling, T. Huang, Q. Yue, Q. Shan, D. Hei, X. Zhang, C. Shi, W. Jia, Improving the estimation accuracy of multi-nuclide source term estimation method for severe nuclear accidents using temporal convolutional network optimized by Bayesian optimization and hyperband, J. Environ. Radioact. 242 (2022) 106787.

[281] S.R. Hanna, G.S. Young, The need for harmonization of methods for finding locations and magnitudes of air pollution sources using observations of concentrations and wind fields, Atmos. Environ. 148 (2017) 361–363.

[282] G.C. Efthimiou, I.V. Kovalets, A. Venetsanos, S. Andronopoulos, C.D. Argyropoulos, K. Kakosimos, An optimized inverse modelling method for determining the location and strength of a point source releasing airborne material in urban environment, Atmos. Environ. 170 (2017) 118–129.

[283] Y. Liao, J. Lu, H. Cai, B. Zhang, F. Li, B. Zhou, A 3D source localization method based on whale optimization algorithm: experiments for locating a time-varying source in a dynamic indoor environment, in: Proceedings of the E3S Web of Conferences, 356, 2022, p. 04002.

[284] F. Li, J. Zhuang, J. Zhang, M. Li, H. Cai, X. Cao, Reconstruction of uncertain parameters in a multizone model based on contam and bayesian inference, in: Proceedings of the E3S Web of Conferences, 356, 2022, p. 04018.

[285] A. Keats, E. Yee, F.S. Lien, Bayesian inference for source determination with applications to a complex urban environment, Atmos. Environ. 41 (2007) 465–479.

[286] E. Yee, F.S. Lien, A. Keats, R. D'Amours, Bayesian inversion of concentration data: source reconstruction in the adjoint representation of atmospheric diffusion, J. Wind Eng. Ind. Aerodyn. 96 (2008) 1805–1816.

[287] D. Ma, J. Gao, Z. Zhang, H. Zhao, Identifying atmospheric pollutant sources using a machine learning dispersion model and Markov chain Monte Carlo methods, in: Stoch. Environ. Res. Risk Assess., 35, 2021, pp. 271–286.

[288] F.K. Chow, B. Kosovic, S. Chan, Source inversion for contaminant plume dispersion in urban environments using building-resolving simulations, J. Appl. Meteorol. Climatol. 47 (2008) 1553–1572.

[289] D. Wade, I. Senocak, Stochastic reconstruction of multiple source atmospheric contaminant dispersion events, Atmos. Environ. 74 (2013) 45–51.

[290] S. Guo, R. Yang, H. Zhang, X. Zhang, New inverse model for detecting fire-source location and intensity, J. Thermophys. Heat Transf. 24 (2010) 745–755.

[291] N. Wu, R. Yang, H. Zhang, L. Qiao, Decentralized inverse model for estimating building fire source location and intensity, J. Thermophys. Heat Transf. 27 (2013) 563–575.

[292] N. Wu, R. Yang, H. Zhang, An advanced fire estimation model for decentralized building control, Build. Simul. 8 (2015) 579–591.

[293] L. Delle Monache, J.K. Lundquist, B. Kosovic, G. Johannesson, K.M. Dyer, R.D. Aines, F.K. Chow, R.D. Belles, W.G. Hanley, S.C. Larsen, G.A. Loosmore, J.J. Nitao, G.A. Sugiyama, P.J. Vogt, Bayesian inference and Markov chain Monte Carlo sampling to reconstruct a contaminant source on a continental scale, J. Appl. Meteorol. Climatol. 47 (2008) 2600–2613.

[294] S.E. Haupt, R.L. Haupt, G.S. Young, A mixed integer genetic algorithm used in biological and chemical defense applications, Soft Comput. 15 (2011) 51–59.

[295] S.E. Haupt, A demonstration of coupled receptor/dispersion modeling with a genetic algorithm, Atmos. Environ. 39 (2005) 7181–7189.

[296] K.J. Long, S.E. Haupt, G.S. Young, Assessing sensitivity of source term estimation, Atmos. Environ. 44 (2010) 1558–1567.

[297] D. Ma, S. Wang, Z. Zhang, Hybrid algorithm of minimum relative entropy-particle swarm optimization with adjustment parameters for gas source term identification in atmosphere, Atmos. Environ. 94 (2014) 637–646.

[298] N. Gunawardena, K.K. Leang, E. Pardyjak, Particle swarm optimization for source localization in realistic complex urban environments, Atmos. Environ. 262 (2021) 118636.

[299] L.C. Thomson, B. Hirst, G. Gibson, S. Gillespie, P. Jonathan, K.D. Skeldon, M.J. Padgett, An improved algorithm for locating a gas source using inverse methods, Atmos. Environ. 41 (2007) 1128–1134.

[300] M. Hutchinson, H. Oh, W.H. Chen, A review of source term estimation methods for atmospheric dispersion events using static or mobile sensors, Inf. Fusion 36 (2017) 130–148.

[301] S. Fang, X. Dong, S. Zhuang, Z. Tian, T. Chai, Y. Xu, Y. Zhao, L. Sheng, X. Ye, W. Xiong, Oscillation-free source term inversion of atmospheric radionuclide releases with joint model bias corrections and non-smooth competing priors, J. Hazard. Mater. 440 (2022) 129806.

[302] M. Krysta, M. Bocquet, B. Sportisse, O. Isnard, Data assimilation for short-range dispersion of radionuclides: an application to wind tunnel data, Atmos. Environ. 40 (2006) 7267–7279.

[303] D. Quelo, B. Sportisse, O. Isnard, Data assimilation for short range atmospheric dispersion of radionuclides: a case study of second-order sensitivity, J. Environ. Radioact. 84 (2005) 393–408.

[304] R. Abida, M. Bocquet, Targeting of observations for accidental atmospheric release monitoring, Atmos. Environ. 43 (2009) 6312–6327.

[305] V. Winiarek, J. Vira, M. Bocquet, M. Sofiev, O. Saunier, Towards the operational estimation of a radiological plume using data assimilation after a radiological accidental atmospheric release, Atmos. Environ. 45 (2011) 2944–2955.

[306] R. Abida, M. Bocquet, N. Vercauteren, O. Isnard, Design of a monitoring network over France in case of a radiological accidental release, Atmos. Environ. 42 (2008) 5205–5219.

[307] P.H. Hiemstra, D. Karssenberg, A. van Dijk, Assimilation of observations of radiation level into an atmospheric transport model: a case study with the particle filter and the ETEX tracer dataset, Atmos. Environ. 45 (2011) 6149–6157.

[308] P.H. Hiemstra, D. Karssenberg, A. van Dijk, S.M. de Jong, Using the particle filter for nuclear decision support, Environ. Model. Soft. 37 (2012) 78–89.

[309] R.E. Kalman, A new approach to linear filtering and prediction problems, J. Basic Eng. 82 (1960) 35–45.

[310] P. Astrup, C. Turcanu, R. Puch, C. Rojas Palma, T. Mikkelsen, Data Assimilation in the Early Phase:Kalman Filtering RIMPUFF (2004) 31.

[311] C. Rojas-Palma, H. Madsen, F. Gering, R. Puch, C. Turcanu, P. Astrup, H. Müller, K. Richter, M. Zheleznyak, D. Treebushny, M. Kolomeev, D. Kamaev, H. Wynn, Data assimilation in the decision support system RODOS, Radiat. Prot. Dosim. 104 (2003) 31–40.

[312] C. Rojas-Palma, F. Gering, H. Madsen, R. Puch-Solis, K. Richter, H. Muller, Theoretical framework and practical considerations for data assimilation in off-site nuclear emergency management, SCK·CEN, Mol. (2001) 1–32.

[313] M. Drews, B. Lauritzen, H. Madsen, Analysis of a Kalman filter based method for on-line estimation of atmospheric dispersion parameters using radiation monitoring data, Radiat. Prot. Dosim. 113 (2005) 75–89.

[314] M. Drews, B. Lauritzen, H. Madsen, J.Q. Smith, Kalman filtration of radiation monitoring data from atmospheric dispersion of radioactive materials, Radiat. Prot. Dosim. 111 (2004) 257–269.

[315] J. Wu, S. Yuan, C. Zhang, X. Zhang, Numerical estimation of gas release and dispersion in coal mine using Ensemble Kalman Filter, J. Loss Prev. Process Ind. 56 (2018) 57–67.

[316] S. Yuan, J. Wu, X. Zhang, W. Liu, EnKF-based estimation of natural gas release and dispersion in an underground tunnel, J. Loss Prev. Process Ind. 62 (2019) 103931.

[317] O. Tichý, V. Šmídl, N. Evangeliou, Source term determination with elastic plume bias correction, J. Hazard. Mater. 425 (2022) 127776.

[318] S. Fang, S. Zhuang, X. Li, H. Li, Automated release rate inversion and plume bias correction for atmospheric radionuclide leaks: a robust and general remediation to imperfect radionuclide transport modeling, Sci. Total Environ. 754 (2021) 142140.

[319] J. Shi, W. Xie, X. Huang, F. Xiao, A. Usmani, F. Khan, X. Yin, G. Chen, Real-time natural gas release forecasting by using physics-guided deep learning probability model, J. Clean. Prod. 368 (2022) 133201.
[320] U.S.NRCReactor Safety study. An assessment of Accident Risks in U. S. Commercial Nuclear Power plants, U.S.NRC, United States, 1975 Executive summary: Main Report[PWR and BWR].
[321] N.E. Wiltbank, C.J. Palmer, Dynamic PRA prospects for the nuclear industry, Front. Energy Res. 9 (2021).
[322] Z.Y. Han, W.G. Weng, An integrated quantitative risk analysis method for natural gas pipeline network, J. Loss Prev. Process Ind. 23 (2010) 428–436.
[323] Z.Y. Han, W.G. Weng, Comparison study on qualitative and quantitative risk assessment methods for urban natural gas pipeline network, J. Hazard. Mater. 189 (2011) 509–518.
[324] B. Zhang, Y. Liu, S. Qiao, A quantitative individual risk assessment method in process facilities with toxic gas release hazards: a combined scenario set and CFD approach, Process Saf. Prog. 38 (2019) 52–60.
[325] B. Zhang, G.M. Chen, Quantitative risk analysis of toxic gas release caused poisoning—a CFD and dose–response model combined approach, Process Saf. Environ. Prot. 88 (2010) 253–262.
[326] D. Courault, I. Albert, S. Perelle, A. Fraisse, P. Renault, A. Salemkour, P. Amato, Assessment and risk modeling of airborne enteric viruses emitted from wastewater reused for irrigation, Sci. Total Environ. 592 (2017) 512–526.
[327] J.d. Hora, E.B. Cohim, S. Sipert, A. Leão, Quantitative microbial risk assessment (QMRA) of campylobacter for roof-harvested rainwater domestic use, in: Proceedings of the AMIA Annual Fall Symposium, 2, 2018.
[328] M.A. Jahne, S.W. Rogers, T.M. Holsen, S.J. Grimberg, I.P. Ramler, Emission and dispersion of bioaerosols from dairy manure application sites: human health risk assessment, Environ. Sci. Technol. 49 (2015) 9842–9849.
[329] Y. Zhao, B. Richardson, E. Takle, L. Chai, D. Schmitt, H. Xin, Airborne transmission may have played a role in the spread of 2015 highly pathogenic avian influenza outbreaks in the United States, Sci. Rep. 9 (2019) 11755.
[330] G. Buonanno, L. Morawska, L. Stabile, Quantitative assessment of the risk of airborne transmission of SARS-CoV-2 infection: prospective and retrospective applications, Environ. Int. 145 (2020) 106112.
[331] H. Gao, T. Hammer, X. Zhang, W. He, G. Xu, J. Wang, Quantifying respiratory tract deposition of airborne graphene nanoplatelets: the impact of plate-like shape and folded structure, NanoImpact 21 (2021) 100292.
[332] T. Hammer, H. Fissan, J. Wang, Determination of the delivered dose of nanoparticles in the trachea-bronchial and alveolar regions of the lung, NanoImpact 14 (2019) 100162.
[333] F.J. Miller, B. Asgharian, J.D. Schroeter, O. Price, Improvements and additions to the multiple path particle dosimetry model, J. Aerosol Sci. 99 (2016) 14–26.
[334] W.J. Bair, The ICRP human respiratory tract model for radiological protection, Radiat. Prot. Dosim. 60 (1995) 307–310.
[335] S. Guha, P. Hariharan, M.R. Myers, Enhancement of ICRP's lung deposition model for pathogenic Bioaerosols, Aerosol Sci. Technol. 48 (2014) 1226–1235.
[336] J. Schmitt, J. Wang, Quantitative modeling of the impact of facemasks and associated leakage on the airborne transmission of SARS-CoV-2, Sci. Rep. 11 (2021) 19403.
[337] J. Schmitt, L.S. Jones, E.A. Aeby, C. Gloor, B. Moser, J. Wang, Protection level and reusability of a modified full-face snorkel mask as alternative personal protective equipment for healthcare workers during the COVID-19 pandemic, Chem. Res. Toxicol. 34 (2021) 110–118.
[338] P. Sachinidou, Y.K. Bahk, M. Tang, N. Zhang, S.S.C. Chen, D.Y.H. Pui, B.A. Lima, G. Bosco, P. Tronville, T. Mosimann, M. Eriksson, J. Wang, Inter-laboratory validation of the method to determine the filtration efficiency for airborne particles in the 3–500nm range and results sensitivity analysis, Aerosol Air Qual. Res. 17 (2017) 2669–2680.
[339] P. Sachinidou, Y.K. Bahk, J. Wang, An integrative model for the filtration efficiencies in realistic tests with consideration of the filtration velocity profile and challenging particle size distribution, Aerosol Sci. Technol. (2016) 1–10.
[340] Z. Sun, M. Tang, Q. Song, J. Yu, Y. Liang, J. Hu, J. Wang, Filtration performance of air filter paper containing kapok fibers against oil aerosols, Cellulose 25 (2018) 6719–6729.
[341] Z. Huang, C. Dang, Z. Sun, H. Qi, High-efficiency air filter media with a three-dimensional network composed of core–shell Zeolitic Imidazolate framework-8@tunicate nanocellulose for PM0.3 removal, ACS Appl. Mater. Interfaces 13 (2021) 57921–57929.
[342] J. Wang, D.R. Chen, D.Y.H. Pui, Modeling of filtration efficiency of nanoparticles in standard filter media, in: A.D. Maynard, D.Y.H. Pui (Eds.), Nanotechnology and Occupational Health, Springer Netherlands, Dordrecht, 2007, pp. 109–115.
[343] S. Vijay, J. Wang, Health benefit/burden, PM2.5 removal effectiveness, and power consumption based comparison of common residential air-cleaning technologies in the United States, Indoor Air 32 (2022) e13080.
[344] J. Wang, S.C. Kim, D.Y.H. Pui, Figure of merit of composite filters with micrometer and nanometer fibers, Aerosol Sci. Technol. 42 (2008) 722–728.
[345] J. Wang, D.Y.H. Pui, Filtration of aerosol particles by elliptical fibers: a numerical study, J. Nanopart. Res. 11 (2009) 185–196.
[346] T. Batt, G. Herwig, S. Annaheim, P. Clement, L. Furrer, C. Hirsch, V. Varanges, B. Caglar, V. Michaud, J. Wang, G. Richner, P. Wick, R. Rossi, Community masks - from an emergency solution to an innovation booster for the textile industry, Chimia 76 (2022) 249 Aarau.
[347] Z. Pan, X. Zhang, Z. Sun, F. Jiang, L. Lin, Y. Liang, M. Tang, J. Wang, High fidelity simulation of ultrafine PM filtration by multiscale fibrous media characterized by a combination of X-ray CT and FIB-SEM, J. Membr. Sci. 620 (2020) 118925.
[348] Z. Sun, Y. Liang, W. He, F. Jiang, Q. Song, M. Tang, J. Wang, Filtration performance and loading capacity of nano-structured composite filter media for applications with high soot concentrations, Sep. Purif. Technol. 221 (2019) 175–182.
[349] H. Gao, W. He, Y.B. Zhao, D.M. Opris, G. Xu, J. Wang, Electret mechanisms and kinetics of electrospun nanofiber membranes and lifetime in filtration applications in comparison with corona-charged membranes, J. Membr. Sci. 600 (2020) 117879.
[350] J. Wang, S.C. Kim, D.Y.H. Pui, Investigation of the figure of merit for filters with a single nanofiber layer on a substrate, J. Aerosol Sci. 39 (2008) 323–334.
[351] H. Gao, W. He, R. Yu, T. Hammer, G. Xu, J. Wang, Aerodynamic property and filtration evaluation of airborne graphene nanoplatelets with plate-like shape and folded structure, Sep. Purif. Technol. 251 (2020) 117293.
[352] J. Wang, Y.K. Bahk, S.C. Chen, D.Y.H. Pui, Characteristics of airborne fractal-like agglomerates of carbon nanotubes, Carbon 93 (2015) 441–450 N Y.
[353] S.C. Kim, J. Wang, M.S. Emery, W.G. Shin, G.W. Mulholland, D.Y.H. Pui, Structural property effect of nanoparticle agglomerates on particle penetration through fibrous filter, Aerosol Sci. Technol. 43 (2009) 344–355.
[354] Z. Sun, Y. Yue, W. He, F. Jiang, C.H. Lin, D.Y.H. Pui, Y. Liang, J. Wang, The antibacterial performance of positively charged and chitosan dipped air filter media, Build. Environ. 180 (2020) 107020.
[355] W. He, Y. Guo, Y.B. Zhao, F. Jiang, J. Schmitt, Y. Yue, J. Liu, J. Cao, J. Wang, Self--supporting smart air filters based on PZT/PVDF electrospun nanofiber composite membrane, Chem. Eng. J. 423 (2021) 130247.
[356] P. Sachinidou, C. Heuschling, J. Schaniel, J. Wang, Investigation of surface potential discharge mechanism and kinetics in dielectrics exposed to different organic solvents, Polymer 145 (2018) 447–453 Guildf.
[357] V. Varanges, B. Caglar, Y. Lebaupin, T. Batt, W. He, J. Wang, R.M. Rossi, G. Richner, J.R. Delaloye, V. Michaud, On the durability of surgical masks after simulated handling and wear, Sci. Rep. 12 (2022) 4938.
[358] W. He, Y. Guo, J. Liu, Y. Yue, J. Wang, Filtration performance degradation of in-use masks by vapors from alcohol-based hand sanitizers and the mitigation solutions, Glob. Chall. 5 (2021) 2100015.
[359] B. Liu, Y. Sun, T. Zheng, X. He, P. Wang, J. Wang, Regeneration of carbon nanotube saturated with tetracycline by microwave-ultraviolet system: performance and degradation pathway, Chem. Eng. J. 394 (2020) 124752.
[360] Y. Yao, S. Liu, T. You, Z. Zhou, X. Zhang, M. Tang, Z. Sun, J. Wang, J. Hu, Application of microfibrillated fibers in robust and reusable air filters with long service time in the ambient with high oily aerosols concentration, Sep. Purif. Technol. 295 (2022) 121263.
[361] W. He, Y.B. Zhao, F. Jiang, Y. Guo, H. Gao, J. Liu, J. Wang, Filtration performance and charge degradation during particle loading and reusability of charged PTFE needle felt filters, Sep. Purif. Technol. 233 (2020) 116003.
[362] ICRP, in: The 2007 Recommendations of the International Commission on Radiological Protection, 37, ICRP, 2007, pp. 9–34. Ann..
[363] B. Nie, M. Ni, S. Wei, Individual dose due to radioactivity accidental release from fusion reactor, J. Hazard. Mater. 327 (2017) 135–143.
[364] J. Shi, B. Chang, F. Khan, Y. Chang, Y. Zhu, G. Chen, C. Zhang, Stochastic explosion risk analysis of hydrogen production facilities, Int. J. Hydrog. Energy 45 (2020) 13535–13550.
[365] J. Shi, J. Li, F. Khan, Y. Chang, Y. Zhu, G. Chen, Explosion risk-based water spray mitigation analysis of ultra-deep-water semi-submersible platforms, Ocean Eng. 239 (2021) 109716.
[366] M. Ruijten, J. Arts, P. Boogaard, P. Bos, H. Muijser, A. Wijbenga, Method for derivation of probit functions for acute inhalation toxicity, Methode Voor De Afleiding Van Probitrelaties Om Acute Sterfte Te Voorspellen Na Inhalatie Van Giftige Stoffen, Rijksinstituut voor Volksgezondheid en Milieu RIVM, 2015.
[367] D.L. Preston, Y. Shimizu, D.A. Pierce, A. Suyama, K. Mabuchi, Studies of mortality of atomic bomb survivors. report 13: solid cancer and noncancer disease mortality: 1950–1997, Radiat. Res. 160 (2003) 381–407.
[368] D.L. Preston, D.A. Pierce, Y. Shimizu, H.M. Cullings, S. Fujita, S. Funamoto, K. Kodama, Effect of recent changes in atomic bomb survivor dosimetry on cancer mortality risk estimates, Radiat. Res. 162 (2004) 377–389 313.
[369] D.L. Preston, E. Ron, S. Tokuoka, S. Funamoto, N. Nishi, M. Soda, K. Mabuchi, K. Kodama, Solid cancer incidence in atomic bomb survivors: 1958–1998, Radiat. Res. 168 (2007) 1–64 64.
[370] N. Hamada, Y. Fujimichi, Classification of radiation effects for dose limitation purposes: history, current situation and future prospects, J. Radiat. Res. 55 (2014) 629–640.
[371] Strahlenschutzkommission, Dose and dose-rate effectiveness factor (DDREF) Recommendation by German commission on radiological protectionGeschäftsstelle Der Strahlenschutzkommission, Bonn, 2014.
[372] R. Wakeford, T. Azizova, W. Dörr, J. Garnier-Laplace, M. Hauptmann, K. Ozasa, P. Rajaraman, K. Sakai, S. Salomaa, M. Sokolnikov, D. Stram, Q. Sun, A. Wojcik, G. Woloschak, S. Bouffler, B. Grosche, M. Kai, M.P. Little, R.E. Shore, L. Walsh, W. Rühm, The dose and dose-rate effectiveness factor (DDREF), Health Phys. 116 (2019).
[373] W. Netkueakul, D. Korejwo, T. Hammer, S. Chortarea, P. Rupper, O. Braun, M. Calame, B. Rothen-Rutishauser, T. Buerki-Thurnherr, P. Wick, J. Wang, Release of graphene-related materials from epoxy-based composites: characterization, quantification and hazard assessment *in vitro*, Nanoscale 12 (2020) 10703–10722.
[374] J. Li, H. Chen, X. Li, M. Wang, X. Zhang, J. Cao, F. Shen, Y. Wu, S. Xu, H. Fan, G. Da, R.J. Huang, J. Wang, C.K. Chan, A.L. De Jesus, L. Morawska, M. Yao, Differing toxicity of ambient particulate matter (PM) in global cities, Atmos. Environ. 212 (2019) 305–315.
[375] J. Wang, L. Schlagenhauf, A. Setyan, Transformation of the released asbestos, carbon fibers and carbon nanotubes from composite materials and the changes of their potential health impacts, J. Nanobiotechnol. 15 (2017) 15.

[376] P. Mantecca, K. Kasemets, A. Deokar, I. Perelshtein, A. Gedanken, Y.K. Bahk, B. Kianfar, J. Wang, Airborne nanoparticle release and toxicological risk from metal-oxide-coated textiles: toward a Multiscale safe-by-design approach, Environ. Sci. Technol. 51 (2017) 9305–9317.
[377] A. Bruinink, J. Wang, P. Wick, Effect of particle agglomeration in nanotoxicology, Arch. Toxicol. 89 (2015) 659–675.
[378] J. Wang, C. Asbach, H. Fissan, T. Hülser, T.A.J. Kuhlbusch, D. Thompson, D.Y.H. Pui, How can nanobiotechnology oversight advance science and industry: examples from environmental, health, and safety studies of nanoparticles (nano-EHS), J. Nanopart. Res. 13 (2011) 1373–1387.
[379] K.A. Ryan, K.R. Bewley, S.A. Fotheringham, Dose-dependent response to infection with SARS-CoV-2 in the ferret model and evidence of protective immunity, Nat. Commun. 12 (2021) 81.
[380] Y.I. Kim, S.G. Kim, S.M. Kim, E.H. Kim, S.J. Park, K.M. Yu, J.H. Chang, E.J. Kim, S. Lee, M.A.B. Casel, J. Um, M.S. Song, H.W. Jeong, V.D. Lai, Y. Kim, B.S. Chin, J.S. Park, K.H. Chung, S.S. Foo, H. Poo, I.P. Mo, O.J. Lee, R.J. Webby, J.U. Jung, Y.K. Choi, Infection and rapid transmission of SARS-CoV-2 in ferrets, Cell Host Microbe 27 (2020) 704–709 e702.
[381] E. Monchatre-Leroy, S. Lesellier, M. Wasniewski, E. Picard-Meyer, C. Richomme, F. Boue, S. Lacote, S. Murri, C. Pulido, J. Vulin, F.J. Salguero, M.A. Gouilh, A. Servat, P. Marianneau, Hamster and ferret experimental infection with intranasal low dose of a single strain of SARS-CoV-2, J. Gen. Virol. 102 (2021) 1–10.
[382] D.K. Chu, E.A. Akl, S. Duda, K. Solo, S. Yaacoub, H.J. Schünemann, A. El-harakeh, A. Bognanni, T. Lotfi, M. Loeb, A. Hajizadeh, A. Bak, A. Izcovich, C.A. Cuello-Garcia, C. Chen, D.J. Harris, E. Borowiack, F. Chamseddine, F. Schünemann, G.P. Morgano, G.E.U. Muti Schünemann, G. Chen, H. Zhao, I. Neumann, J. Chan, J. Khabsa, L. Hneiny, L. Harrison, M. Smith, N. Rizk, P.Giorgi Rossi, P. AbiHanna, R. El-khoury, R. Stalteri, T. Baldeh, T. Piggott, Y. Zhang, Z. Saad, A. Khamis, M. Reinap, Physical distancing, face masks, and eye protection to prevent person-to-person transmission of SARS-CoV-2 and COVID-19: a systematic review and meta-analysis, Lancet N. Am. Ed. 395 (2020) 1973–1987.
[383] T. Watanabe, T.A. Bartrand, M.H. Weir, T. Omura, C.N. Haas, Development of a dose-response model for SARS coronavirus, Risk Anal. 30 (2010) 1129–1138.
[384] X. Zhang, J. Wang, Dose-response relation deduced for coronaviruses from coronavirus disease 2019, severe acute respiratory syndrome, and middle east respiratory syndrome: meta-analysis results and its application for infection risk assessment of aerosol transmission, Clin. Infect. Dis. 73 (2021) e241–e245.
[385] Á. Leelőssy, R. Mészáros, A. Kovács, I. Lagzi, T. Kovács, Numerical simulations of atmospheric dispersion of iodine-131 by different models, PLoS One 12 (2017) e0172312.
[386] J.M. Carcione, J.E. Santos, C. Bagaini, J. Ba, A simulation of a COVID-19 epidemic based on a deterministic SEIR model, Front. Public Health 8 (2020) 1–13.
[387] X.L. Zhang, W.G. Weng, H.Y. Yuan, J.G. Chen, Empirical study of a unidirectional dense crowd during a real mass event, Phys. A 392 (2013) 2781–2791.
[388] X.L. Zhang, W.G. Weng, H.Y. Yuan, Empirical study of crowd behavior during a real mass event, J. Stat. Mech. Theory Exp. 2012 (2012) P08012.
[389] J.Y. Wang, W.G. Weng, X.L. Zhang, New insights into the crowd characteristics in Mina, J. Stat. Mech. Theory Exp. 2014 (2014) P11003.
[390] W. Jiayue, W. Wenguo, Z. Xiaole, Comparison of turbulent pedestrian behaviors between mina and love parade, Procedia Eng. 84 (2014) 708–714.
[391] D. Efimov, R. Ushirobira, On an interval prediction of COVID-19 development based on a SEIR epidemic model, Annu. Rev. Control 51 (2021) 477–487.
[392] N. Zhang, P. Cheng, W. Jia, C.H. Dung, L. Liu, W. Chen, H. Lei, C. Kan, X. Han, B. Su, S. Xiao, H. Qian, B. Lin, Y. Li, Impact of intervention methods on COVID-19 transmission in Shenzhen, Build. Environ. 180 (2020) 107106.
[393] P. Douglas, E.T. Hayes, W.B. Williams, S.F. Tyrrel, R.P. Kinnersley, K. Walsh, M. O'Driscoll, P.J. Longhurst, S.J.T. Pollard, G.H. Drew, Use of dispersion modelling for environmental impact assessment of biological air pollution from composting: progress, problems and prospects, Waste Manag. 70 (2017) 22–29 Oxford.